THESE DE DOCTORAT

NNT : 2022UPASG048

Optimization of ridesourcing services for the future deployment of connected and autonomous vehicles in urban areas

Optimisation des services de "ridesourcing" pour le déploiement futur des véhicules autonomes et connectés en milieu urbain

Thèse de Doctorat de l'Université Paris-Saclay et de l'Université de Tongji

Ecole Doctorale n° 580 : Science et Technologies de l'Information et de la Communication (STIC)

Spécialité de doctorat : Automatique

Graduate School : Informatique et Science du Numérique

Référent : Université d'Evry

Thèse préparée dans le laboratoire PICS-L (Université Gustave Eiffel, Versailles, France) et The Key Laboratory of Road and Traffic Engineering (Université de Tongji, Shanghai, Chine) sous la direction de Dominique GRUYER, Ye LI, et Olivier ORFILA

Thèse soutenue à Paris-Saclay, le 14 juin 2022, par

Meiting TU

Jury Members

CHEN Shiyi	Prof. (Fudan University)	Présidente
RAKOTONIRAINY Andry	Prof. (Queensland University of Technology)	Rapporteur
ZARGAYOUNA Mahdi	CR HDR (University Gustave Eiffel)	Rapporteur
CHEN Xiaohong	Prof. (Tongji University)	Examinatrice
NOUVELIERE Lydie	MCF HDR (Université Paris-Saclay)	Examinatrice
YE Jianhong	Prof. (Tongji University)	Examinatrice
GRUYER Dominique	Prof. (University Gustave Eiffel)	Directeur de thèse
LI Ye	Prof. (Tongji University)	Directeur de thèse
ORFILA Olivier	CR HDR (ITE VEDECOM)	CoDirecteur de thèse
EL GANAOUI-MOURLAN Ouafae	Prof. (IFP School)	Invitée
SUN Haihao	Prof. (Tongji University)	Invité

ABSTRACT

On-demand ridesourcing services have become increasingly popular due to their convenience. There are some debates claiming that ridesourcing services could increase congestion and pollution. Ridesplitting, a new shared mobility service, is a more sustainable travel mode for improving traffic efficiency and reducing air pollution. Therefore, the motivation of this study is to propose an optimization framework for the shared mobility system (SMS). The SMS ecosystem can be modeled with four specific research domains: city infrastructures, users, shared mobility system, and connected and autonomous vehicles (CAVs) technologies. Critical results and conclusions could be summarized into the following four aspects:

1) City infrastructures

Exploring nonlinear effects of the built environment on ridesplitting service

We use a machine learning method, gradient boosting decision tree model, to identify the impacts of the built environment on the ridesplitting ratio. The results show that most built environment features have a strong nonlinear effect on the ridesplitting ratio. Partial dependence plots could provide policy implications for the shared mobility system to improve the ridesplitting service.

2) Users

Improving the demand prediction of ridesourcing services with an Optimized Spatiotemporal Encoder-Decoder Neural Network

We propose a novel ridesourcing demand prediction framework. We use a combination of a graph convolutional network and a read-first long short-term memory network and a dynamic spatiotemporal attention mechanism. The experimental results show that the proposed framework outperforms state-of-the-art models for both single-step demand prediction and multi-step prediction.

3) Ridesourcing system

Optimizing ridesourcing system based on a shareability network on a city level

We optimize the ridesourcing system based on a shareability network and evaluate the gap between the potential and actual level of ridesplitting. We explore the potential of ridesplitting during peak hours using empirical ridesourcing data in Chengdu, China. The results show that the percentage of potential cost savings, time savings and shared trips could reach up to 18.47%, 25.75% and 90.69%, while the actual level is 1.22%, 2.38% and 7.85%. CAVs are also applicable in the proposed system.

4) CAVs technologies

Proposing a resilient and robust control strategy for connected and autonomous vehicles to resist the threat of cyberattacks

In anticipation of applying the previous models and solutions to CAVs, cyberattacks are an urgent problem for CAVs. We explore how cyberattacks work on CAVs. A resilient and robust control strategy (RRCS) for cyberattacks is developed and its impacts on the mixed traffic flow are explored. Finally, sensitivity analyses are conducted in different platoon compositions, vehicle distribution and cyberattack intensities. The results show that the proposed RRCS of cyberattacks is robust and can resist the negative threats of cyberattacks on the CAV platoon.

The originality and innovative aspects of this dissertation could be summarized according to 2 perspectives. For the value of theory and methodology, the proposed framework for the SMS could provide a systematic methodology for the modelling and simulation. The proposed artificial intelligent algorithms could provide a better understanding for the researches of travel behaviors analysis and spatiotemporal modelling. For the value of practical application, the proposed shared mobility system could help improve ridesplitting service to build a low carbon transport, which could incorporate CAVs for the future mobility.

Key Words: ridesourcing, ridesplitting, connected and autonomous vehicles, shared mobility services, optimization, machine learning

Résumé

Les services de transport à la demande sont de plus en plus populaires en raison de leur commodité. Cependant, certaines études font apparaitre que ces services pourraient augmenter les congestions et le niveau de pollution. Le ridesplitting, un nouveau service de mobilité partagée, est un moyen plus durable de se déplacer pour améliorer l'efficacité des transports et réduire les émissions de polluants. Dans ce contexte, ce travail propose un cadre d'optimisation pour un Système de Mobilité Partagée (SMP). Dans cette thèse, l'écosystème SMP est traité sur quatre domaines de recherche : l'infrastructure urbaine, les utilisateurs, le système de mobilité partagée et les Véhicules Connectés et Autonomes (CAVs) :

1) Infrastructures urbaines

L'objectif est d'explorer les effets non linéaires de l'environnement bâti sur le service de ridesplitting en utilisant une méthode d'apprentissage automatique (modèle d'arbre de décision avec boosting de gradient). Les résultats montrent que la plupart des caractéristiques de l'environnement bâti ont un effet fortement non linéaire sur le taux de ridesplitting. Ces résultats peuvent fournir des préconisations importantes sur les politiques de transport impliquant les opérateurs de transport dans le but d'améliorer les services de covoiturage.

2) Utilisateurs

L'objectif est d'améliorer la prévision de la demande de services de ridesplitting à l'aide d'un réseau neuronal encodeur-décodeur spatio-temporel optimisé avec une couche d'encodage basée sur une combinaison de réseaux (réseau convolutif de graphes et réseau de mémoire à long terme à lecture prioritaire). Les résultats expérimentaux montrent que le cadre proposé surpasse les résultats obtenus dans l'état de l'art aussi bien pour la prédiction de la demande en une seule étape, que pour la prédiction en plusieurs étapes.

3) Système de répartition des trajets

A partir des résultats précédents, nous proposons une optimisation du système de répartition des trajets sur la base d'un réseau de partage pour améliorer le système de répartition des trajets et évaluons l'écart entre le potentiel et le niveau réel de répartition des trajets. A partir de données empiriques de répartition des trajets à Chengdu (Chine), nous avons exploré le potentiel de la répartition des trajets pendant les heures de pointe.

Les résultats montrent que le pourcentage d'économies potentielles, de gains de temps, et de trajets partagés pourrait atteindre respectivement 18,47%, 25,75% et 90,69%, alors que le niveau réel est de 1,22%, 2,38% et 7,85%. La solution proposée est générique et applicable au déploiement des CAV.

4) CAV

En prévision d'appliquer les modèles et solutions précédentes aux CAV, la résilience et la robustesse des CAV en cas de cyber-attaques a été étudiée en développant une stratégie de contrôle résiliente et robuste (RRCS).

Cette RRCS est appliquée sur un modèle de poursuite et son impact sur le flux de trafic mixte et la stabilité d'un peloton est étudié en cas de cyber-attaques et de défaillances. Des analyses de sensibilité ont été menées pour différentes compositions de pelotons, distributions de véhicules, et cyber-attaques. Les résultats montrent que la RRCS proposée est robuste et efficace pour garantir la sécurité d'un peloton de CAV.

L'originalité et les aspects innovants développés dans cette thèse sont aussi bien théoriques et méthodologiques, qu'appliqués.

Du point de vue théorique et méthodologique, le cadre proposé pour le SMP fournit une méthodologie systématique et générique pour la modélisation et la simulation. Les algorithmes d'IA proposés permettent d'analyser et de mieux comprendre les comportements de déplacement des usagers et leur modélisation spatio-temporelle.

Pour ce qui est de l'application pratique de ces travaux, le SMP proposé peut améliorer significativement les services de ridesplitting tout en réduisant l'empreinte carbone. De plus, ce SMP est facilement extrapolable aux CAV et aux futurs systèmes de mobilités.

Mots clés : ridesourcing, ridesplitting, véhicules connectés et autonomes, services de mobilité partagée, optimisation, machine learning

摘要

网约车公司运营的按需乘车服务因其便利性而越来越受欢迎，其发展也面临一些争论，有研究发现网约车服务可能会加剧交通拥堵和空气污染问题。因而，网约车服务也逐步实现向共享出行服务的巨大转变，比如拼车服务。拼车是一种新型的共享出行服务，相较于非拼车出行，是一种更可持续的出行方式。然而，拼车出行在网约车出行占比非常低，对于其影响因素、作用机理、框架设计以及不确定性还有待深入研究。因此，智能网联背景下如何充分利用多源数据中蕴含的丰富信息，优化实现精准高效的共享出行系统，并探寻自动驾驶技术对系统的影响，是目前城市智能交通领域工程应用的热点方向，也是亟需解决的前沿科学问题。

因此，本研究的目标是提出一个共享出行系统研究框架，该研究框架从以下四个要素进行建模：城市基础设施，用户，共享出行系统和自动驾驶技术。本文的研究内容和成果主要包括以下四个方面：

1) 城市基础设施

探究建成环境对拼车行为的影响机制并进行阈值效应分析

使用机器学习方法--梯度提升决策树模型，来探究建成环境对拼车率的影响机制。结果表明，大多数建成环境特征对拼车率有很强的非线性影响。到市中心的距离、土地利用的多样性和道路密度是影响拼车率的关键解释变量。基于部分依赖图发现建成环境因素的非线性阈值效应，可为政府和网约车公司改善拼车服务提供重要参考。

2) 用户

提出一种新的基于时空编码器-解码器神经网络的网约车需求预测框架

网约车需求预测是共享出行系统优化调度和运力调整的重要依据。我们提出了一种基于时空编码器-解码器神经网络的新型网约车需求预测框架。对于编码器层，我们结合使用图卷积网络和读优先长短时神经网络，它可以全面捕获时空特征。对于解码器层，我们使用长短时神经网络模型和动态时空注意机制，自适应地将历史时空特征与当前预测有效关联起来。实验结果证明了所提出的框架的有效性。

3) 共享出行系统

优化了自动驾驶场景下城市规模级别的拼车调度及基于可共享网络进行潜力分析

我们基于可共享网络优化城市规模级别的拼车调度系统，并探究拼车的潜在效益和实际水平之间的差距。我们利用中国成都市的网约车数据，结果表明了优化车队规模和调度管理以提高拼车效率的巨大潜力：当使用自动驾驶车辆提供拼车服务时，潜在的出行成本节约、出行时间节约和拼车出行的比例最高可达 18.47%、25.75%和 90.69%，而实际水平为 1.22%、2.38%和 7.85%。

4) 自动驾驶技术

探究网络攻击对自动驾驶车辆的作用机理并提出抵御其不利影响的控制策略

自动驾驶技术会促进本研究提出的共享出行系统的建立，但网络攻击对于自动驾驶车辆是亟需解决的问题。我们探究了网络攻击对自动驾驶车辆的作用机理并开发了应对网络攻击不利影响的控制策略，研究了该控制策略在不同网络攻击类型下对混合交通流的影响。最后，对车队组成、车辆分布和网络攻击强度进行敏感性分析。结果表明，所提出应对网络攻击的控制策略具有较强鲁棒性，可以减弱网络攻击对自动驾驶车辆的负面威胁，提高自动驾驶车辆的安全性。

综上所述，本论文的创新点可以从两个方面来概括：对于理论创新和方法创新，所提出的共享出行系统研究框架为交通网络的建模和仿真提供系统的方法论，所提出的人工智能算法可以为交通行为分析和时空建模的研究提供更好的理解。对于实际应用价值创新，提出的共享出行系统可以帮助改善拼车服务，践行低碳交通发展，并且可以结合自动驾驶车辆，为未来出行实现更多可能。

关键词：网约车、拼车、网联和自动驾驶汽车、共享出行服务、最优化、机器学习

Contents

LIST OF FIGURES

LIST OF TABLES

Chapter 1 Introduction

HIGHLIGHTS

1) The background and motivations of the research
2) The research questions to be addressed
3) Overview of the research framework for addressing the research questions
4) The main contributions of the research
5) The outline of the dissertation

1.1 Background and motivations

Vehicular traffic congestion and air pollution during rush hours are two difficult problems for urban areas worldwide. The cost of congestion in the United States alone is approximately $121 billion per year, representing 1% of the GDP, which includes 5.5 billion hours of time lost and an extra 2.9 billion gallons of fuel burned (Schrank et al., 2012). The CO_2 emissions have increased greatly during these years, so it is necessary to advocate the low-carbon transport (Luo et al., 2017). Additionally, the road transport sector is now the leading cause of air-pollution-related deaths (Roskilly et al., 2015). Therefore, it is imperative and urgent to mitigate congestion and air pollution. Recently, countries around the world have made commitments to spare no efforts to achieve carbon peaking and carbon neutrality to slow the trend of global warming. Transportation emissions account for a large proportion of carbon emissions. The development of low-carbon cities and low-carbon transportation is crucial to achieve carbon neutrality.

The current revolutions of sharing, automation and electrification are reshaping the way we travel, with broad implications for future mobility management (Yang, 2021). Ridesourcing services will be the first application scenario in a wave of revolutions of sharing, automation and electrification. Much uncertainty remains about how these disruptive technologies would exactly impact the ridesourcing system. It is meaningful to explore the opportunities and challenges of smart shared mobility system with connected and autonomous vehicles in a wave of revolutions.

Carbon peaking and carbon neutrality guidance

Climate change and CO2 emissions mitigation have drawn an extensive attention in recent years. Because of its continuously growing share in overall energy consumption, the transport sector has been acknowledged as one of the most important contributors to global emissions (Nakamura & Hayashi, 2013). According to the International Energy Agency, world energy-related CO2 emissions increase from 32.3 billion metric tons in 2012 to 35.6 billion metric tons in 2020 and to 43.2 billion metric tons in 2040 (Conti et al., 2016). Besides, 7.38 million tons of CO2 was generated due to oil consumption in the global transport sector in 2013, accounting for 23% of the total fossil fuel-related CO2 emissions (IEA, 2015). In addition, with the continuous development of the urban economy and acceleration of the motorization process, cities account for 75% of global energy consumption and 80% of greenhouse gas emissions (Yan, 2010). Therefore, the urban transport sector has become one of the major contributors to global CO2 emissions. In addition, 1960-2001 was a key period during which the world urbanization level rose from 33% to 45% and global CO2 emissions increased from approximately 190 billion tons to approximately 370 billion tons (Guan et al., 2013).

At the virtual Leaders' Summit on Climate in April 2021 (Warm-up meeting for the United Nations Climate Change Conference in November 2021 in Glasgow), participating countries announced ambitious new climate targets ensuring the emission reductions to keep the goal of limiting global warming to 1.5-degrees C within reach globally. U.S. has made a solemn commitment to reduce greenhouse gas emissions by 50 to 52 percent by 2030 compared to the emissions in 2005. The EU has made a solemn commitment to the world to reduce greenhouse gas emissions by 50% by 2030 and strive to reach 55% compared to the emissions in 1990, which guarantees the carbon neutrality (net-zero emissions) by 2050. Japan has also announced it will strengthen its climate goals, aiming to reduce emissions to below 44% of 2005 levels by 2030. Canada also updated its climate goals, pledging to cut emissions by 40 to 45 percent by 2030 compared to the emissions in 2005. China has pledged to strive to achieve carbon peaking by 2030 and carbon neutrality by 2060 (TheWhiteHouse, 2021).

Three revolutions of transportation in the future (Sperling, 2018)

The revolution of transportation is a major historical opportunity to solve the above problems for the rise of new cities. The previous revolutions in transportation have given birth to the rise and development of emerging cities. At present, the world's transportation sector is about to face "three new revolutions": vehicle electrification, automation, and shared mobility (sharing of vehicle trips), which have started three major battles in transportation:

Shared mobility Campaign: L4 will revolutionize the attributes of cars，which promotes the development of shared mobility.

Automation Campaign: Market demand drives the "intelligence" and "connectivity" of automobiles.

Electrification Campaign: International Convention on "Carbon Emissions" promotes "Electrification" of Vehicles.

Shared mobility Campaign

In this context, car consumers (ownership) will gradually transition to car users (use rights), and autonomous vehicles can be controlled and allocated through the unified data center, which will effectively reduce the idle time of cars and improve utilization efficiency.

The shared mobility platforms represent a new mobility paradigm, a win-win practice for both drivers and passengers, capable of reducing each traveler's costs, offering a new way to decrease environmental impact (Casprini et al., 2019). Shared mobility has become a popular choice, which can effectively reduce car ownership, improve car usage efficiency, and ease the traffic environment. At the same time, when fully autonomous driving technology is realized in the future, the future shared cars will inevitably be combined with autonomous driving technology, which will inevitably subvert the existing service model and become a more advanced and convenient service method that is superior to the existing traditional taxis.

Shaheen et al. (2015) offer an explicit classification of shared mobility, see Figure 1-1. Shared mobility services can be divided into two categories: sharing a vehicle and sharing a passenger ride. For the sharing a vehicle, the services include carsharing, e-scooter, e-motorcycle and shared bikes.

For the sharing a passenger trip, the services include ridesourcing, E-hailing, ridesharing and microtransit services. There are some confusing terms relating to shared mobility for academic transportation researchers.

In summary, ridesourcing refers to transportation services that connect drivers

who drive private cars (instead of commercial vehicles) with passengers via smartphone applications (Rayle et al., 2016). Ridesplitting is a form of ridesourcing wherein riders with similar routes are matched to the same driver and vehicle in real time (S. Shaheen et al., 2016). Ridesourcing is different from ridesharing. Drivers who provide ridesourcing services are usually not travelers, and they drive for the purpose of making money. In contrast, in ridesharing, including carpooling and vanpooling, drivers are travelers who share similar origins/destinations with their riders for the purpose of conserving resources, saving money, or saving time (Jin et al., 2018). E-hailing is a kind of on-demand taxi service.

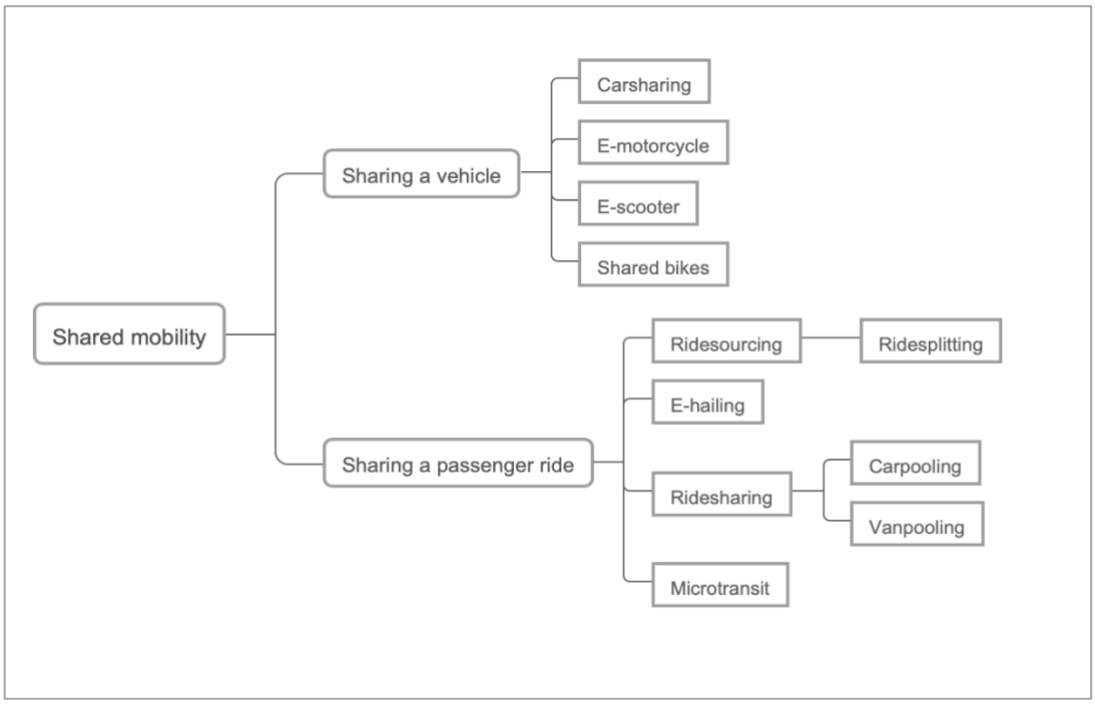

Figure 1-1: Classification of shared mobility
[Source: modified from (Shaheen et al., 2015)]

It should be noted this study focuses on the ridesourcing and ridesplitting services, which are typical shared mobility platforms nowadays. Prearranged and on-demand ride services that match drivers and passengers using smartphone applications have rapidly spread worldwide due to their convenience. As shown in the Figure 1-2, ridesourcing services have spread all over the world.

Figure 1-2: The distribution of some typical ridesourcing platforms worldwide
[Source: (Audenhove et al., 2020)]

Table 1-1 presents the development of some typical ridesourcing platforms, such as Uber, Lyft and DiDi Chuxing. As of 2022, Uber operated in 84 countries in over 1110 cities (Uber Estimator, 2022). Uber served 118 million users and provided 6.3 billion trips globally in 2020, even with the coronavirus pandemic shutting down its operations for most of the year (Iqbal, 2022b). As of 2020, Lyft has offered services in 644 US cities and served 12.5 million users globally (Iqbal, 2022a). As of 2021, DiDi Chuxing has provided 41 million trips per day on average in approximately 4000 cities globally. In addition, the numbers of annual active users and drivers have reached 493 million and 15 million, respectively, on the DiDi Chuxing platform (DiDi Chuxing, 2021). Many ridesourcing companies have launched ridesplitting services to improve transportation efficiency, thus reducing carbon emissions. Lyft Line and UberPOOL are leading companies that allow passengers whose routes overlap to split rides and fares (Shaheen et al., 2015). As of April 2018, more than 2.4 million users travel through DiDi ExpressPool (including ridesplitting services) per day over 60 cities (DiDi Chuxing, 2018a).

Table 1-1 The development of some typical ridesourcing platforms
[Source: (Audenhove et al., 2020)]

	Uber	lyft	cabify	DiDi	Careem	Grab	FREENOW	OLA	Yandex Taxi	
Year of foundation	2009	2012	2011	2012	2012	2012	2009 (formerly MyTaxi, Hailo)	2011	2011	
Key shareholders	▪ SoftBank Corp (16%) ▪ IPO in May 2019	▪ Public ▪ IPO in 2019	▪ Rakuten	▪ Alibaba ▪ Tencent ▪ Baidu	▪ Uber (acquired in March 2019)	▪ Temasek Holdings ▪ SoftBank Corp	▪ BMW Group ▪ Daimler AG	▪ SoftBank Corp	▪ Yandex	
HQ	US	US	Spain	China	UAE	Singapore	Germany	India	Russia	
Main offerings/ business model	▪ "PHV ride-hailing platform" ▪ "taxi ride-hailing platform" ▪ DRPT	▪ "PHV ride-hailing platform" ▪ "taxi ride-hailing platform"	▪ "PHV ride-hailing platform"	▪ "PHV ride-hailing platform" ▪ "taxi ride-hailing platform" ▪ DRPT	▪ "PHV ride-hailing platform" ▪ "taxi ride-hailing platform"	▪ "PHV ride-hailing platform" ▪ "taxi ride-hailing platform"	▪ "PHV ride-hailing platform" ▪ "taxi ride-hailing platform"	▪ "PHV ride-hailing platform" ▪ "taxi ride-hailing platform"	▪ "PHV ride-hailing platform" ▪ "taxi ride-hailing platform"	*50+ other players globally* Bolt Gett
Number of cities	63 countries >700 cities	2 countries >660 cities	12 countries >130 cities	>400 cities in China >1,000 cities globally via partnerships	>14 countries >90 cities	>500 cities in Southeast Asia	>100 cities in Europe	4 countries >150 cities	18 countries >300 cities	
Est. fleet size	93 million active users	2 million drivers	Hundreds of thousands of drivers	>550 million users >31 million drivers	>30 million users >1 million drivers	>45 million users >1 million drivers	>21 million users >250,000 drivers	>1.5 million vehicles	>200,000 drivers	

Automation Campaign

At present, intelligent vehicles have become an important strategic direction for the transformation and upgrading of the global automobile industry. Countries have accelerated their strategic deployment and promoted the development of the intelligent vehicles.

In the United States, the government has improved the environment for the development of the intelligent and connected vehicles (ICV) industry by continuously strengthening strategic planning, accelerating testing and application, and other measures. In January 2021, the US Department of Transportation released the "Comprehensive Plan for Autonomous Vehicles" to further clarify the vision and goals of realizing autonomous vehicles. In April 2020, the United States released the "ITS Strategy 2020~2025". More than 30 states in the United States have passed the revision of policies and regulations to accelerate testing and demonstration. Among them, California, Arizona and other places actively promote the exploration of commercial applications. Michigan plans to build the first 40-mile-long road between Detroit and Ann Arbor exclusively for connected and autonomous vehicles.

The European Union (EU) promotes EU-level consensus and cross-industry collaboration about intelligent vehicles through strategic planning, technology roadmaps, and support for innovative research projects. European countries have adopted the revision of policies and regulations to promote the commercial application of L3 intelligent driving. In April 2021, the UK completed the Compliance with the

new automated lane keeping systems (ALKS) technical consultation, launched the revision of the Roads Act, and promoted the commercial application of the ALKS function in the UK by the end of 2021. In May 2021, the German Bundestag and the Bundesrat successively passed the "Autonomous Driving Law", allowing L4-level autonomous vehicles to operate on German public roads in 2022. In July 2021, France promulgated the autonomous driving decree to establish a complete regulatory framework for the deployment of autonomous vehicles, and hopes to take the lead in promoting the application of ALKS by the end of 2021 (National ICV & China SAE, 2021).

Japan has carried out a large number of top-level design plans to develop autonomous driving through the deep integration of automobiles with intelligent transportation and smart cities. Japan released the *"ITS Concept Roadmap for Officials and Civilians"* which indicates that by 2025, private cars and trucks will achieve L4-level autonomous driving on highways, and driverless travel will be realized nationwide.

In China, ICV industry has been incorporated into the national top-level plan. China is exploring the technical path of Chinese solutions, accelerating cross-industry collaboration, and promoting testing and demonstration. Since 2021, important documents such as *Application Management Specifications (Trial)* and *Several Provisions on Automotive Data Security Management (Draft for Comments)* have been adopted to support the safe development of the ICV industry. From January to October 2021, the penetration rate of L2-level intelligent connected passenger vehicles will exceed 20%, and the penetration rate in new energy vehicles will be as high as 30% (National ICV & China SAE, 2021).

Electrification Campaign

It can be seen that we have just experienced a battle of electrification of automobiles in the past five years. Traditional cars are slowly being replaced by electric vehicles, and this battle is not over yet.

US could have up to 35 million electric vehicles on roads by 2030 according to a report by smart electric power alliance. In China, the number of new energy vehicles will reach 7.84 million in 2021, accounting for 2.60% of the total number of vehicles, an increase of 2.92 million or 59.25% over 2020. Among them, there are 6.4 million pure electric vehicles, accounting for 81.63% of the total number of new energy vehicles. In 2021, 2.95 million new energy vehicles will be newly registered

nationwide, accounting for 11.25% of the total number of newly registered vehicles, an increase of 1.78 million or 151.61% over the previous year (The Ministry of Public Security of China, 2022).

In summary, how could the shared mobility system with connected and autonomous vehicles be defined? From a high-level overview, this complex system can be summarized with the following definition: the shared mobility system with connected and autonomous vehicles (CAVs) is made up of the **users** who use/interact/cooperate with **city infrastructures** and **CAVs technologies** on **shared mobility system** to move efficiently and optimally according to 3 main criteria (efficiency/energy-consumption/safety) for personal or economic goals. Figure 1-3 gives a diagram of this shared mobility system with a set of existing researches dedicated to the use, improvement, management, and modeling of the four key domains: city infrastructures (built environment, R5G, connected infrastructures, road signs and road markings, adaptive infrastructures, etc.), the users (demand prediction, human factors, cognitive model of behaviors visibility and perception, H/M Interaction and ergonomics, etc.), shared mobility system (optimization of the system, connected and cooperative systems, dispatching strategies, MaaS, incentive mechanisms, etc.), and technologies (cyber-security, autonomous/automated vehicles, sensors and environment perception, path planning and copilot, operating safety, mixed traffic management, etc.). Obviously, these four domains have strong interactions and dependency with each other. The studies on each domain aim to optimize the shared mobility system with respect to three key issues (efficiency, energy-consumption, and mobility). The research results could provide the decision makers with policy implications for a low-carbon transport and help the society better understand how the shared mobility services with CAVs should be developed in the future.

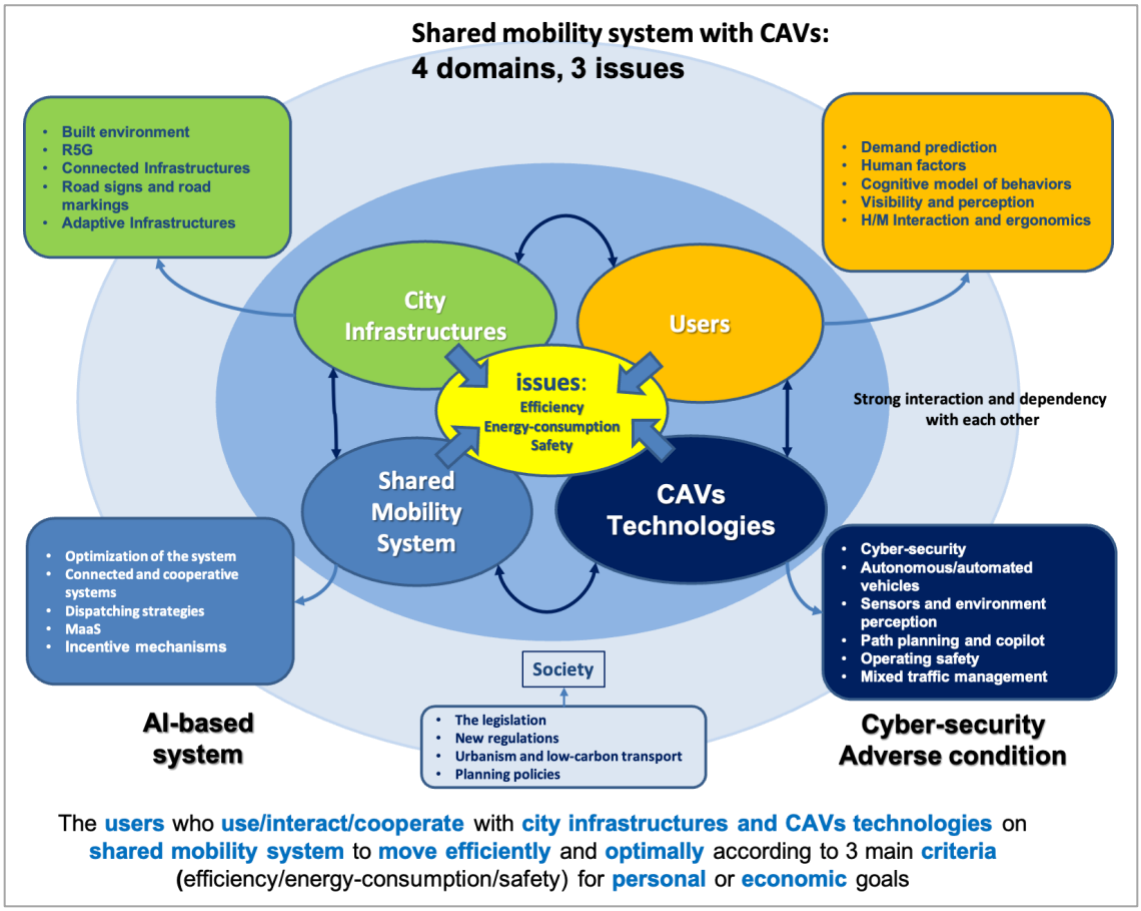

Figure 1-3 A diagram illustration of shared mobility system with CAVs
[Source: modified from (Gruyer et al., 2021) in Gustave Eiffel University]

Developing low-carbon cities and low-carbon transportation is crucial to achieve carbon neutrality worldwide. Shared mobility is one possible and effective way to reduce the adverse effects of transportation with respect to air pollution, energy consumption, and congestion in urban areas. In the context of the three major revolutions in the future, the combination of shared mobility and connected and automated vehicles will bring earth-shaking changes, not only for the automobile industry, but also for human travel in the future. They have the potential to provide an efficient and convenient complementary service to existing mobility solutions in urban areas, however, if not properly regulated, they may also drive-up congestion impacting the overall performance of mobility systems (Audenhove et al., 2020). The motivation of this study is to provide a systematic framework for the shared mobility system. The proposed shared mobility system could help improve ridesplitting service to build a low carbon transport, which could incorporate CAVs for the future mobility to provide a forward-looking reference for transportation network companies and the government

to better understand and manage future mobility trends.

1.2 Research questions and methodologies

As mentioned in the previous section, the shared mobility system with CAVs is made up of **users** who use/interact/cooperate with **city infrastructures** and **CAVs technologies** on **ridesourcing system** to move efficiently and optimally according to 3 main criteria (efficiency/energy-consumption/safety) for personal or economic goals. This dissertation follows the proposed framework (seen from Figure 1-3) and further proposes 4 research questions in the four domains. The detailed research questions and corresponding research objectives can be summarized as shown in Figure 1-4:

Domain 1: City infrastructures

Research question 1: What are the factors which influence the ridesplitting service?

Research objective 1: Exploring nonlinear effects of the built environment on ridesplitting service

Domain 2: Users

Research question 2: How to improve the ridesourcing demand prediction using artificial intelligent algorithms?

Research objective 2: Improving the demand prediction of ridesourcing services with an Optimized Spatiotemporal Encoder-Decoder Neural Network

Domain 3: Ridesourcing system

Research question 3: How to model and optimize the ridesourcing system?

Research objective 3: Optimizing ridesourcing system based on a shareability network on a city scale

Domain 4: CAVs technologies

Research question 4: What are the Impacts of Cyber Attacks on CAVs?

Research objective 4: Proposing a resilient and robust control strategy for connected and autonomous vehicles to resist the threat of cyberattacks

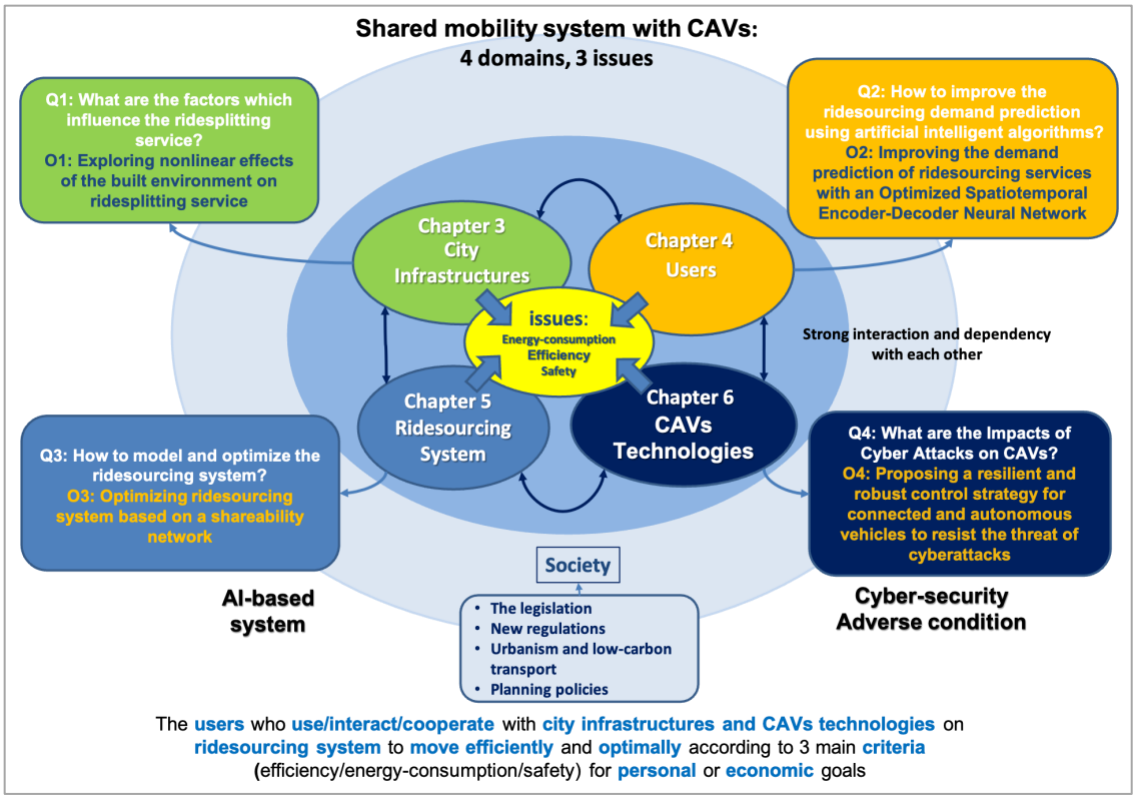

Figure 1-4 The research framework and research questions of the dissertation

The work of this study focuses on the thriving ridesourcing service, one kind of shared mobility service. This study aims to propose an optimization framework for the shared mobility system (SMS) and help decision makers better understand how the shared mobility services including potential CAVs will develop in the future. This study aims to answer the above 4 research questions in the proposed framework as shown in Figure 1-4. First, we explore the influencing factors on the ridesplitting service. Then we propose a novel ridesourcing demand prediction framework based on artificial intelligence algorithms. Moreover, we optimize the ridesourcing system based on a shareability network and evaluate the gap between the potential and actual level of ridesplitting. Finally, we explore how cyberattacks work on CAVs and propose a resilient and robust control strategy (RRCS) against cyberattacks in anticipation of applying the proposed models and solutions to CAVs. Figure 1-5 shows the components and their relationships in a typical ridesourcing system. There are three main components: passenger side, vehicle side and platform side. 4 research questions are also presented in Figure 1-5. Specific contributions of the 4 research questions are shown in section 1.3.

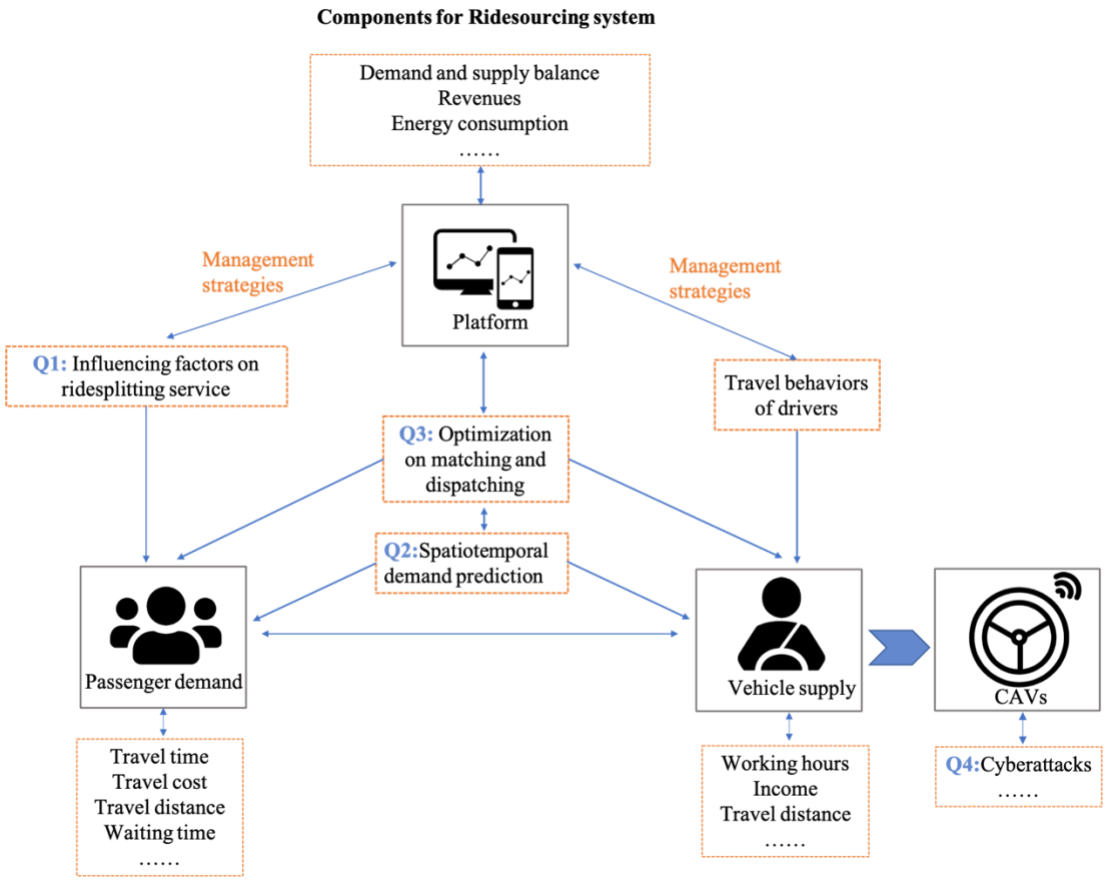

Figure 1-5: The components of a typical ridesourcing system
[Source: modified from (Wang & Yang, 2019)]

1.3 Major contributions

In this section, we resume the major contributions of this dissertation. To answer the above listed research questions, the following contributions were achieved:

What are the factors which influence the ridesplitting service?

In chapter 3, we answer this research question. The main contributions in this chapter can be summarized as follows: we use a machine learning method, gradient boosting decision tree (GBDT) model, to identify the important features of the built environment at the origins and destinations of ridesplitting services. We explore the nonlinear relationship between the ridesplitting service and key explanatory variables, which could provide insightful results to better understand how the built environment, demographic factors and travel time impact ridesplitting services. Partial dependence plots could provide policy implications for the shared mobility system to improve the

ridesplitting service.

How to improve the ridesourcing demand prediction using artificial intelligent algorithms?

In chapter 4, we answer this research question. The main contributions in this chapter can be summarized as follows: we propose a novel ridesourcing demand prediction framework. We use a combination of a graph convolutional network and a read-first long short-term memory network and a dynamic spatiotemporal attention mechanism. The experimental results show that the proposed framework outperforms state-of-the-art models for both single-step demand prediction and multi-step prediction, which demonstrate the effectiveness of the proposed framework.

How to model and optimize the ridesourcing system?

In chapter 5, we answered this research question. The main contributions in this chapter can be summarized as follows: we optimize the ridesourcing system on a city scale based on a shareability network and evaluate the gap between the potential and actual level of ridesplitting. The proposed shared mobility system could help improve ridesplitting service to build a low carbon transport, which could incorporate CAVs for the future mobility to provide a forward-looking reference for transportation network companies and the government.

What are the Impacts of Cyber Attacks on CAVs?

In chapter 6, we answered this research question. The main contributions in this chapter can be summarized as follows: we explore how cyberattacks work on CAVs and propose a resilient and robust control strategy (RRCS) against cyberattacks in anticipation of applying the proposed models and solutions to CAVs. This could help traffic flow under cyberattacks restore the stability and enhance the security of CAVs.

1.4 Dissertation Organization

The dissertation is organized as follows, as shown in Figure 1-6: following this overview chapter, a thorough literature review of literature is provided. The literature review covers the state-of-the-art researches related to ridesourcing services; which followed by a summarized review for the implemented and research studies for the

ridesourcing services in a connected and automated environment in the future. Chapter 3 investigates the influencing factors of ridesplitting service using a machine learning algorithm. Chapter 4 proposes a novel ridesourcing demand prediction framework, the optimized spatiotemporal encoder-decoder neural network (O-STEDN) to improve the prediction accuracy and balance demand and supply. Chapter 5 aims to optimize the ridesourcing services based on a shareability network and explore the potential on the ridesplitting service. Chapter 6 explores the impacts of cyberattacks on mixed traffic in a connected and autonomous environment. Finally, chapter 7 concludes the research efforts, findings, and future perspectives of this work.

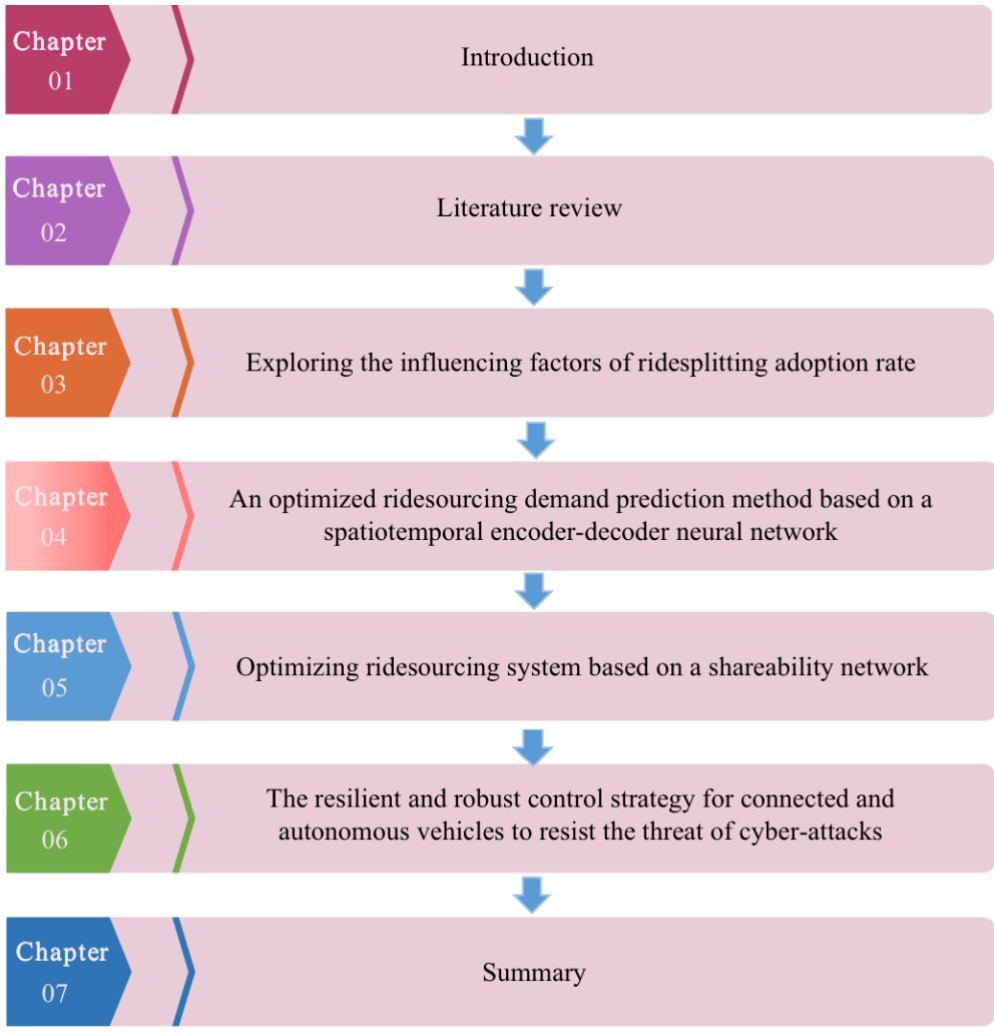

Figure 1-6 The organization of the dissertation

Chapter 2 Literature Review

HIGHLIGHTS

1) The general visual analyses of the existing literature review
2) The state-of-the-art literature review in the research topics
3) The interesting findings in the existing literature review
4) The research gap to be addressed in the research topics

2.1 General

We use the VOS viewer software and Web of Science, a bibliographic database file, to visualize the network map of the existing literature review. We look for articles with subject headings containing the following keywords: connected and automated vehicles, ridesourcing, ridesplitting and ridesharing to look for the articles. 4731 references are selected to make the further analysis and visual maps. It can be seen that there are 4 heat clusters in the network map, as shown in Figure 2-1.

Cluster 1: demand responsive transport, smart mobility, public transport, travel, transit, autonomous vehicles, urban mobility, …

The studies in cluster 1 explore the on-demand mobility services with autonomous vehicles from a global perspective.

Cluster 2: ridesharing, behavior, adoption, service, preferences, automated vehicle…

The studies in cluster 2 focus on the travel behavior analysis of ridesharing services, such as adoption rate and preferences.

Cluster 3: optimization, demand, simulation, urban areas, operations…

The studies in cluster 3 focus on the optimization and simulation of transportation services operation. Besides, demand management is a very important research hotspot in the optimization system.

Cluster 4: impacts, ridesourcing, connected vehicles, autonomous vehicle, transportation system...

The studies in cluster 4 focus on the two aspects. On the one hand, they want to

explore the impacts of ridesharing services with connected and autonomous vehicles in ideal conditions. On the other hand, they want to explore the impacts on mixed traffic with connected and automated vehicles in adverse conditions.

We can find more mainstream keywords: optimization, demand, behavior, impacts, adoption and transportation system, etc., as shown in the overlay map Figure 2-2 and the heat map Figure 2-3.

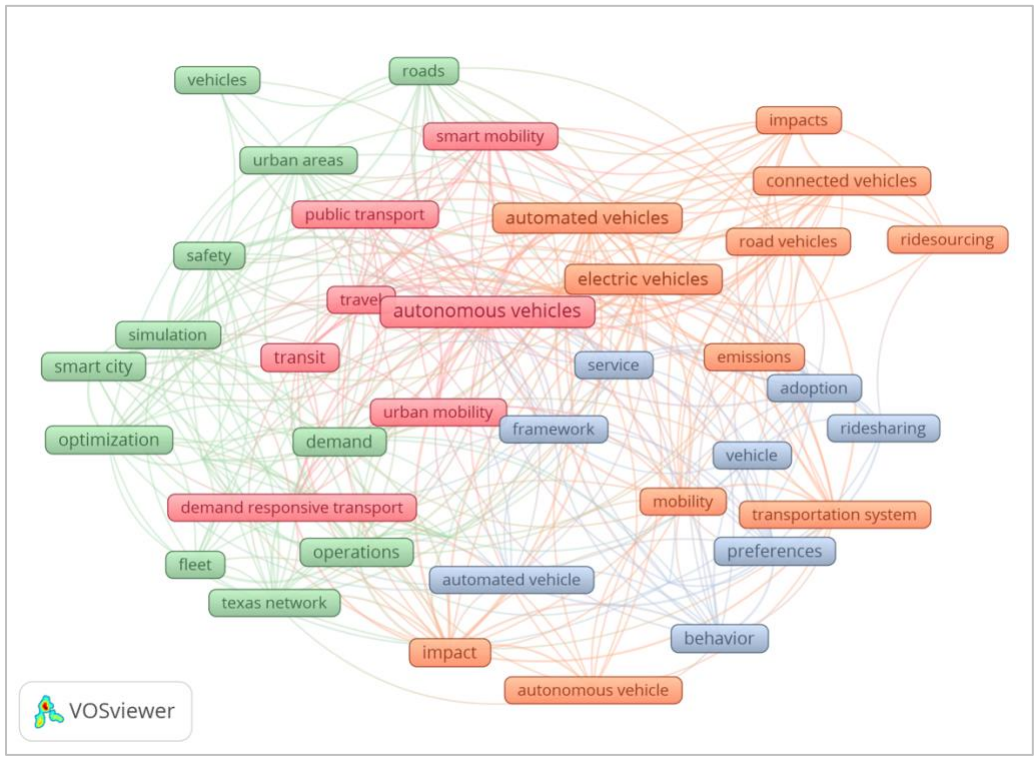

Figure 2-1 The network map of the keywords of related literature review

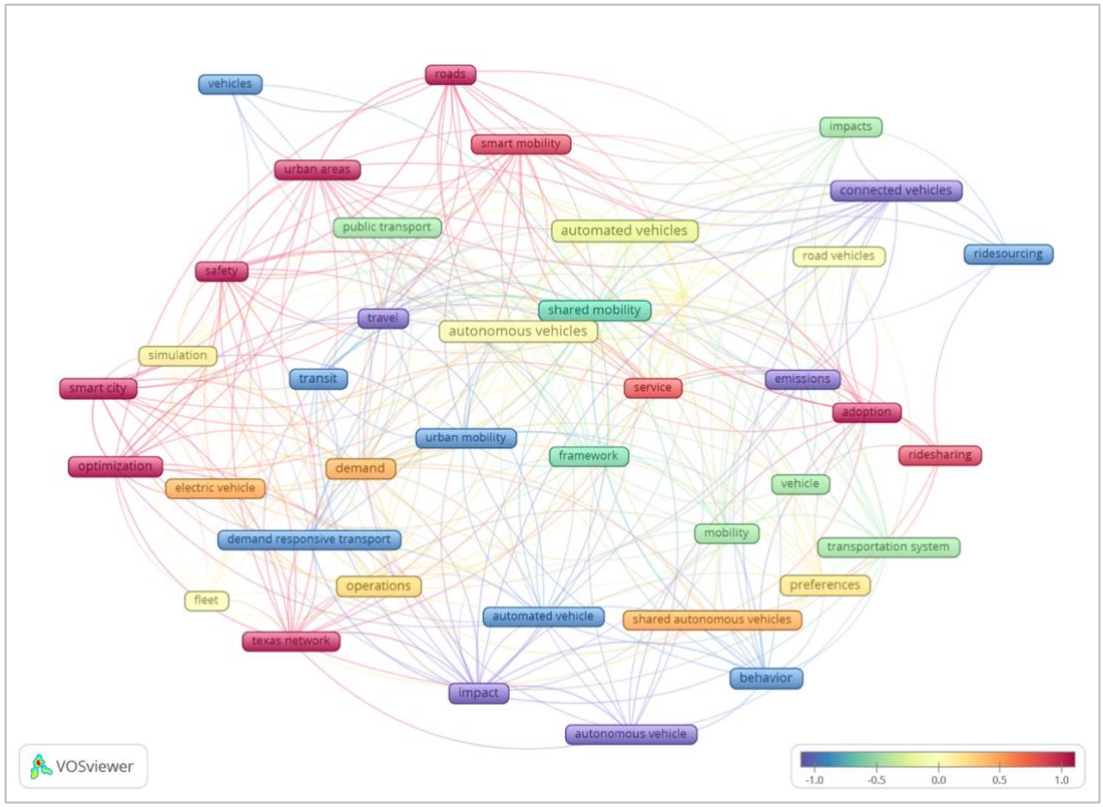

Figure 2-2 The overlay map of the keywords of related literature review

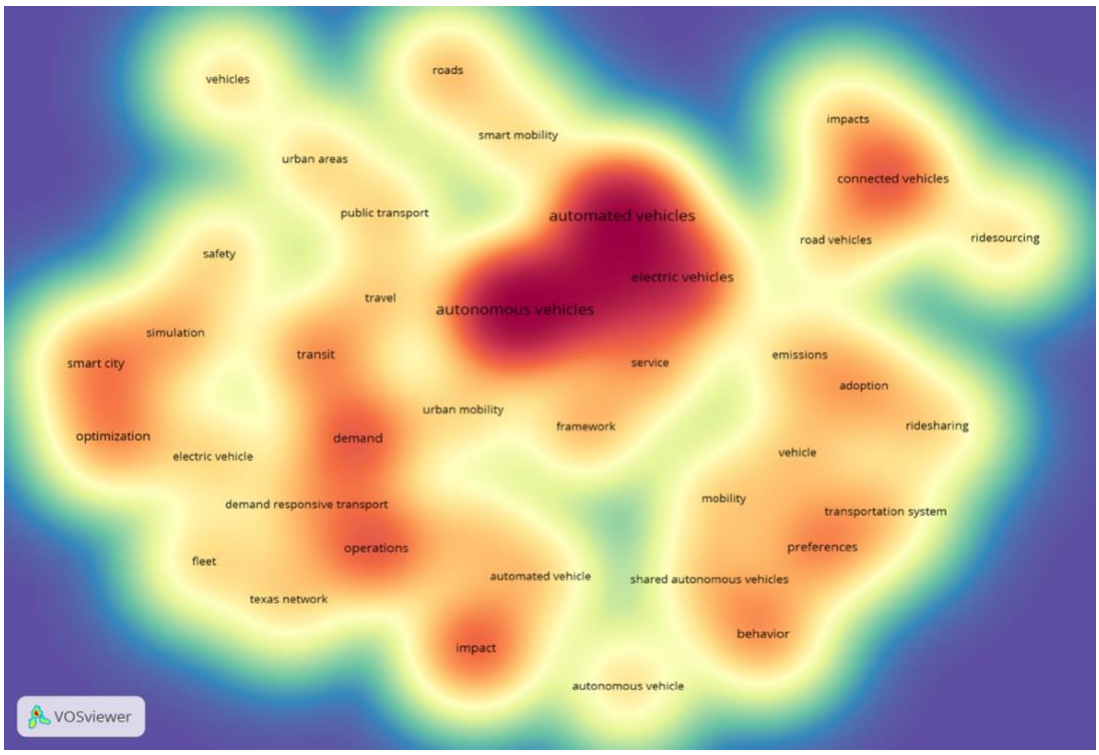

Figure 2-3 The heat map of the keywords of related literature review

In summary, we can synthesize the existing references into four mainstream research topics, which are interrelated to each other. Detailed literature review in every

research topic is described in the remainder of this chapter.

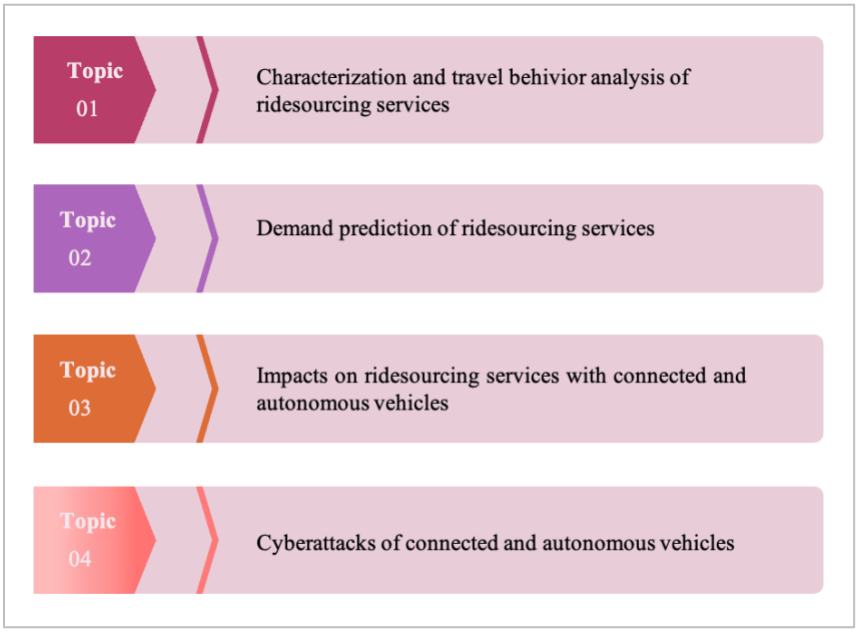

Figure 2-4 Synthesis of the literature review

2.2 Influencing factors of ridesplitting adoption rate

2.2.1 Built environment features

Many studies that identify the relationship between the built environment and travel behaviors attract people's attention because the findings can be used to design our built environment better and thus make the whole transportation system more efficient. In these studies that are published in mainstream academic journals, the terms used to reflect built environment features often start with a "D". Cervero and Kockelman (1997) proposed the initial "three Ds": density (e.g., population), diversity (e.g., land use mixture), and design (e.g., road density or percentage of 4-way intersections). These features were extended to the "five Ds" by adding destination accessibility and distance to transit (Ewing & Cervero, 2001, 2010). Demand management (e.g., dynamic parking charges) is the sixth D, and demographics is the seventh D (Ewing & Cervero, 2010). Many studies that identify the relationship between the built environment and travel behaviors attract people's attention because the findings can be used to design our built environment better and thus make the whole transportation system more efficient.

2.2.2 The influence factors of travel behaviors

We summarized the literature to show the different effects of built environment features on various travel behaviors, which can be classified by different traffic modes, as shown in Table 2-1.

For rails and metros, Durning and Townsend (2015) find that population density, intersection density, and three main land use ratios, industrial/commercial/residential ratios, have significant positive associations with the ridership of rapid rail transit. Ding et al. (2019) apply a GBDT model and show that the number of bus stops, compact and mixed land use development, and car ownership play a key role in determining station-level Metrorail ridership. With respect to buses, Chakour and Eluru (2016) find that transit facilities, the presence of parks and public transport services have a positive effect on ridership, while the presence of highways has a negative effect. For bikes, El-Assi et al. (2017) identify that network intersection density and bicycle infrastructure, such as bike lanes and path situations, have significant effects on bike-sharing demands. For walking, Tao et al. (2020) confirm that job density, population density, land use diversity, and pedestrian road density have strong nonlinear relationships with walking distance to transit. For private vehicles, Ding et al. (2018) identify the strong nonlinear relationship between driving distance and built environment factors, as well as demographics in Oslo.

For ridesourcing, Yan et al. (2020) find that socioeconomic and demographic variables, travel impedance, built environment characteristics, and transit-related factors have strong correlations with the ridesourcing demand in Chicago. Sabouri et al. (2020) reveal that Uber demand is positively correlated with the land use mix or entropy, total population and employment, activity density, and transit stop density of a census block group. In addition, intersection density and destination accessibility have negative impacts on Uber demand. Yu and Peng (2019) identify that there are strong relationships between ridesourcing demand and built environment factors such as density, land use, infrastructure, and transit accessibility in Austin, Texas, using a geographically weighted Poisson regression model.

Table 2-1 Literature review exploring the relationship between built environment and travel behaviors in different traffic modes

Traffic modes	Travel behaviors	Methodologies

Rail/Metro	Ridership of rail rapid transit systems (Durning & Townsend, 2015)	Bootstrapped ordinary least squares regression model
	Metro ridership at station level (Ding et al., 2019)	GBDT
Bus	Bus ridership in Montreal (Chakour & Eluru, 2016)	Ordered regression model
Bike	Bike sharing demand in Toronto (El-Assi et al., 2017)	Ordinary Least Square (OLS) regression model
Walking	Walking distance to transit (Tao et al., 2020)	GBDT
Private vehicles	Driving distance of private vehicles in Oslo (Ding et al., 2018)	GBDT
Ridesourcing	The number of OD ridesourcing ridership in Chicago (Yan et al., 2020)	Random forest model
	Uber demand (Sabouri et al., 2020)	Mixed linear regression model
	Spatial variation of ridesourcing demand in Austin, Texas (Yu & Peng, 2019)	Geographically Weighted Poisson regression model

In summary, the above studies have confirmed the strong relationship between the built environment and travel behaviors for different traffic modes, namely rail and metro, bus, bike, walking, private vehicles and ridesourcing services. However, to the best of our knowledge, there is no existing research exploring the relationship between ridesplitting and the built environment, which should be investigated. By exploring the relationship between the built environment and ridesplitting, urban planners can better understand how the features of the built environment impact ridesplitting and improve traffic efficiency by way of a more reasonable design and planning of built environment.

Most studies use statistical modeling to explore the relationship between the built environment and travel behaviors, whereas it should be noted that modeling is just one way to explore the relationship. The widely used models can be summarized as follows: ordinary least squares (OLS) models; discrete choice models, such as logit models and probit models; and geographically weighted regression (GWR) models.

For example, Durning and Townsend (2015) applied a bootstrapped OLS regression model to identify the association between station boardings of the Canadian rapid rail transit and 44 socioeconomic, built environment, and system attributes. Alemi et al. (2018) used a binomial logit model to analyze the key factors, such as the built environment and travel distance, affecting the travel demand of ridesourcing services using comprehensive survey data on 2400 residents in California. Choudhury et al. (2018) applied a nested logit model using data from the Stated Preference (SP) survey in Lisbon, Portugal to analyze the influencing factors of travelers' departure times and ridesharing mode choices. However, OLS and discrete choice models can be used for only global estimations that do not consider spatial heterogeneity (Brunsdon et al., 1996).

The GWR is a regression model that uses local estimation rather than global estimation to address spatially nonstationary processes. Specifically, GWR involves the generation of a regression for each location rather than using a global regression for the entire research area. GWR models have been used to analyze the relationship between the built environment and travel behaviors. For example, Torun et al. (2020) applied a logistic GWR model to explore how urban form factors and sociodemographic factors impact transportation walking. However, this kind of model assumes a prior hypothesis of a particular function, such as a linear or log linear relationship, which could lead to modeling biases.

Due to the development of new technology for big data analyses, increasingly more intelligent algorithms are used to explore the characterization of travel behaviors. In recent years, machine learning models such as GBDT models have performed well when applied to explore the characterization of different transport modes. Friedman developed the first GBDT model, which could provide highly robust, outstanding, and interpretable regression and classification problems (Friedman, 2001). (Gan et al., 2020) used a GBDT model to examine the nonlinear effects of the built environment on OD metro ridership in Nanjing, China; this model performed better than the multiplicative model. (Ding et al., 2018) employed a GBDT model to investigate the relationship between the built environment and driving distance in Oslo. GBDT is a machine learning method without a prior hypothesis of a particular function and can predict the target variable more accurately, even the nonlinear relationships with explanatory variables.

2.2.3 Summary

The existing literature has proven that the built environment has a strong relationship with travel behaviors (Ding et al., 2019; Ding et al., 2018; Durning & Townsend, 2015; Tao et al., 2020). However, to the best of our knowledge, no existing research has investigated how the built environment impacts ridesplitting services. To fill this gap, the aim of this research part is to explore the relationship between the built environment and origin-destination (OD) ridesplitting ratio.

2.3 Demand prediction

2.3.1 Spatial-Temporal Traffic Prediction

The spatial-temporal traffic prediction problem plays an important role in the transportation field. The forecasting objectives include traffic volumes (Song et al., 2018), congestion levels (Wen et al., 2019), travel speeds (Zhang et al., 2021), travel times (Zhang & Haghani, 2015), air pollution (Idir et al., 2021; B. Zhang et al., 2021) and traffic demand (Du et al., 2020; Geng et al., 2019; Y. Liu et al., 2019; Zhao et al., 2019) across the dimensions of time and space. For traffic demand prediction, different traffic modes have their own characteristics, such as bus ridership (Chakour & Eluru, 2016), metro ridership(Ding et al., 2019; Gan et al., 2020), bikes (El-Assi et al., 2017) and ridesourcing demand (Tu et al., 2021; Yan et al., 2020). Ridesourcing demand prediction is a key and feasible way to optimize a dispatching system and reach the great potential of ridesourcing services (Tu et al., 2019).

2.3.2 Methodologies for Spatial-Temporal Traffic Prediction

According to the characteristics of the existing traffic demand forecasting research, we can basically divide the available techniques into two categories: traditional time series methods and machine learning approaches.

Traditional spatial-temporal demand prediction models

Traditional demand prediction models include the historical model (HA) and autoregressive integrated moving average (ARIMA) model (L. Liu et al., 2019; Williams & Hoel, 2003). The HA uses the average value of the historical data at the

same time every day as the predicted value at the same time instant in the future prediction task (L. Liu et al., 2019). ARIMA is a traditional time series prediction method that combines a moving average and autoregressive components to model historical time series data, and its variants have been widely used in traffic prediction tasks(Williams & Hoel, 2003). Recent studies have proven that the demand prediction task with time series is affected not only by the time dimension but also by the space dimension. However, traditional time series methods are based on prior knowledge, theoretical assumptions, simple mathematical statistics and time series analyses. The challenges they face are the inability to extract the nonlinear characteristics of the input variables, the inability to extract the spatial and temporal correlations among the input variables, and the difficulty of fully utilizing and learning the distribution characteristics and laws of the input data from the perspective of big data.

Traditional machine learning models for spatial-temporal demand prediction

Machine learning algorithms can make fuller use of historical data and obtain satisfactory performance through complex modeling and training processes. Compared with traditional time series forecasting methods, they can determine the correlations between complex input variables and thus exhibit better forecasting performance. According to statistics, machine learning methods can be divided into two important branches: traditional machine learning methods and deep learning methods. Traditional machine learning methods include eXtreme gradient boosting (XGBoost) (Shi et al., 2019), gradient boosting decision trees (GBDTs) (W. Wu et al., 2020), support vector machines (SVMs) (Sapankevych & Sankar, 2009), and multiple linear regression (MLR) (Shams et al., 2021), etc. (Castro-Neto et al., 2009; Zaki et al., 2020; Zhu et al., 2018). In demand prediction tasks, compared with traditional time series methods, traditional machine learning methods have achieved greater performance improvements(Castro-Neto et al., 2009; Sapankevych & Sankar, 2009; Shams et al., 2021; Shi et al., 2019; Z. Wu et al., 2020; Zaki et al., 2020; Zhu et al., 2018). However, by processing massive spatiotemporal data from non-Euclidean census tracts for multi-step ridesourcing demand prediction, traditional time series methods and traditional machine learning algorithms have encountered some problems (X. Chen et al., 2021; Chu et al., 2019; Du et al., 2020; Geng et al., 2019; Shu et al., 2020; Yao et al., 2018; Zhao et al., 2019).

Deep learning for spatial-temporal prediction models

In recent years, deep learning technology has performed well in dealing with regression problems. Recently, deep learning methods have become the main technology applied in related fields such as computer vision and natural language processing. This has also successfully prompted researchers to apply deep learning techniques to traffic prediction problems. Various neural networks based on back propagation algorithms are used to improve traffic demand forecasting performance. RNN, GRU, and LSTM are used to extract the time series features of input variables and have better prediction performance than traditional models (Kontou et al., 2020; C. Li et al., 2019; L. Liu et al., 2019; Liu & Shoji, 2019; Mackenzie et al., 2018; Z. Wang et al., 2020; Xu et al., 2017; C. Zhang et al., 2021). LSTM was used to predict taxi demand (Kontou et al., 2020; Wen et al., 2019). IA multilevel RNN (MLRNN) model combining the development of cluster-level and global-level prediction modules was proposed to extract intra- and inter-cluster features to achieve accurate taxi demand prediction(C. Zhang et al., 2021). However, if only LSTM is used to process the time series characteristics of demand data, the impact of spatial correlation on forecasting may be ignored (G. Chen et al., 2021; Chu et al., 2019; Du et al., 2020; Geng et al., 2019; Yao et al., 2018; Zhao et al., 2019).

To solve the problem encountered by LSTM, Yao et al. proposed a deep multiview spatial-temporal network (DMVST-Net) framework to simulate spatial and temporal relationships (Yao et al., 2018); that is, a CNN was used to extract the spatial correlations, and LSTM is used to model the correlations between future demand values and near-time points. Similar to the research on DMVST-Net, Chu et al. proposed a deep learning network called multiscale convolutional LSTM (MultiConvLSTM) that considers both time and spatial correlations to achieve more accurate predictions of future travel demand and on-demand traffic (Chu et al., 2019). The common problem with these methods is that they extract spatial correlation features through CNNs, but traditional CNNs deal with this issue in the context of Euclidean space and are not suitable for non-Euclidean spaces (Zhao et al., 2019). Regarding the spatial distribution of traffic demand, long-distance areas may have stronger correlations than neighboring areas (Du et al., 2020). Therefore, CNN-based processing of traffic demand data has great defects.

Acquiring complex spatial dependencies is a key problem in ridesourcing demand prediction. The traditional CNN can obtain local spatial features (Ke et al., 2018), but it can only be used in a Euclidean space, such as a picture or a regular grid (G. Chen et

al., 2021). An urban area network has the form of a graph rather than a two-dimensional grid, which means that a CNN model cannot reflect the complex topological structure of this network and thus cannot accurately capture spatial dependencies. Recently, the generalization of CNNs to GCNs, which can handle arbitrary graph-structured data, has received widespread attention (Defferrard et al., 2016; Kipf & Welling, 2016; Niepert et al., 2016; Z. Wu et al., 2020). GCN models have been successfully used in traffic prediction tasks, including ridesourcing demand prediction (Du et al., 2020; Geng et al., 2019; Guo et al., 2020; Ke et al., 2021; Z. Li et al., 2020; Yu et al., 2020; Zhang et al., 2019; Zhao et al., 2019). Geng et al. (2019) proposed a spatiotemporal multigraph convolution network (ST-MGCN), which encoded the non-Euclidean pairwise correlations among regions into multiple graphs, and then used an RNN and a GCN to model these correlations. Ke et al. (2021) proposed a Spatio-temporal encoder-decoder residual multi-graph convolutional network (ST-ED-RMGC), which uses RMGC to encode spatially dependent features, uses LSTM to encode temporal features, and finally uses RMGC as a decoder to predict the origin-destination ridesourcing demand at the next moment. Du et al. (2020) proposed a dynamic transition-based CNN (DTCNN), which is a novel dynamic transition-based GCN method and provides an effective method for traffic demand prediction. However, these studies did not consider the impact of the temporal and spatial characteristics of the input variables on the current prediction, and they focused only on the single-step prediction task for the next time period.

2.3.3 Summary

Ridesourcing demand prediction is a feasible way to increase these occupancy rates. The vehicles can be dispatched properly to decrease the idle time according to the demand prediction results. Then, passengers could also wait for less time when using ridesourcing services. Therefore, it is important to obtain high-accuracy ride-souring demand predictions for transportation network companies to balance demand and supply.

Existing studies related to traffic demand prediction have focused on single-step prediction for the next time period (L. Liu et al., 2019; Williams & Hoel, 2003). However, it is more beneficial for ridesourcing services to make multi-step demand predictions, which can help transportation network companies dispatch vehicles more properly in advance. In summary, existing studies focus on single-step prediction,

which not only limits the practical application value of the resultant model but also presents the problem of insufficient prediction ability. To fill these gaps, the primary objective of this research part is to propose a new ridesourcing demand prediction framework to improve the single-step and multi-step demand prediction.

2.4 Optimization on the ridesourcing services

2.4.1 Studies on ridesourcing services

The future landscape of urban mobility will be reshaped by shared mobility services and CAVs (Nazari et al., 2018). Shared mobility services and CAVs are gaining momentum in recent years (Greenblatt & Shaheen, 2015; Nazari et al., 2018). It is predicted that all vehicles will be autonomous by the middle of the century (Anderson et al., 2014). AVs are driverless and accordingly available at every time and every place (Vosooghi et al., 2019). People assume that CAVs will be more relevant to the "sharing-concept". In recent years, more and more researchers have gradually integrated CAVs into sharing services or shared autonomous vehicle (SAV) services. Meanwhile the widespread adoption of SAV services could provide benefits to society (Krueger et al., 2016).

Most studies on ridesourcing focus on three specific aspects: (1) identifying the characteristics of passengers who use ridesourcing services and their preferences (Nielsen et al., 2015; S. A. Shaheen et al., 2016; Wang et al., 2010); (2) exploring the impacts of ridesourcing services on passengers, such as waiting time (Hughes & MacKenzie, 2016; Rayle et al., 2014), drivers, such as income (Angrist et al., 2021; M. K. Chen et al., 2019; Hall et al., 2018), the environment (Kent, 2014), other traffic modes (Chan & Shaheen, 2012; Zhang & Zhang, 2018); and (3) optimizing ridesplitting operations, such as matching and dispatching strategies (Tang et al., 2019; Tu et al., 2019). The literature suggests that ridesourcing services have been increasingly important in the entire transportation system.

Four data sources have typically been used to research the problem of sharing a passenger ride: (a) survey data, (b) mobile phone data, (c) empirical data on taxis, and (d) empirical data on ridesourcing services collected directly from transportation network companies. Ridesourcing surveys mainly collect data through questionnaires, including intercept surveys (Handke & Jonuschat, 2012) and telephone surveys (Hara

Associates Inc., 2013); this method has several weaknesses, including the limited number of respondents who can be surveyed, the incomplete representation of the ridesourcing market, and the huge investment of time and resources. Mobile phone data refer to average daily origin-destination (OD) trips from mobile phone call detail records (Alexander & González, 2015); but the observations are recorded only when an individual interacts with his or her device, resulting in heterogeneous sampling frequencies and an incomplete picture of daily behavior across users, therefore the data lack full authenticity to assess the impacts of sharing a passenger ride. Some studies used empirical data on taxis to quantify the benefits of ridesplitting in New York (Alonso-Mora et al., 2017; Santi et al., 2014; Simonetto et al., 2019). These articles assume that all passengers using taxis are willing to use the ridesplitting service and that there is only one passenger in each ride. However, passengers using taxis are distinct from passengers using ridesourcing services. Taxi services are regarded as premium services. Passengers using taxis probably are not willing to use ridesplitting services because of the issues of time value and privacy. Furthermore, the average number of passengers per ride for taxis in New York was 1.6 in 2014 (King & Saldarriaga, 2017). Therefore, the actual passenger capacity is much larger than what is assumed in the two studies.

Few studies use empirical data on ridesourcing services to evaluate the impacts of ridesplitting because transportation network companies are reluctant to share their ridesourcing data with the public due to privacy protection. X. M. Chen et al. (2017) used empirical data from DiDi Chuxing to predict the ridesplitting choices of individual passengers. X. Chen et al. (2021) analyzed ridesplitting behaviors and the associated impact on multimodal mobility. However, these two studies do not investigate the potential of ridesplitting to evaluate the benefits.

2.4.2 Optimization models of ridesourcing services

The objectives of shared mobility-related models can be summarized as follows: (a) maximizing the number of ridesplitting trips, (b) minimizing the total travel time or minimizing the vehicle miles of all trips, and (c) maximizing the value saved by ridesplitting.

The maximum number of ridesplitting trips can ideally satisfy passengers' trip demand with a minimum fleet size. Two shared trips can be served by a single vehicle instead of two. Thus, shared trips can be used to reduce the required fleet size to

mitigate traffic congestion for society. This also benefits passengers by enhancing their mobility. Generally, the cost is proportional to the travel time or vehicle miles. Therefore, an optimization objective is proposed for the purpose of minimizing the cost to society.

The Senseable City Laboratory of MIT uses empirical taxi data to quantify the benefits of ridesplitting in the future based on the above two objectives (Santi et al., 2014; Vazifeh et al., 2018). However, the delay experienced by passengers is not included in the objective function.

Maximizing the cost saved by ridesplitting is considered from two aspects: on the one hand, we want to minimize the total time and travel distance of all trips from the perspective of the ridesplitting system. On the other hand, the optimal solution for the whole society may not necessarily be optimal for individual passengers, since the travel time is the time actually spent in the vehicle and does not include delays caused by detours. This objective takes the value of the delay experienced by individual passengers into consideration to guarantee the rights of passengers when using the ridesplitting service. Kleiner et al. (2011) presented an objective of maximizing saved value by carpooling while simultaneously considering the tradeoff of a tolerable delay for commuters due to the detour distance. However, as demonstrated in the definitions we mentioned above, they focus on the ridesharing for commuters rather than ridesplitting.

Problems related to sharing a passenger ride can be regarded as "pick-up and delivery" problems with desired time windows in which multi-vehicles and multi-passengers should be matched efficiently (Cortés et al., 2010; Ropke et al., 2007). Traditionally, such problems are solved by complex mathematical programming with a large number of variables and constraints. This method can be used to address problems with only a few thousand vehicles and trips at most (Baker & Ayechew, 2003; Laporte, 1992); thus, it is not applicable for the hundreds of thousands of trips and vehicles on a large city scale. Ma et al. (2013) take the first step toward solving the taxi ridesharing problem with dynamic large scales. The Senseable City Laboratory of MIT (Santi et al., 2014) proposes an efficient "shareability network" method that translates spatiotemporal sharing problems into a graph-theoretic framework to realize shared taxi services. Furthermore, these researchers address the minimum fleet problem using a "vehicle sharing network" (Vazifeh et al., 2018).

The problem of maximum matching in ridesharing is NP hard. There are two main

algorithms for solving NP hard problems: exact algorithms and approximation algorithms. Exact algorithms, such as branch-and-bound algorithms (Ignall & Schrage, 1965), branch-and-cut methods (Cortés et al., 2010; Ropke et al., 2007), and cut-and-price algorithms (Fukasawa et al., 2006), can be used to solve the ridesharing problem only for small-scale trip requests due to computational challenges. There are many approximation algorithms:1) classical heuristic algorithms, such as saving algorithm (Clarke & Wright, 1964), sweep algorithm (Gillett & Miller, 1974), cluster fist-route second (Fisher & Jaikumar, 1981), and petal algorithms (Renaud et al., 1996); 2) metaheuristic algorithms such as local search, population search, learning mechanisms, and the hybridizations. Local search algorithms include simulated annealing algorithms (Osman, 1993), deterministic annealing algorithms (Groër et al., 2010), tabu search algorithms (Braekers et al., 2014; Kirchler & Calvo, 2013), iterated local search algorithms(Nogueira et al., 2018; Penna et al., 2013), and variable neighborhood search algorithms (Li et al., 2016; Parragh et al., 2010). Population search algorithms include genetic algorithms (Baker & Ayechew, 2003), scatter search and path relinking algorithms (Yoshizaki, 2009). Learning mechanisms include ant colony optimization (Dorigo et al., 2006) and machine learning algorithms (Accorsi et al., 2022). Hybridizations refer to the combination of above metaheuristic algorithms, such as the combination of local search and population search (Santos & Mariani, 2006).

2.4.3 Impacts of connected and autonomous vehicles on the shared mobility

(1) Impacts on economic costs: Clements and Kockelman (2017) synthesized the impact of autonomous vehicles on 13 major industries in the United States, and the results showed that it is estimated that the United States could save 1.2 trillion US dollars per year. Duncan (2011) sought to quantify the potential travel cost savings for people using shared autonomous vehicles, and the results showed that the cost could be decreased significantly.

(2) Impacts on traffic behavior and land use: Hawkins and Nurul Habib (2019) found that the emergence of autonomous vehicles will not only affect the transportation system, but also affect the future pattern of land use development. Davidson and Spinoulas (2016) pointed out that ridesplitting services could significantly improve network efficiency.

(3) Impacts on traffic congestion, fuel consumption and private car ownership: Maciejewski and Bischoff (2016) explored the impact of autonomous taxis in the city on traffic congestion based on the analysis of the Berlin area using MATSim. It is founded that the autonomous fleets have a positive impact on urban traffic if the road capacity is increased. However, without an increase in road capacity, autonomous vehicles should not be introduced on a large scale, as the induced additional traffic flow would exacerbate traffic congestion. Y. Chen et al. (2019) developed an analytical framework to quantify the impact of autonomous vehicles on fuel consumption in the United States, and the results showed that the percentage of the fuel saving could be 45% in the optimistic case, but the fuel consumption could be increased by 30% in the pessimistic case.

(4) Impacts on the environment: Fagnant and Kockelman (2014) used Chester and Horvath to estimate that after using SAV vehicles, the emissions of VOC and CO decreased significantly, and the emissions of PM10 and GHG also decreased, but not significantly. Firnkorn and Müller (2011) explored the environmental impact of the car-sharing system, Car2go, in Ulm, Germany. The result showed that CO2 emissions could be reduced significantly.

2.4.4 Summary

In summary, ridesourcing is an attractive option for many travelers without their own vehicles. However, there are some debates claiming that on-demand ridesourcing services could increase congestion and pollution (Union of Concerned Scientists, 2020).

However, ridesourcing service has also triggered a seismic shift towards shared mobility service. Ridesplitting, a new shared mobility service, is a more sustainable travel mode for improving traffic efficiency and reducing traffic congestion and air pollution problems. Policy makers have realized the benefits of ridesplitting services and encouraged ridesourcing companies to launch ridesplitting services for passengers.

Previous studies on the potential of ridesourcing that used observed data are quite limited, and empirical research on ridesplitting is even sparser because of the lack of data. To our knowledge, this research part is one of the first investigations to quantify the actual level and potential of ridesplitting on a city scale. This research part aims to explore the potential of ridesplitting for the future mobility system. The findings can help reveal the potential benefits of ridesplitting, which will be crucial for

transportation management agencies and ridesourcing companies in developing sensible policies to promote the use of ridesplitting services.

2.5 Impacts of cyberattacks on connected and autonomous vehicles

2.5.1 Types of cyberattacks on connected and autonomous vehicles

Cyberattacks on vehicles can be classified into different types according to different perspectives. From the perspective of the position of cyberattacks, cyberattacks can be classified into in-vehicle cyberattacks and inter-vehicle cyberattacks (Aliwa et al., 2021; Khan et al., 2020; Mousavinejad et al., 2019; P. Wang et al., 2020). The former injects malicious information into the in-vehicle networks that could disrupt the function of CAN (Controller Area Network), On-board diagnostics (OBD), Telematics Box (T-box), and Electric Control Units (ECUs). And the latter is intended to disable the vehicular wireless communication (i.e., Vehicle-to-Everything or V2V) information to influence vehicles' behaviors through DSRC (Dedicated Short-Range Communications) and/or LTE-V (Long-Term Evolution-Vehicle).

Some previous studies explored the impacts of cyberattacks from the perspective of in-vehicle. For example, Palomar et al. (2012) successfully prevented the propagation of false warning events in VANETs by applying certificates and Proof-of-Work (POW) systems. To deal with the serious threat to vehicle safety and driver privacy caused by cyberattacks, Liu et al. (2017) summarized the previous methods of cyberattacks and proposed the countermeasures of in-vehicle networks. Asuquo et al. (2018) introduces the privacy enhancement technology and encryption method to provide location privacy in the vehicle and mobile networks. Taylor et al. (2018) combined recurrent neural network and multivariate Markov chain to develop anomaly detector for identifying cyberattacks and malicious traffic, and designed an attack framework to verify the effectiveness of the detectors through simulation. Tariq et al. (2020) proposed CAN Bus Message Attack Detection Framework (CAN-ADF), which can generate, detect and evaluate comprehensive exceptions for a CAN bus. Moreover, the real vehicle design experiments show that the proposed method has high detection accuracy. Katragadda et al. (2020) designed a sequence mining approach to detect low-

rate injection attacks in Control Area Network (CAN), which can detect sophisticated injection attacks and supply real-time intrusion detection for the vehicle.

Besides, the researchers also focus on the inter-vehicle cyberattacks. They pay attention to the impacts of cyberattacks on CAV platoons and traffic flow by using different vehicle control models based on vehicle dynamics modeling. This will help us understand the impact mechanism of cyberattacks on traffic flow evolution, and lay a foundation for us to design response strategies (Khattak et al., 2021; Li et al., 2018; Noei et al., 2021; P. Wang et al., 2020).

This research part focuses on the inter-vehicle cyberattacks, which can be further divided into three kinds of categories according to the consequences on the vehicles: bogus messages, replay/delay messages and collusion attacks, as shown in Table 2-2 (P. Wang et al., 2020).

Table 2-2 Cyberattack classification

Category	Description
Bogus messages	These attacks could transmit bogus messages such as erroneous velocity or position through masquerading a legal vehicle or tampering a piece of messages
Replay/delay	Due to the jammed communication channel or being injected with a replay virus, the communication data is fraudulently repeated or delayed
Collusion attacks	Two or more vehicles are attacked simultaneously by cooperatively adversaries

2.5.2 Modeling of cyberattacks on connected and autonomous vehicles

In order to effectively resist to cyberattacks and improve traffic safety performance, scholars have conducted a lot of researches on cyberattacks from different perspectives. Alipour-Fanid et al. (2017) investigated the influence of mobile reactive jamming attacks on the stability of CACC platoon, and the results showed that the attack will reduce the stability of traffic flow system. P. Wang et al. (2018) proposed an extended car-following model to describe connected traffic dynamics under

cyberattacks, the results showed that the proposed model will help to avoid collision and reduce traffic congestion under the influence of cyberattacks. Li et al. (2018) studied and evaluated the impact of slight cyberattacks on CAV longitudinal security through modeling and simulation. The results showed that the impact of communication location attacks is worse than that of speed attacks. In addition, the impact of cyberattacks in vehicle acceleration phase is more severe and dangerous than that in vehicle deceleration phase. P. Wang et al. (2020) proposed a bi-bi-layer architecture composed of both a vehicle layer and a cyber layer to explore the impact of cyberattacks on CAV platoon safety and efficiency. Dong et al. (2020) proposed an evaluation framework to measure the impact of cyberattacks on traffic flow performance, and analyzed and studied the impact from the aspects of attack intensity, attack range and traffic demand through numerical simulation. Zhai and Wu (2021) designed a new continuous feedback controller based on lattice hydrodynamic model to suppress the impact of cyberattacks, and the effectiveness of the controller in dealing with cyberattacks and reducing traffic congestion were analyzed and verified by stability analysis and numerical simulation. Khattak et al. (2021) used an infrastructure-based communication platform to discuss the impact of cyberattacks on the safety and stability of connected and automated vehicle platoons under lane changes. Noei et al. (2021) proposed a traffic microsimulation tool that can simulate conventional, automated, and connected and automated vehicles in a platoon under fault, failure, and cyberattack with optimized accuracy and simulation speed to maximize throughput and without compromising safety or string stability.

2.5.3 Summary

Scholars have also carried out some researches to demonstrate the great potential benefits of CAVs (Li et al., 2013; Rios-Torres & Malikopoulos, 2016; Sukuvaara & Nurmi, 2009; Van Arem et al., 2006; Zhao & Sun, 2013). However, with the help of diverse and advanced communication technology, the “intelligent” information exchange between vehicles and the surrounding environment/world is realized all the time. So, such an open-access communication environment system increases the risk of vehicles being exposed to cyberattacks, which is an urgent and critical challenge to be solved. In order to effectively resist to cyberattacks and improve traffic safety

performance, scholars have conducted a lot of researches on cyberattacks from different perspectives.

Although some studies investigated the impact of cyberattacks and put forward the corresponding strategies, there are two important issues to be revealed:

- There are different types of vehicles on the actual road, such as cars, buses, trucks and so on, so the characteristics and performances of the different vehicles are also different. Therefore, it's an important problem to build a vehicle dynamics model for CAV in a mixed traffic flow considering cyberattacks.
- Some of the existing cyberattacks response strategies are formulated from the perspective of intrusion detection, privacy protection, etc., so when the cyberattacks have reached the vehicle level and produced negative effects, it will be an urgent problem to formulate the control strategy from the perspective of vehicle dynamics to resist the harmful threat brought by the cyberattacks.

.

Chapter 3 Exploring the influencing factors of ridesplitting adoption rate

HIGHLIGHTS

1) Built environment factors have strong non-linear effects on the ridesplitting ratio
2) Gradient Boosting Decision Trees model is used to analyze the effects.
3) Distance to the city center is the most important among built environment factors
4) Land use diversity and road density also have strong impacts on ridesplitting ratios
5) Non-linear thresholds of built environment factors are identified to guide the planning

3.1 Introduction

On-demand ridesourcing services, operated by transportation network companies, match passengers and drivers through intelligent mobile phone applications (Rayle et al., 2016). Ridesourcing services have become increasingly popular due to their convenience. Ridesplitting, one form of ridesourcing services, matches riders with similar routes to the same driver, such as "UberPool" and "Lyft Line" (S. Shaheen et al., 2016). There are some debates claiming that on-demand ridesourcing services could increase congestion and pollution (Union of Concerned Scientists, 2020). However, ridesplitting, a new shared mobility service, is a more sustainable travel mode for improving traffic efficiency and reducing traffic congestion and air pollution problems. Policy makers have realized the benefits of ridesplitting services and encouraged ridesourcing companies to launch ridesplitting services for passengers. For DiDi Chuxing, the number of passengers who choose ridesplitting services has continued to increase since its launch at the end of 2015. By the end of 2019, the cumulative number of users reached 2.9 billion, with a compound annual growth rate

of 143.3%. The passenger volume using ridesplitting services was equivalent to 1.2 times the civil aviation passenger volume in 2019 (Didi Chuxing, 2020).

However, the current ridesplitting ratio in key ridesourcing services provided in the city of Chengdu is low, only 7% (W. Li et al., 2019). The average time usage rate of private cars in China is only 7% (Accenture, 2016), while the rate is only 4% in the United Kingdom (Bates & Leibling, 2012) and 17% in the United States (Santos et al., 2011). This low utilization rate leads to a serious waste of resources. With the development of technology for autonomous driving, idle private cars could be used for autonomous ridesourcing services or ridesplitting services in the future. Tu et al. (2019) showed that such ridesplitting services could potentially have great benefits in the city of Chengdu, specifically by improving the percentage of cost savings and time savings to 17% and 23%, respectively.

Specifically, this chapter involves three main tasks. First, we use a machine learning method, gradient boosting decision tree (GBDT) model, to identify the important features of the built environment at the origins and destinations of ridesplitting services. Second, we explore the nonlinear relationship between the ridesplitting service and key explanatory variables by creating partial dependence plots. Third, we provide insightful results that can help transportation network companies improve existing ridesplitting services and have policy implications for urban planners seeking to better understand how the built environment, demographic factors and travel time impact ridesplitting services.

The remainder of this chapter is organized as follows. Section 3.2 presents the data and variables used in this chapter. The GBDT model is described in section 3.3. Section 3.4 presents the results in detail and discusses the related insights regarding how the built environment features, demographic factors and travel time impact ridesplitting services. The final section 3.5 summarizes the main findings, presents some policy implications and proposes future research directions.

3.2 Data and Variables

3.2.1 Study area

Chengdu is the capital of Sichuan Province and is one of the three most populous cities in Western China. As of 2020, the total area in Chengdu was 14335 square

kilometers, the local population was 16.58 million, the urban population was 12.34 million, and the urbanization rate was 74.42% (Chengdu Bureau of Statistics, 2020).

Since the launch of ridesplitting services on the DiDi Chuxing platform in 2015, the number of passengers who chose ridesplitting services has continued to increase. Chengdu is one of the leading cities that actively advocate for and promote ridesplitting services. Chengdu government keeps taking active part in developing the ridesourcing and ridesplitting services with Didi Chuxing to mitigate the congestion level and air pollution problems. In 2018, the users of ridesplitting services provided by the DiDi platform shared more than 800 million kilometers with other riders across China, which is equivalent to reducing fuel consumption by 43 million liters and reducing CO_2 emissions by 97,000 tons (DiDi Chuxing, 2018b). For 2018 and 2019, the DiDi Chuxing platform reduced carbon dioxide emissions across China by a total of 1.303 million tons, and Chengdu city ranked first. The ridesharing and ridesplitting services provided by this platform reduced carbon dioxide emissions by 913 thousand tons and 158 thousand tons, respectively (Didi Chuxing, 2020). Thus, we choose the municipal districts of Chengdu as the study area, as shown in Figure 3-1.

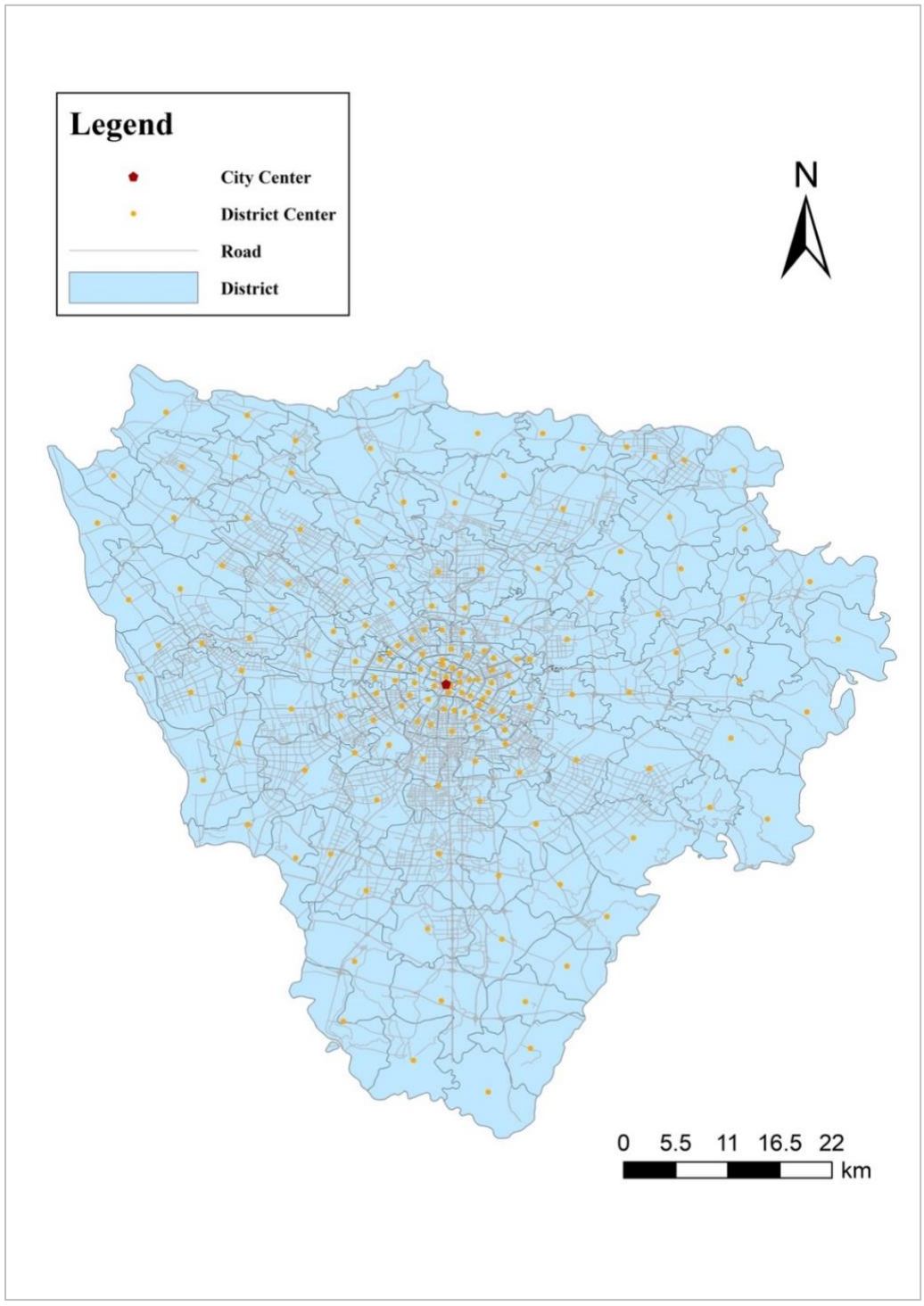

Figure 3-1 Study area

3.2.2 Data sources

Ridesourcing order and GPS data. These data were obtained from the DiDi platform through the DiDi GAIA Initiative, which compiles an open dataset (DiDi Chuxing, 2018b). The dataset includes the complete trajectory and order data of DiDi

Express and DiDi Premier Services in Chengdu, China, from November 1st to November 30th, 2016. The fields of the trajectory dataset are anonymous driver ID, order ID, longitude, latitude, and timestamp, with an average interval time of 3 s. The fields of the order dataset are order ID, pick-up and drop-off locations, start timestamp and end timestamp. We cleaned the data and removed outliers such as order data with travel times less than 120 s or more than 7200 s. Furthermore, we divide the ride orders into single rides and shared rides based on the ridesplitting trip identification algorithm proposed by W. Li et al. (2019). Then, the ridesplitting ratio of each OD pair can be calculated.

GIS layers. We choose the central urban areas of Chengdu as the study area. We divide Chengdu into 162 census tracts based on the administrative boundaries and obtain data on the road networks from OpenStreetMap. The city center is Tianfu Square (Yu & Gao, 2011), which is not only Chengdu's economic, cultural and commercial center but also a comprehensive transportation hub.

Built environment data. The built environment is measured by the four Ds, namely, density, design, land use diversity and distance to the city center. Density measures include population density, local population density, park density, public transportation density, public services density, point of interest (POI) density, and the ratios of industrial, residential and commercial land use (Li et al., 2017). Population density and local population density are from the sixth nationwide population census survey in China. Other density factors are calculated by dividing the number of corresponding facilities by the area. The number of corresponding facilities is obtained by using the POI search API of the Gaode Map Web Services (Gaode Map, 2021). Public service density is measured by the number of health care, government, and education institutions per unit area. Public transportation density is measured by the number of airports, train stations, metro stations and bus stops per unit area. The commercial ratio is measured by the number of financial institutions, shopping places, restaurants, entertainment facilities, and hotels per unit area. Design is measured by the road density, which is calculated by dividing the road length by the area. Land use diversity is measured by the entropy index, which ranges between 0 and 1, where 0 indicates that the land use is homogenous, and 1 indicates that all land use types are equally distributed (Cervero & Kockelman, 1997).

Demographic data. Demographic characteristics are employed to allow for the exploration of the effects of the demographic variables on the ridesplitting ratio. These

variables include the population density who are younger than 14 years old and older than 64 years old, per capita gross domestic product (PGDP), and average housing price. They are measured at the scale of census tract. The population density of individuals younger than 14 years old and older than 64 years old is calculated by dividing the population of individuals younger than 14 years old and older than 64 years old by the area. PGDP data and average housing prices are obtained from the sixth nationwide population census survey in China and the Lianjia website in Chengdu (http://cd.lianjia.com/).

Travel time is used to explore the effects of travel impedance factors on the ridesplitting ratio and is an important factor for passengers deciding whether to choose ridesplitting services. It is the average travel time of all OD pairs from the DiDi order dataset.

3.2.3 Variables description

Based on the data available, we determined the dependent variable and several independent variables. The ridesplitting ratio of each OD pair is chosen as the dependent variable. Then, we divide the explanatory variables into 4 categories, namely, *the built environment at the origin locations, the built environment at the destination locations, demographic factors and travel time*. Then, a descriptive analysis of all the variables was carried out, as shown in Table 3-1. The spatial distributions of some explanatory variables are shown in Figure 3-2.

Table 3-1 Variable definitions and statistics.

Variables	Variable Description	Mean	S.D.	Min	Max
Orders					
Ridesplitting orders	Number of ridesplitting orders from November 1st to 30th in 2016	26.58	63.81	0	1597
Ridesourcing orders	Number of ridesourcing orders from November 1st to 30th in 2016	431.71	984.20	1	33477
Ridesplitting ratio	Number of ridesplitting orders/number of ridesourcing orders	21.85%	33.32%	0	99.94%
Built Environment					
Population density	Population/area size (person per km^2)	11142.95	14545.89	155.07	67557.29
Local population density	Local population/area size (person per km^2)	6132.88	8789.07	151.72	41861.45
Park density	Number of parks and square/area size (park per km^2)	0.60	0.85	0	5.11
Industrial ratio	Number of industrial locations/number of POI	3.22%	5.03%	0	39.74%
Transportation density	Number of transportation facilities/area size (facility per km^2)	5.14	4.41	0.33	17.75

Residential ratio	Number of residential locations/number of POI	8.78%	5.56%	0	22.78%
Commercial ratio	Number of commercial locations/number of POI	67.66%	13.52%	28.57%	91.76%
Public density	Number of public service facilities/area size (facility per km^2)	29.43	41.48	0.30	174.02
POI density	Number of POI/area size (facility per km^2)	221.96	328.50	0.46	1699.44
Land use diversity	Entropy index of the land use mix	0.80	0.10	0.44	0.99
Area	Area of every tract (km^2)	22.70	20.08	0.64	82.31
Road density	Length of the road/area size (km/km^2)	4.28	3.01	0.22	12.28
Distance to city center	Straight line distance from city center (km)	20.92	14.50	1.07	54.80
Demographic Characteristics					
Population density (less than 14 years old)	Population less than 14 years old/area size (person per km^2)	1000.03	1244.20	25.20	6588.39
Population density (more than 64 years old)	Population more than 64 years old/area size (person per km^2)	1131.36	1697.28	20.64	9473.61
PGDP	Gross domestic product/population (10^4 RMB per capita)	10.79	2.87	7.71	15.75
Housing price	Average price per square meter (RMB/m^2)	13656.02	4951.05	4661	31245
Travel Impedance variables					
Travel time	Average travel time for OD ridesourcing orders (s)	2178.00	1339.14	120	7200

Note: Samples: 14,121 OD pairs

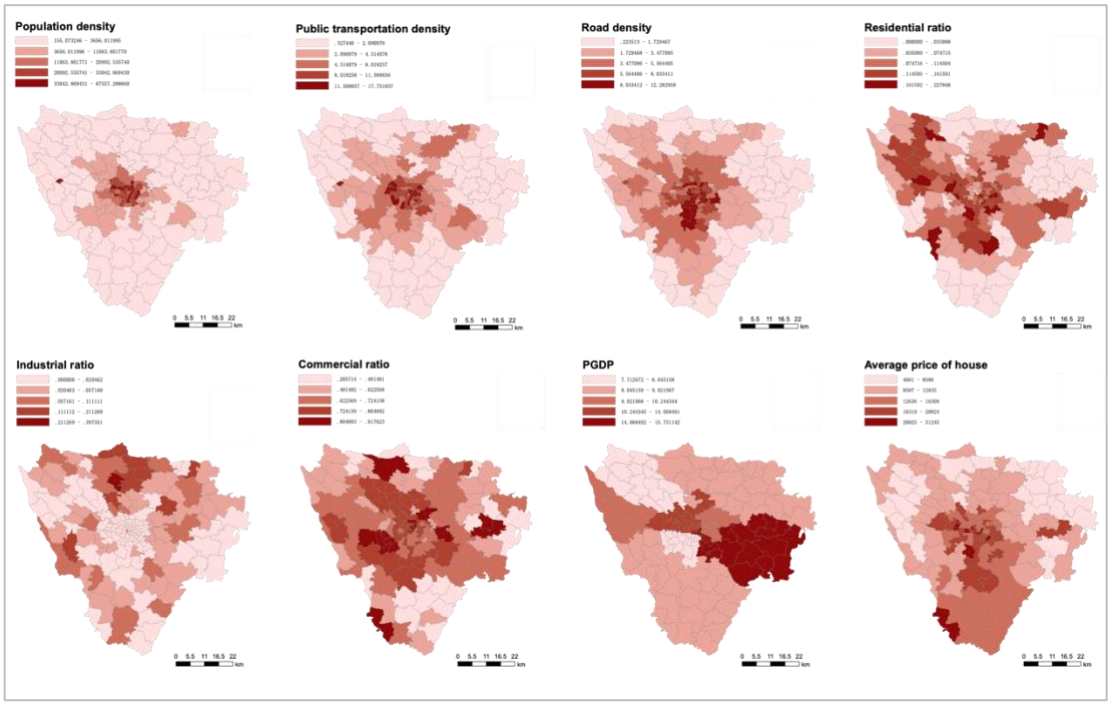

Figure 3-2 Distributions of some explanatory variables

3.3 Methodology

We choose the built environment features that are measured by the 'four Ds', namely, density, land use diversity, design, and distance to city center. Then, we use the GBDT model to predict the OD ridesplitting ratio and investigate the relative importance ranking of all the explanatory variables. Furthermore, we explore the nonlinear relationship between the ridesplitting ratio and key explanatory variables by generating partial dependence plots. We find some useful thresholds from the partial dependence plots, which could provide a reference for policy makers.

3.3.1 GBDT model

A GBDT model is an additive model that uses decision trees f(x) to estimate the function F(x). The objective of the algorithm is to minimize the loss function $L\big(y, F(x)\big) = (y - F((x))^2$.

$$F(\mathrm{x}) = \sum_{m=1}^{M} f_m(x) = \sum_{m=1}^{M} \beta_m h(x; a_m) \tag{3.1}$$

where x is a set of explanatory variables (i.e., built environment features, demographic factors and travel time) and F(x) is an approximation function of the dependent variable (i.e., OD ridesplitting ratio). a_m is the mean of split locations and the terminal node for each splitting variable for each tree. M represents the mth iteration.

The function F(x) is updated according to the gradient descent direction as follows:

$$F_m(\mathrm{x}) = F_{m-1}(\mathrm{x}) + \beta_m h(x; a_m) \tag{3.2}$$

$$\beta_m = \arg\min_{\beta} \sum_{i=1}^{n} L(\mathrm{y}_i, \mathrm{F}_{m-1}(\mathrm{x}_i) + \beta\, \mathrm{h}(\mathrm{x}_i; a_m)) \tag{3.3}$$

where β_m is expected to minimize the value of the loss function.

A shrinkage parameter ξ ($0<\xi<1$), also called the learning rate, can be used to avoid the overfitting problem (Friedman, 2001) by means of scaling the contributions

of each tree.

$$F_m(\mathrm{x}) = F_{m-1}(\mathrm{x}) + \xi * \beta_m h(x; a_m) \tag{3.4}$$

3.3.2 Relative importance and partial dependence of the explanatory variables

Compared to most machine learning algorithms regarded as 'black-box' algorithms, the GBDT model can be used to determine the relative importance ranking of all explanatory variables. The relative importance of variable x_i can be obtained as follows:

$$I^2_{x_i} = \frac{1}{M}\sum_{m=1}^{M} I^2_{x_i}(T_m) \tag{3.5}$$

$$I^2_{x_i}(T_m) = \sum_{j=1}^{J-1} d_j \tag{3.6}$$

where j is the number of leaves on each tree and d_j represents the improvement in the squared error term by making the j^{th} split based on the variable x_i.

The GBDT model can also generate a partial dependence plot to illustrate the relationships between the explanatory variables and dependent variables. The partial dependence plot shows the marginal effect of one or two features on the predicted response variable (Friedman, 2001) The partial dependence of F(x) on x_s can be defined as follows (Hastie et al., 2009):

$$F_{x_S}(\mathrm{x}_S) = E_{x_C}[\mathrm{F}(\mathrm{x}_S, \mathrm{x}_C)] = \int \mathrm{F}(\mathrm{x}_S, \mathrm{x}_C) dP(\mathrm{x}_C) \tag{3.7}$$

$$F_{x_S}(\mathrm{x}_S) = \frac{1}{n}\sum_{i=1}^{n} F(x_S, x_C^i) \tag{3.8}$$

Where x_s are the features that we want to know the specific effect on the OD ridesplitting ratio and x_c are the other features used in the chapter. n represents the number of samples.

3.4 Results and Discussion

3.4.1 Performance of the GBDT model

We use a five-fold cross-validation procedure to obtain the optimal parameter settings and a robust result. We fit the models with different numbers of trees (5000, 10000, 15000), shrinkages (0.005, 0.05, 0.01, 0.1) and tree complexities (1, 3, 5, 7) based on the experimental findings of previous studies. We fit the model 240 times and find that the best performance is obtained when the number of trees, shrinkage and tree complexity are set as 5000, 0.005 and 7, respectively.

As shown in Table 3-2, the values of testing pseudo-R^2, mean absolute error (MAE) and mean squared error (MSE) for the GBDT model are 0.7415, 0.1070 and 0.0293, respectively. The corresponding values for the traditional linear regression model are 0.3449, 0.2104 and 0.0727. The pseudo-R^2 is improved by 114.99%, and the MAE and MSE are decreased by 49.14% and 59.70%, respectively.

Table 3-2 Comparison of the GBDT model and basic linear regression model.

Metrics	**GBDT**	**Linear regression**	**Percentage of improvement**
R^2	0.7415	0.3449	+114.99%
MAE	0.1070	0.2104	-49.14%
MSE	0.0293	0.0727	-59.70%

3.4.2 Relative importance of the explanatory variables

Figure 3-3 The importance ranking of all the explanatory variablesshows the relative importance of the explanatory variables and their rankings in predicting the OD ridesplitting ratio. The total importance of all explanatory variables equals 100% because it is measured in a relative way.

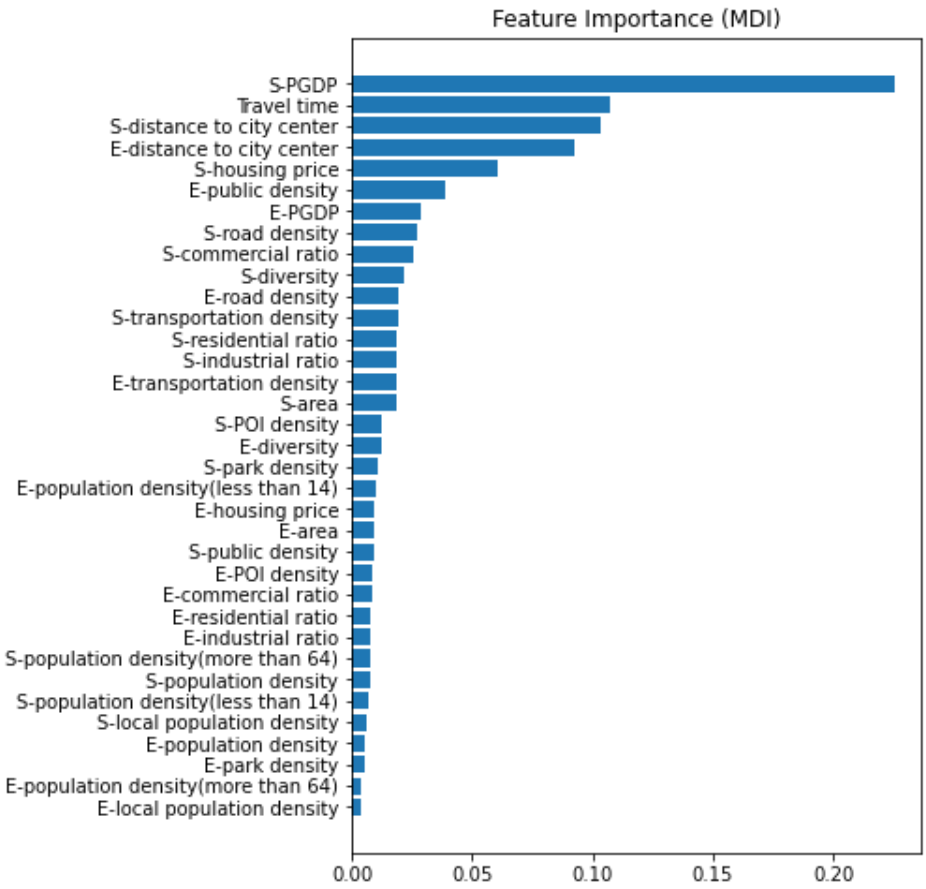

Note: 'S-' represents features at the origin locations and 'E-' represents features at the destination locations

Figure 3-3 The importance ranking of all the explanatory variables

As shown in Table 3-3, the built environment features at the origin locations contribute 29.97%, whereas the contribution of the features at the destination locations is 23.98%. The built environment features at the origin locations have larger effects on the OD ridesplitting ratio than the destination locations. In addition, the collective contribution of the demographic factors is 35.31%. Moreover, travel time contributes 10.74%, which is also an important feature.

For the built environment features at the origin locations, distance to city center, road density, commercial ratio, land use diversity, and public transportation density are the top five important explanatory variables, which contribute to 10.35%, 2.75%, 2.56%, 2.20% and 1.92%, respectively. The three least important features at the origin locations are local population density, population density and public service density, which contribute to 0.59%, 0.75% and 0.90%, respectively.

For the built environment features at the destination locations, distance to city center, public service density, road density, public transportation density, and land use

diversity are the five variables with the highest relative importance, which contribute to 9.26%, 3.92%, 1.97%, 1.83% and 1.24%, respectively. The three least important features at the destination locations are local population density, park density and population density, which contribute to 0.41%, 0.55% and 0.55%, respectively.

Table 3-3 The relative importance ranking of all the explanatory variables.

Built environment features at origin locations	**Relative importance**	**Ranking**
S-distance to city center	10.35%	3
S-road density	2.75%	8
S-commercial ratio	2.56%	9
S-diversity	2.20%	10
S-transportation density	1.92%	12
S-residential ratio	1.89%	13
S-industrial ratio	1.87%	14
S-area	1.82%	16
S-POI density	1.26%	17
S-park density	1.10%	19
S-public density	0.90%	23
S-population density	0.75%	29
S-local population density	0.59%	31
Sum	29.97%	--
Built environment features at destination locations	**Relative importance**	**Ranking**
E-distance to city center	9.26%	4
E-public density	3.92%	6
E-road density	1.97%	11
E-transportation density	1.83%	15
E-diversity	1.24%	18
E-area	0.95%	22
E-POI density	0.88%	24
E-commercial ratio	0.83%	25
E-residential ratio	0.79%	26
E-industrial ratio	0.78%	27
E-population density	0.55%	32
E-park density	0.55%	33
E-local population density	0.41%	35
Sum	23.98%	--
Demographic factors	**Relative importance**	**Ranking**
S-PGDP	22.56%	1
S-housing price	6.07%	5
E-PGDP	2.84%	7
E-population density (less than 14)	1.04%	20
E-housing price	0.96%	21
S-population density (more than 64)	0.77%	28
S-population density (less than 14)	0.66%	30
E-population density (more than 64)	0.42%	34
Sum	35.31%	--
Travel impedance feature	**Relative importance**	**Ranking**
Travel time	10.74%	2

For the demographic factors, PGDP at the origin locations is the most important factor in all the explanatory variables, accounting for 22.56%. The average price of the house at the origin locations contributes to 6.07%, which is the second most important demographic feature to predict the ridesplitting ratio. The least important demographic factor is the population density of people who are more than 64 years old, which contributes to 0.42%.

3.4.3 Nonlinear effects of built environment features

Figure 3-4 demonstrates the effects of four key built environment variables of the origin locations on the ridesplitting ratio. Figure 3-4 (a) shows that the distance to the city center at the origin locations has a positive association with the OD ridesplitting ratio. People are more likely to use ridesplitting services when they depart from areas far away from the city center than those near the city center. People are reluctant to use ridesplitting services when the distance to the city center at the origin locations is less than 5 km. However, the OD ridesplitting ratio increases substantially when the distance to the city center is more than 32 km.

Figure 3-4 (b) displays the relationship between public transportation density at the origin locations and the OD ridesplitting ratio, which shows a significant nonlinear pattern: first decreasing then steady and then increasing slightly. The OD ridesplitting ratio decreases with increasing public transportation density at the destination locations from 0 to 6 per km^2, and the ridesplitting ratio differs by approximately 4%. The ridesplitting ratio remains steady when the public transportation density is between 6 and 13 per km^2. The ridesplitting ratio increases slightly when the public transportation density at the origin locations is greater than 13 per km^2. The above results show that the ridesplitting ratio is relatively high in the districts where public transportation density is less than 6 per km^2. Therefore, transportation network companies should provide enough ridesplitting services to satisfy ridesplitting demand and guarantee the service quality in areas with low accessibility to public transportation. This threshold could also provide a reference for the government to achieve a good balance of ridesplitting services and public transportation services.

Figure 3-4 (c) demonstrates that the road density at the origin locations is negatively correlated with the OD ridesplitting ratio. First, the ridesplitting ratio remains high and steady when the road density is less than 2.5 km/km^2. Then, the ratio decreases with an increase in road density between 2.5 km/km^2 and 6 km/km^2. The OD

ridesplitting ratio remains almost stable when road density exceeds 6 km/km^2.

Figure 3-4 (d) generally shows a positive association between land use diversity at the origin locations and the ridesplitting ratio. Land use diversity at the origin locations has almost no effect when it is less than 0.8. However, the OD ridesplitting ratio increases substantially when it reaches 0.85. Then, the ratio remains constant when the land use diversity exceeds 0.85.

To summarize the above results in the origin locations, we can say that the ridesplitting ratio is higher when:

a) The origin area is close to the city center (>32 km)
b) The public transportation services at the origin locations have a low density (< 6.0 number/km^2)
c) The road density at the origin locations is low (<4.0 km/km^2)
d) The land use diversity at the origin locations is high (>0.85)

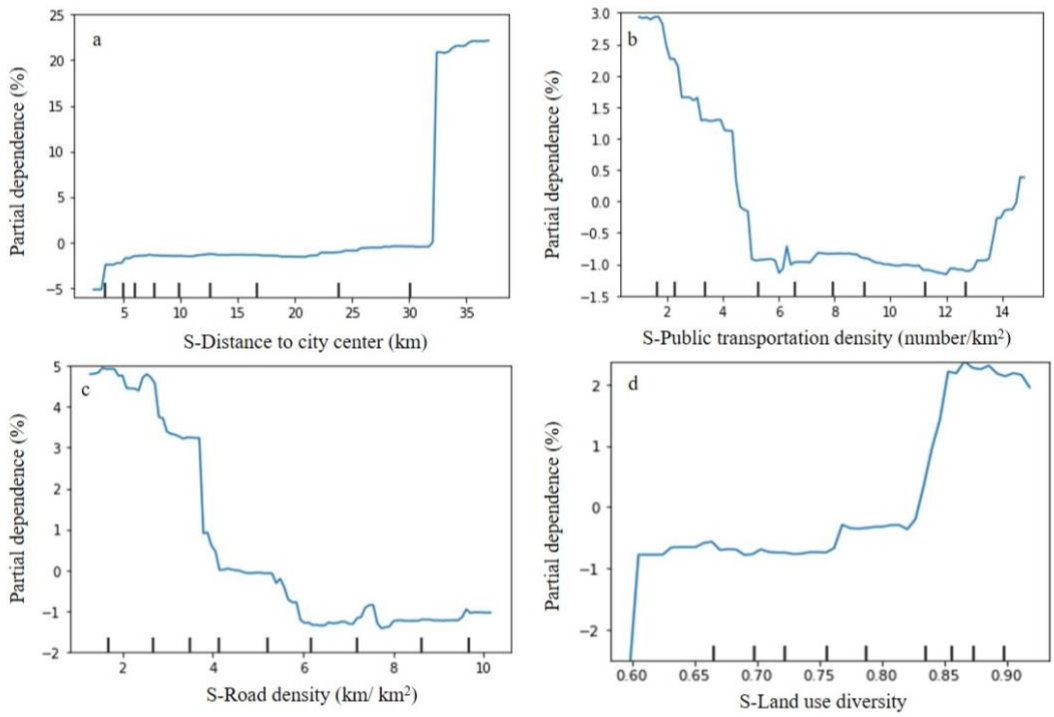

Figure 3-4 The effects of the key built environment variables of the origin locations on the ridesplitting ratio

Figure 3-5 demonstrates the effects of four key built environment variables of the destination locations on the ridesplitting ratio. The partial dependence plot for the distance to the city center at the destination locations is presented in Figure 3-5 (a).

The plot shows that the distance to the city center at the destination locations is positively associated with the OD ridesplitting ratio. First, the difference in the ridesplitting ratio could reach 20% between the destinations near the city center and those 33 km away from the city center. Distance to the city center at the destination locations has almost no effect when it is less than 20 km. Within this range, the ridesplitting ratio only differs by approximately 5%. However, the OD ridesplitting ratio increases substantially when it exceeds 20 km.

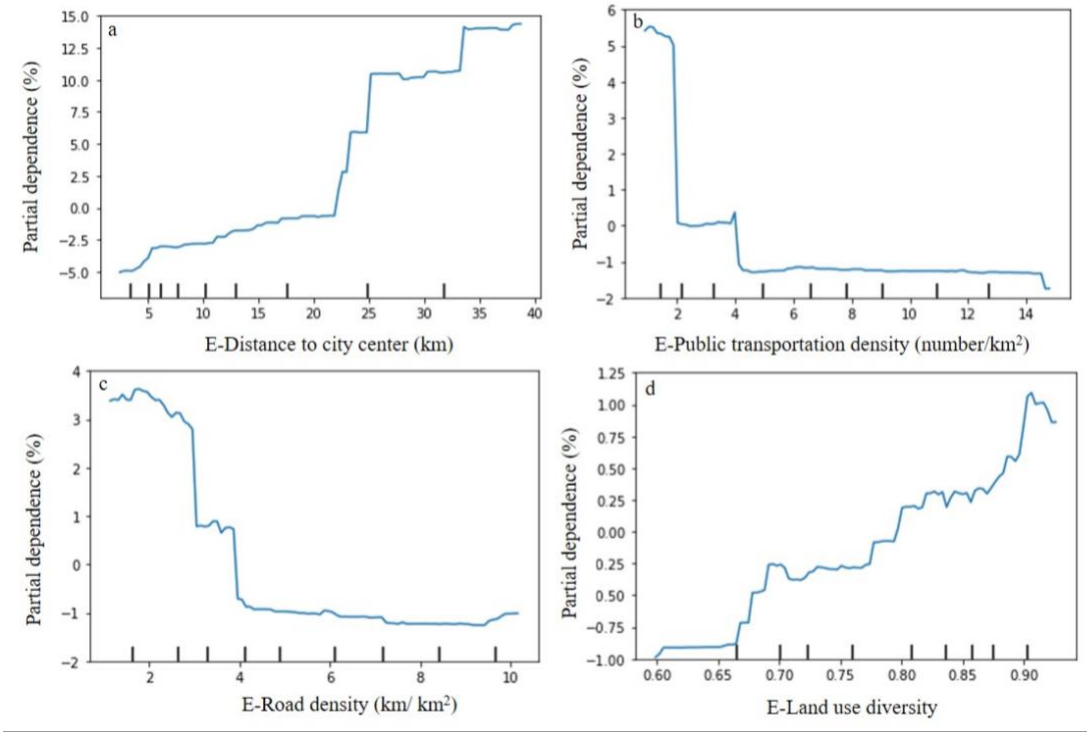

Figure 3-5 The effects of the key built environment variables of the destination locations on the ridesplitting ratio

Figure 3-5 (b) indicates that public transportation density at the destination locations is negatively associated with the ridesplitting ratio, which is similar to the relationship between the public transportation density at the origin locations and the ridesplitting ratio. The OD ridesplitting ratio decreases with increasing public transportation density at the destination locations ranging from 0 to 2 per km^2, and the ridesplitting ratio differs by approximately 5%. The ridesplitting ratio remains steady when the public transportation density is between 2 and 4 per km^2. The ridesplitting ratio decreases slightly when the public transportation density at the destination locations is 4 per km^2 and remains steady beyond this range. The above results show

that the ridesplitting ratio is higher in districts where the public transportation density is lower than 2 per km^2.

Figure 3-5 (c) demonstrates that the road density at the destination locations is negatively correlated with the OD ridesplitting ratio, which is similar to the relationship between the road density at the origin locations and the ridesplitting ratio. First, the ridesplitting ratio remains high and steady when the road density is less than 2.5 km/km^2. Then, the ratio decreases with an increase in the road density between 2.5 km/km^2 and 4 km/km^2. The OD ridesplitting ratio remains almost stable when the road density exceeds 4 km/km^2. Figure 3-4(c) and Figure 3-5 (c) demonstrate that road density is negatively correlated with the ridesplitting ratio at both the origin and destination locations. This result can be explained by other studies finding that road density has a positive correlation with public transportation services such as buses and metros (Tu et al., 2018; Zhao et al., 2014; Gan et al., 2019). Therefore, the share of ridesplitting services can be replaced by public transportation services in areas with high road density.

Figure 3-5 (d) shows a positive association between the land use diversity at the destination locations and the ridesplitting ratio in general. The land use diversity at the origin locations has almost no effect when it is less than 0.65. However, the OD ridesplitting ratio keeps increasing when the land use diversity increases from 0.65 to 0.9.

To summarize the above results in the destination locations, we can say that the ridesplitting ratio is higher when:

a) The destination area is far from the city center (>20 km)
b) The public transportation services at the destination locations have a low density (< 4 number/km^2)
c) The road density at the destination locations is low (<4.0 km/km^2)
d) The land use diversity at the destination locations is high (>0.85)

To be specific, we choose two typical census tracts for further analysis. In census tract No. 77, the distance to the city center is 44.39 km, the density of public transportation is 0.8 number/km^2, the road density is 1.70 km/ km^2 and the land use diversity is 0.93. For all ridesourcing trips departing from the No. 77 census tract, the average real ridesplitting ratio is 74.66%. For all ridesourcing trips arriving at No. 77 census tract, the average real ridesplitting ratio is 53.00%. In census tract No. 137, the

distance to the city center is 7.41 km, the density of public transportation is 14.93 number/km^2, the road density is 8.03 km/ km^2 and the land use diversity is 0.72. The number of ridesourcing trips departing from No.137 census tract is 81054, and the average real ridesplitting ratio is zero. For all ridesourcing trips arriving at No.137 census tract, the average real ridesplitting ratio is 19.61%. The real ridesplitting situation related to these two census tracts is consistent with the result provided by the proposed model.

3.4.4 Other explanatory variables

Figure 3-6 demonstrates the effects of key demographic variables on the OD ridesplitting ratio. Figure 3-6 (a) displays the relationship between PGDP at the origin locations and OD ridesplitting ratio. The partial dependence plot indicates that the ridesplitting ratio is relatively low when the PGDP is less than 100,000 RMB/year. However, the OD ridesplitting ratio increases substantially when the PGDP increases to 100,000 RMB/year. The ridesplitting ratio remains steady from 100,000 to 125,000 RMB/year and then decreases slightly between 125,000 and 140,000 RMB/year. Then, the ridesplitting ratio increases from 140,000 to 155,000 RMB/year. The difference in the ridesplitting ratio can reach 30% between areas where the PGDP is 155,000 RMB/year and those where the PGDP is approximately 90,000 RMB/year.

Figure 3-6 (b) demonstrates the relationship between the PGDP at the destination locations and the OD ridesplitting ratio. The per capita GDP at the destination locations has little effect on the ridesplitting ratio.

The partial dependence plot for the average price of housing at the origin locations is presented in Figure 3-6 (c). In general, this plot indicates that the average price of housing is negatively correlated with the OD ridesplitting ratio. The OD ridesplitting ratio decreases when the average price of housing at the origin locations increases from 6,000 to 10,000 RMB per m^2. This result indicates that people who live in houses with relatively low prices prefer to choose ridesplitting services. This is consistent with reality because these homeowners want to use ridesplitting services due to the low price. Figure 3-6 (d) demonstrates that the average price of housing at the destination locations has little effect on the ridesplitting ratio.

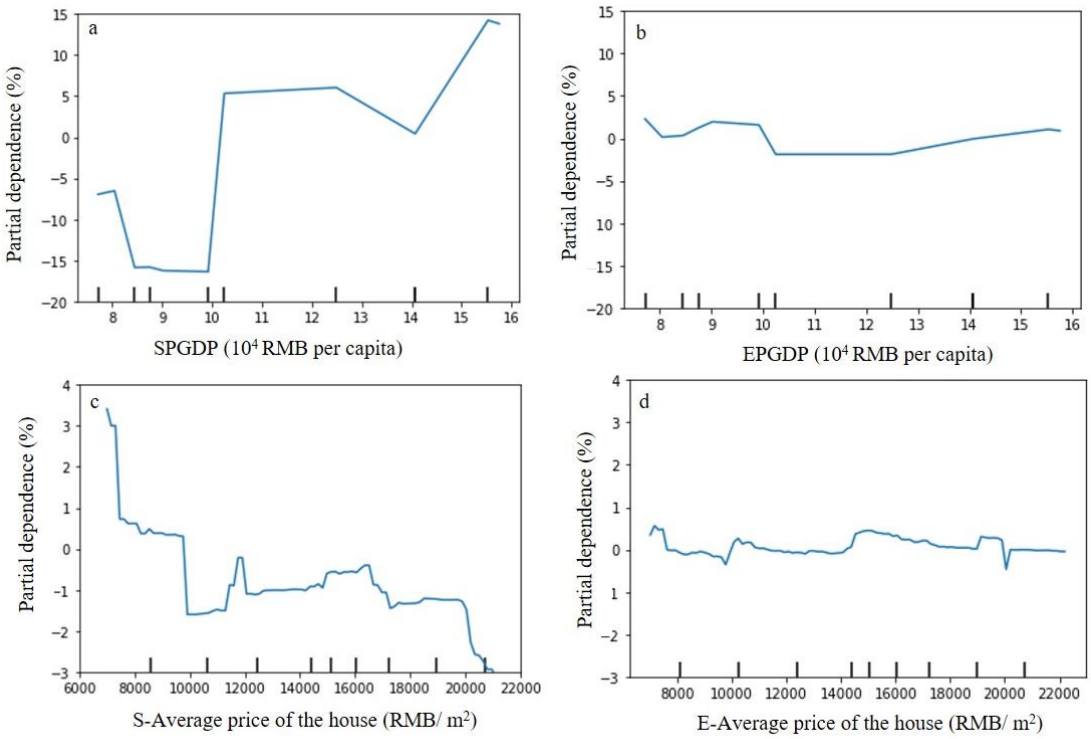

Figure 3-6 The effects of the key demographic variables on the OD ridesplitting ratio

The partial dependence plot demonstrates the relationship between travel time and OD ridesplitting ratio in Figure 3-7. The results show that travel time has a significant and positive effect on the OD ridesplitting ratio in general. A subpeak exists when the travel time is approximately 20 minutes. Travel time has almost no effect when it is less than approximately 35 minutes, while OD ridesplitting ratio increases gradually when travel time exceeds 35 minutes. Beyond this range, people are more likely to choose the ridesplitting service with the increase of the travel time. Furthermore, the ridesplitting ratio remains nearly the same when the travel time increases to 70 minutes.

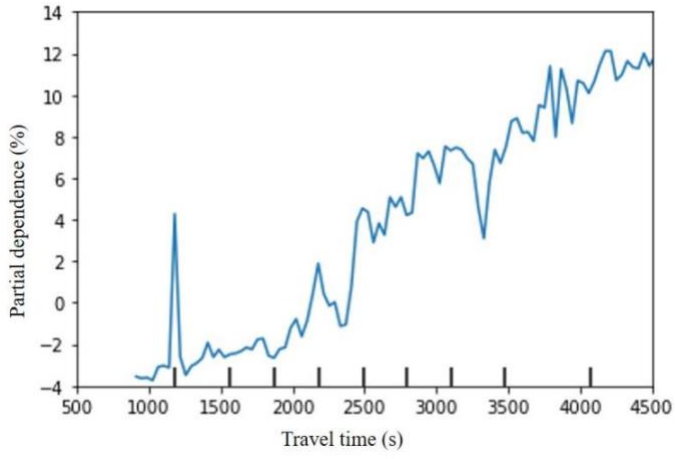

Figure 3-7 The effects of the travel time on the OD ridesplitting ratio

3.4.5 Multi-predictor partial dependence plots

Figure 3-8 demonstrates the combined impacts of the residential ratio and commercial ratio of the origin locations on the OD ridesplitting ratio. The result indicates that when the residential ratio ranges from 0.16 to 0.18 and the commercial ratio ranges from 0.55 to 0.65, the ridesplitting ratio reaches its highest value. This result could provide a significant reference for both policy makers such as urban planners and commercial managers such as transportation network companies.

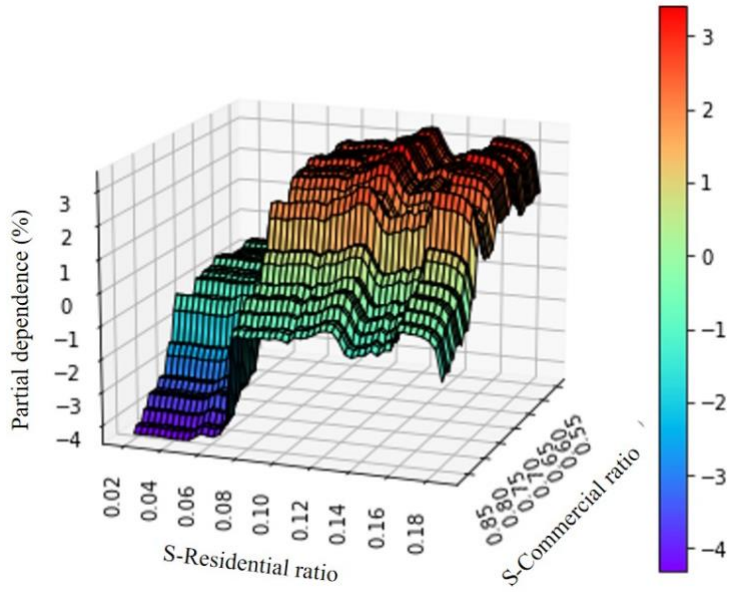

Figure 3-8 The combined effects of S-residential ratio and S-commercial ratio on the OD ridesplitting ratio

Figure 3-9 depicts the impacts of POI density and land use diversity of the origin locations on the OD ridesplitting ratio. The OD ridesplitting ratio increases with increasing land use diversity at the origin locations. When the land use diversity increases to 0.85, the ridesplitting ratio increases by 5%. The result indicates that when land use diversity ranges from 0.85 to 1 and the POI density is less than 600 per km^2, the ridesplitting ratio remains relatively steady and high.

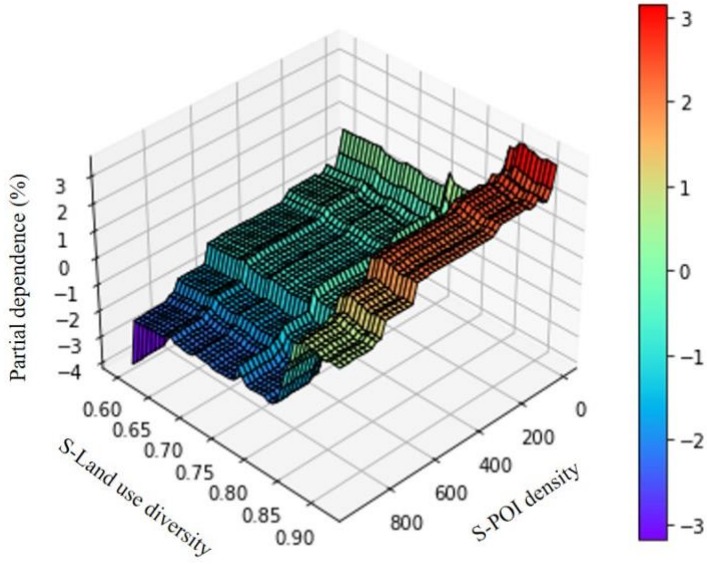

Figure 3-9 The combined effects of S-POI density and S-land use diversity on the OD ridesplitting ratio

3.5 Conclusions and Implications

To explore the effects of built environment features, demographic factors and travel time on the OD ridesplitting ratio, this chapter employs a GBDT model using observed ridesplitting data of Chengdu obtained from DiDi's open data project. GBDT is a machine learning method without a prior hypothesis of a particular function such as a linear or log linear relationship. The GBDT model can be used to predict the OD ridesplitting ratio and even the nonlinear relationships with the explanatory variables more accurately. The results of this chapter verify that the performance of the GBDT model is much better than that of the traditional linear regression model.

Four categories of explanatory variables are used in this chapter: the built environment at the origin locations and destination locations, demographic factors and travel time. The GBDT model provides the relative importance ranking of all the explanatory variables. The results indicate that the built environment at the origin locations has a larger effect on the OD ridesplitting ratio than that of the destination locations. The collective influence of the built environment is larger than that of demographics and travel time. The built environment at the origin locations contributes 29.97%, whereas the contributions of the features at the destination locations are 23.98%. In addition, the collective contribution of the demographic factors is 35.31%. Travel time contributes to 10.74%.

For the built environment features at the origin locations, distance to city center, road density, commercial ratio, land use diversity, and public transportation density are the five most important explanatory variables. For the built environment features at the destination locations, distance to city center, public service density, road density, public transportation density, and land use diversity are the five most important variables. It can be found that distance to city center, land use diversity, road density and public transportation density rank highest in terms of importance for both the origin and destination locations, indicating that they play key roles in impacting the ridesplitting ratio.

Distance to the city center has a positive association with the ridesplitting ratio at both the origin locations and destination locations. People are more likely to use ridesplitting services when they depart from areas far away from the city center than those near the city center. The difference in the ridesplitting ratio could reach 20% between the destinations near the city and those 33 km away from the city center. In addition, road density is identified to be negatively correlated with the ridesplitting ratio at both the origin and destination locations. In general, land use diversity is positively associated with the ridesplitting ratio both at the origin locations and at the destination locations. Therefore, urban planners should pay more attention to the planning of land use and residential/commercial/industrial ratios, and develop reasonable designs based on the specific thresholds identified in the partial dependence plots. The insightful findings could enhance their understanding of ridesplitting services and be used for land use planning to design a ridesplitting-friendly city.

Public transportation density also plays an essentially important role in the impact on the ridesplitting ratio at both the origin and destination locations. A negative association between public transportation and the ridesplitting ratio can be seen both at the origin locations and at the destination locations. The results show that the ridesplitting ratio is relatively high in the districts where public transportation density is less than 4 per km^2. The government could set a threshold of the available ridesplitting services nearby for transportation network companies to guarantee the service quality, especially in areas with low accessibility to public transportation. This threshold could also provide a reference for the government to achieve a good balance of ridesplitting services and public transportation services.

With respect to demographics, PGDP and the average price of housing at the origin locations are the two most important factors impacting the ridesplitting ratio.

The results demonstrate that a positive association exists between the PGDP at the origin locations and the ridesplitting ratio, whereas a negative association exists between the average price of housing at the origin locations and the ridesplitting ratio.

The findings of this chapter could help to better understand how the built environment, demographic factors and travel time impact ridesplitting services and provide policy implications for decision makers. For urban planners, the insightful results could enhance their understanding of ridesplitting services and be used for land use planning, design, and related features. For the transportation network companies, the results could help them optimize their long-term ridesplitting capacity to satisfy ridesplitting demand and improve the transportation efficiency. These companies should provide enough ridesplitting services in areas with high ridesplitting demand to guarantee service quality and reduce ridesplitting capacity in areas with low ridesplitting demand to reduce empty travel by vehicles.

Ridesplitting, a form of ridesourcing services that matches riders with similar routes to the same driver, is a high occupancy travel mode that can bring considerable benefits. However, the current ratio of ridesplitting in the ridesourcing services is relatively low and its influencing factors remain unrevealed. Therefore, this chapter uses a machine learning method, gradient boosting decision tree model, to identify the impacts of the built environment on the origin-destination ridesplitting ratio. The results show that most built environment features have a strong nonlinear effect on the ridesplitting ratio. Distance to city center, land use diversity and road density are the key explanatory variables impacting the ridesplitting ratio. The non-linear thresholds of built environment factors are found based on partial dependence plots, which could provide policy implications for the government and transportation network companies to promote the ridesplitting. In the next chapter, an optimized ridesourcing demand prediction method will be proposed to improve the ridesourcing service efficiency.

Chapter 4 An optimized ridesourcing demand prediction method based on an encoder-decoder neural network

HIGHLIGHTS

1) Improve the demand prediction accuracy for ridesourcing platform
2) Tackle both spatiotemporal single-step prediction and multi-step prediction
3) Develop an encoder-decoder neural network framework for spatiotemporal prediction.
4) Build a dynamic spatiotemporal attention mechanism for the network

4.1 Introduction

On-demand ridesourcing services have become crucially important for daily travel worldwide due to the development of mobile internet technology and market demand. Ridesourcing services match passengers and drivers through intelligent mobile phone applications (Rayle et al., 2016). Uber has launched services in over 890 cities in 71 countries through 2020 (Uber, 2020). In 2019, Uber served 111 million users and provided 6.9 billion trips worldwide. There is no doubt that on-demand ridesourcing services can bring convenience for passengers. However, it is known that on-demand ridesourcing services also cause some negative effects, such as aggravating traffic congestion and air pollution, for the whole transportation system because of the low occupancy rates of the vehicles. Ridesourcing demand prediction is a feasible way to increase these occupancy rates. The vehicles can be dispatched properly to decrease the idle time according to the demand prediction results. Then, passengers could also wait for less time when using ridesourcing services. Therefore, it is important to obtain high-accuracy ride-souring demand predictions for transportation network companies to balance demand and supply.

Compared to the traditional time series methods, machine learning methods have an absolute advantage (G. Chen et al., 2021; Chu et al., 2019; Du et al., 2020; Geng et al., 2019; Xu et al., 2017; Yao et al., 2018; B. Zhang et al., 2021; C. Zhang et al., 2021; Zhao et al., 2019). To date, machine learning methods have been widely used in

classification and regression prediction tasks (K. Chen et al., 2017; Du et al., 2020; Geng et al., 2019; Guo et al., 2019; J. Li et al., 2020; Minaee et al., 2021; G. Wang et al., 2018; B. Zhang et al., 2021; Zhang et al., 2020; Zhao et al., 2019), including computer vision (Guo et al., 2019; G. Wang et al., 2018), natural language processing (K. Chen et al., 2017; J. Li et al., 2020), and traffic demand prediction (Du et al., 2020; Geng et al., 2019; Zhao et al., 2019). In particular, many existing works and experimental results in the field of traffic demand prediction prove that deep learning methods have better performance than traditional time series methods and traditional machine learning algorithms. In view of these findings, we propose a novel and simple optimized spatiotemporal encoder-decoder neural network (O-STEDN) for ridesourcing demand prediction in this chapter.

More specifically, this chapter involves 3 tasks. First, we divide the study area according to its administrative districts to guarantee the integrity of the districts and perform a characterization analysis of the ridesourcing demand in Chengdu. Second, we propose our own prediction model, which combines temporal and spatial characteristics to accurately complete the multi-step prediction of future ridesourcing demand. Finally, we compare our model with other existing advanced methods to validate the efficiency of the proposed model. The main contributions of this chapter can be summarized as follows:

1) To the best of our knowledge, this is the first time that multi-step ridesourcing demand prediction has been performed based on integral administrative districts at the city scale. These results can provide highly meaningful references for both government and transportation network companies in advance.
2) Different from existing methods, our approach uses a combination of a GCN and an RLSTM network as the spatiotemporal feature extractor. The advantage is that the GCN overcomes the shortcomings of traditional convolutional neural networks (CNNs) and can deeply extract the spatial correlation features of discrete regions in non-Euclidean space. Compared with time series feature extraction methods, including recurrent neural network (RNN), gated recurrent unit (GRU), and LSTM, RLSTM can better extract and memorize time-related features.
3) For the ridesourcing demand prediction task, there is a high degree of spatiotemporal correlation between the current prediction value and the input

variables. Therefore, we use a global attention mechanism to associate the spatiotemporal features with the current prediction, that is, to consider the impacts of the input variables on the prediction.

4) In addition, predictive models based on neural networks are generally prone to information loss and internal covariate shift during the feature extraction process. Therefore, we add residual connections and layer normalization tricks in both the encoder layer and the decoder layer. In the experiment, we evaluate our model on the typical task of next-step prediction and a multi-step prediction task. The results of our evaluation show that our approach outperforms state-of-the-art models.

The remainder of this chapter is organized as follows. Section 4.2 describes the methodology and framework of our method for predicting ridesourcing demand. Section 4.3 presents the experiments in detail. Comparative results and further discussions are proposed in Section 4.4. Conclusions and policy implications are presented in Section 4.5. The final section concludes the chapter's contributions and limitations.

4.2 Methodology

Our O-STEDN model uses a graph convolutional network (GCN) and a read-first long short-term memory (RLSTM) network as encoders to extract the spatiotemporal correlation features of the input variables (W. Wu et al., 2020; B. Zhang et al., 2021) and uses LSTM and a spatiotemporal dynamic attention mechanism as decoders to achieve multi-step prediction (Cho et al., 2015; Hochreiter & Schmidhuber, 1997; Luong et al., 2015). Note that the dynamic spatiotemporal attention mechanism considers the influence of the spatiotemporal features extracted at each moment in the history of the current prediction, and we also add residual connections and layer normalization tricks to the entire network to prevent network information loss and internal covariate shift problems.

In summary, the main differences between our proposed O-STEDN method and the existing approaches are that, first, we consider the correlations between the predictions at each moment and the spatiotemporal characteristics of the historical input variables; second, we achieve precise multi-step demand forecasting; third, we consider the information loss and internal covariate shift in the feature extraction process (Chen et al., 2020; He et al., 2016; Ioffe & Szegedy, 2015). The specific

description of the methodology is in the remainder of this section.

4.2.1 Framework Overview

Ridesourcing demand prediction is a specific problem of time series analysis. If we measure the input ridesourcing demand data at a certain frequency, such as one sample per 15 min, we obtain a sequence of ridesourcing demand data in a time series form; this is denoted by $\{x_i | -\infty < i < +\infty\}$, in which $x_i \in R^{N \times \boldsymbol{d_x}}$ and N is the number of area nodes. The core of this problem involves how to reveal the spatial and temporal correlations of ridesourcing demand data. Thus, we use the O-STEDN to learn the spatial and temporal properties hidden in data.

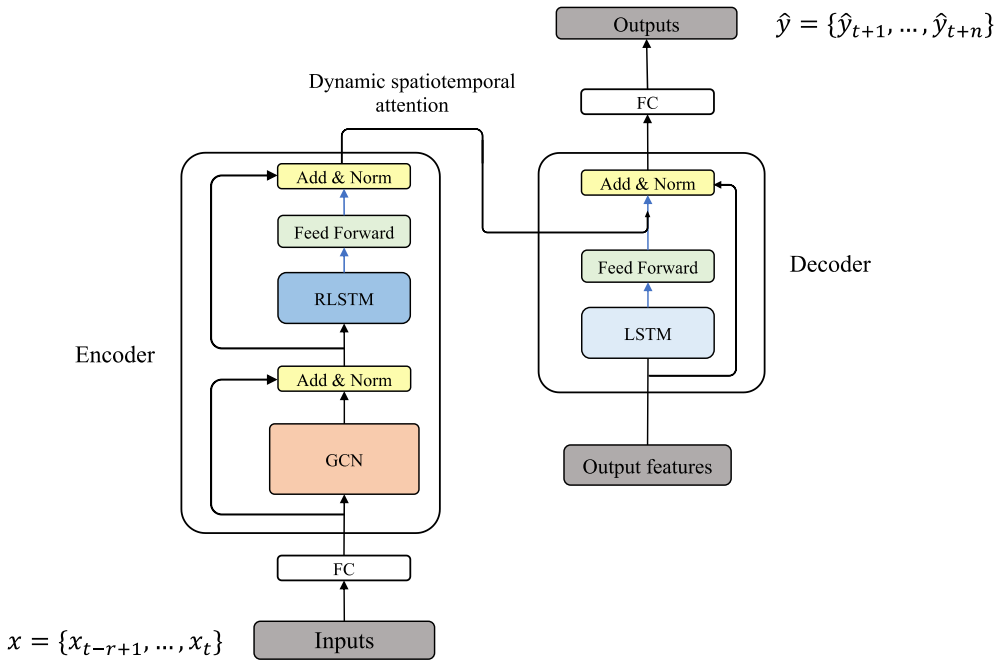

Figure 4-1 The framework of the proposed O-STEDN.

The framework of the proposed O-STEDN is illustrated in Figure 4-1. There are two steps required to implement the proposed method:

Encoder The ridesourcing demand sequence data are pipelined into the proposed O-STEDN to learn its spatiotemporal features by a stacked encoder. We use a GCN to extract the spatial features of the ridesourcing demand data in all areas and use RLSTM to extract the temporal features of the spatial correlation features output by the GCN. At each time step, the input data of the encoder are $x_: \in R^{N \times d_x}$, where d_x includes five factors (year, month, day, hour, and demand), the output of the GCN is $H_: \in R^{N \times d_g}$, and the output of RLSTM is $h_: \in R^{N \times d_r}$. Here, d_g and d_r represent the embedding dimensions of the GCN output and RLSTM output, respectively, and N is the number

of regions studied in this chapter.

Decoder Based on the output of the encoder network $\{h_{t-r+1}, \dots, h_t\}$, we can make predictions for the ridesourcing demand at future times $\hat{y} = \{\hat{y}_{t+1}, \dots, \hat{y}_{t+n}\}, \hat{y}_: \in R^{N\times 1}$ with the decoder layer. It is worth noting that our prediction at each moment is based on the output of the encoder and decoder and is implemented through the dynamic spatiotemporal attention method.

For the above O-STEDN, we also add residual connections and layer normalization tricks to the whole network to prevent network information loss and internal covariate shift problems. In the following sections, we describe each step of the proposed method in detail.

4.2.2 GCN

The GCN model constructs a filter in a non-Euclidean space, and the filter is used to extract the spatial features between the central node of the graph and its first-order neighbor nodes; that is, the GCN model is constructed by stacking multiple convolutional layers. As shown in Figure 4-2, assuming that the red node is the central area, the GCN model can obtain the topological relationships between the central area and its surrounding areas, encode the topological structure of the area network and the attributes of the areas, and then obtain the resulting spatial correlation features. In this chapter, we use the GCN model to learn spatial features from historical Ridesourcing demand data.

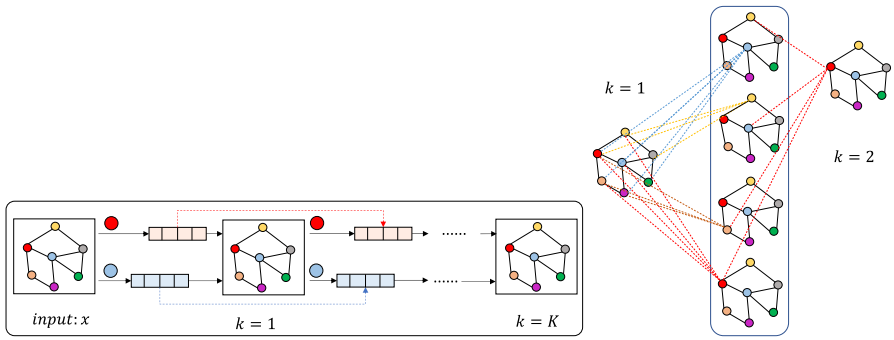

Assuming that the red node is the central area, the blue, yellow, and orange nodes indicate the areas connected to the central area. (a) We use a residual connection to add the input and output of the GCN. (b) We obtain spatial features by obtaining the topological relationships between the central area and the surrounding areas. When $k = 1$, we can extract the spatial features of the red node and the neighboring nodes with depths of 1. When $k = 2$, on the basis of $k = 1$, we can also extract the spatial features of the red node and the nodes with depths of 2.

Figure 4-2 GCN model

For each node $v \in V$, we use H^0 to denote the node initial embeddings, which usually contain the input feature x_i of each node. In a graph G, the key idea of a GCN is to stack K steps in a recursive feature propagation manner to learn node embeddings. For each node v, the feature aggregation step aggregates the embeddings from the graph neighbors N_v and its own embedding H_v^k at the previous layer k. We input the output of feature aggregation into a standard nonlinear transformation layer to generate the $(k+1)$-th layer embeddings of the graph nodes as:

$$H^{(k+1)} = \mathrm{ReLU}(\widetilde{D}^{-0.5}\tilde{A}\widetilde{D}^{-0.5}H^{(k)}) \tag{4.1}$$

After iteratively executing equation (4.1) in each layer with a defined depth K (such as $K = 2$), the final embeddings of graph nodes at a depth K are denoted as $H^{(K)}$, as shown in Fig. 2 (b). To protect the feature information of the original node, we use a residual connection layer to connect the input and output hidden features, as shown in Fig. 2 (a). A GCN model can be expressed as:

$$H^{(k+1)} = \mathrm{LayerNorm}(H^{(k+1)} + W_{res}H^{(k)}) \tag{4.2}$$

where ReLU is a nonlinear activation function (rectified linear unit) and LayerNorm represents layer normalization (Ba et al., 2016). We use $\widetilde{D}^{-0.5}\tilde{A}\widetilde{D}^{-0.5}$ to denote the normalized adjacency matrix with added self-connections, $\tilde{A} = A + I$ is the adjacency matrix of the graph with added self-connections, and I is the identity matrix. $\widetilde{D}$ is the degree matrix of $\tilde{A}$; W^k and W_{res} are the weight matrices of transformation layer and residual connection layer, respectively.

As shown in Figure 4-2, we use a K-depth GCN to extract the spatial correlation features of the historical ridesourcing demand data. Finally, we learn the spatial correlation features of each area node through the GCN and use the learned spatial features as the inputs of the RLSTM network in time series order.

4.2.3 Spatiotemporal Prediction Model

4.2.3.1 RLSTM Encoder

RLSTM is a novel model (proposed by us) for extracting the temporal features of long-term sequence tasks, and it has been successfully used in pollutant concentration prediction-based research tasks (B. Zhang et al., 2021). To better extract the temporal correlation features of ridesourcing demand data, we use RLSTM as the temporal feature extractor. Its structure is shown in Figure 4-3, and the feature extraction steps are described as Figure 4-4.

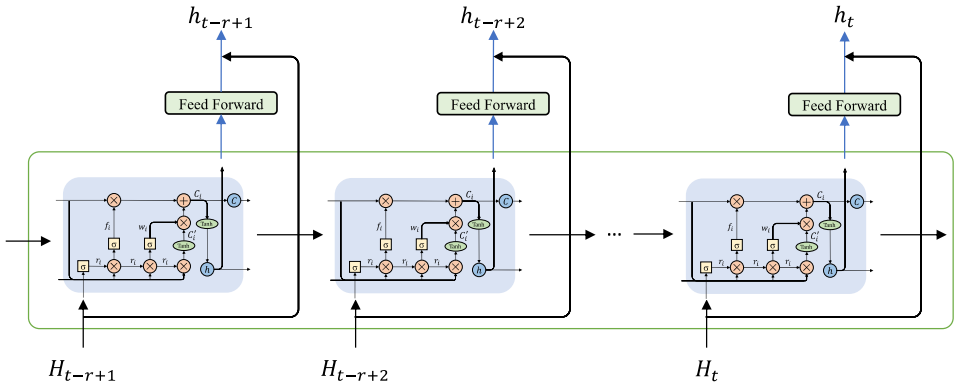

Figure 4-3 The architecture of the RLSTM model.

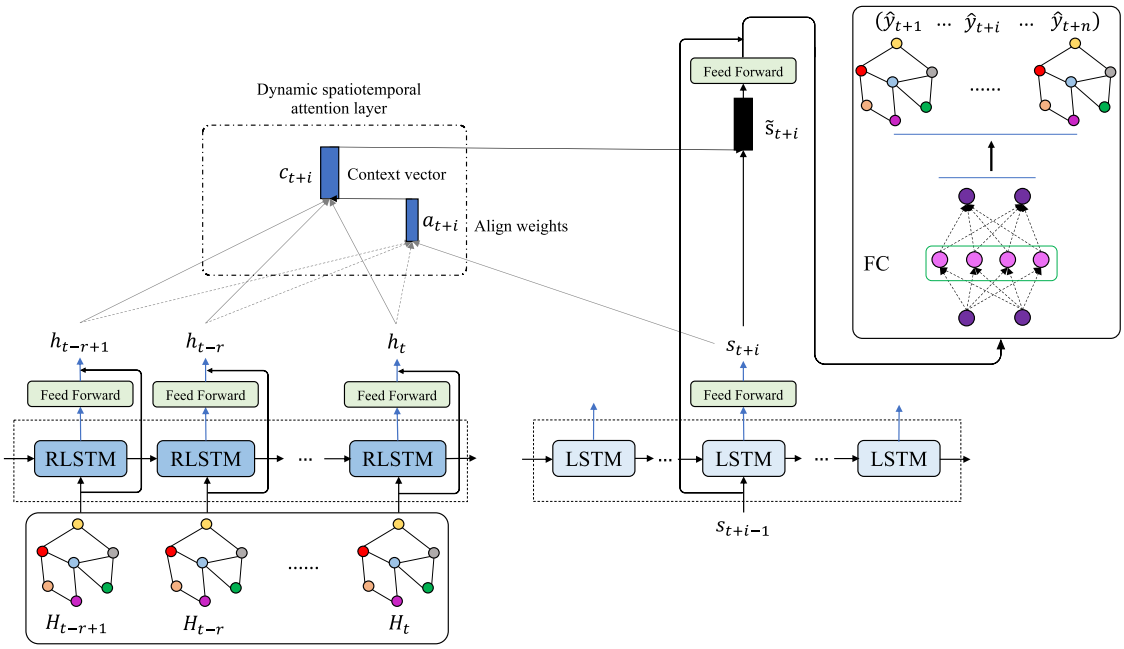

Left, we use the RLSTM network to extract the temporal features. Right, we use LSTM and a dynamic spatiotemporal attention mechanism to complete ridesourcing demand prediction.

Figure 4-4 Spatiotemporal prediction model

1) We use a read gate to extract the important information of the input features and adaptively filter out the redundant information in the input variables. The filtering method is similar to an attention mechanism and uses a sigmoid function to weight the input features $[\hat{h}_{t-j-1}, H_{t-j}, c_{t-j-1}]$. The whole weighting process is completed by training the network; a small weight indicates that the importance of the feature information is low, and the weight range is between [0.0, 1.0]. '$\circ$' denotes the Hadamard product. This process is shown in equation (4.3):

$$r_{t-j} = \sigma(W_r[\hat{h}_{t-j-1}, x_{t-j}, c_{t-j-1}] + b_r) \tag{4.3}$$

2) RLSTM uses the sigmoid function as the activation function of the forget gate to forget the feature information with a small contribution in the memory unit c_{t-j-1} according to the output of the read gate r_{t-j} and the current input $[\hat{h}_{t-j-1}, H_{t-j}, c_{t-j-1}]$. By multiplying the output of the memory unit c_{t-j-1} and the forget gate f_{t-j}, part of the memory information is forgotten.

$$f_{t-j} = \sigma(W_f(r_i \circ [\hat{h}_{t-j-1}, H_{t-j}, c_{t-j-1}]) + b_f) \tag{4.4}$$

$$\hat{c}_{t-j} = f_{t-j} \circ c_{t-j-1} \tag{4.5}$$

3) The write gate w_{t-j} is based on the outputs of the read gate r_{t-j} and the input $[\hat{h}_{t-j-1}, H_i, c_{t-j-1}]$ at the current time $t-j$ and selects some important feature information for updating the information of the memory unit $\hat{c}_{t-j}$ at the current time. Therefore, the write gate w_{t-j} updates the memory unit information based on the important features selected by the read gate r_{t-j}, thereby reducing redundant information residuals. This is shown in equations (4.6), (4.7), (4.8), and (4.9):

$$w_{t-j} = \sigma(W_w(r_{t-j} \circ [\hat{h}_{t-j-1}, H_{t-j}, c_{t-j-1}]) + b_w) \tag{4.6}$$

$$c'_{t-j} = Tanh(W_c(r_{t-j} \circ [\hat{h}_{t-j-1}, H_{t-j}, c_{t-j-1}]) + b_c) \tag{4.7}$$

$$c_{t-j} = \hat{c}_{t-j} + w_{t-j} \circ c'_{t-j} \tag{4.8}$$

$$\hat{h}_{t-j} = Tanh(c_{t-j}) \tag{4.9}$$

Finally, the result is the unit state c_{t-j} output at time $t-j$, as shown in equation (9). To prevent network information loss and internal covariate shift, we add residual connections and layer normalization tricks to the RLSTM layer.

$$h_{t-j} = W_s(\text{LayerNorm}(W_c\hat{h}_{t-j} + W_r H_{t-j})) \tag{4.10}$$

In the above, we describe the time feature extraction process of RLSTM in detail. As shown in Figure 4-4, we use the temporal features $\{h_{t-r+1}, \ldots, h_{t-j}, \ldots, h_t\}$ extracted by the encoder at each moment as the inputs of the decoder and dynamic spatiotemporal attention layer for Ridesourcing demand prediction.

4.2.3.2 LSTM Decoder

The ridesourcing demand prediction for the i-th time step is affected not only by the predicted value at the previous time $t+i-1$ but also by all historical spatiotemporal features $h = \{h_{t-r+1}, \ldots, h_{t-j}, \ldots, h_t\}$. To realize the multi-step prediction of ridesourcing demand in the future, we use LSTM as a decoder for prediction purposes. The LSTM input containing the spatiotemporal features is obtained using the method described in the previous section, that is, via a GCN and RLSTM. LSTM is used to extract temporal features from the prediction periods, which is advantageous for processing long-term time dependence problems, and it outputs the final prediction result. Assume that $\bar{c}_{t+i}$ is the cell state, and $\bar{h}_{t+i}$ is the cell output state at time $t+i$. Additionally, i, f and o represent the input gate, forge gate and output gate, respectively. The prediction process of the LSTM at each time series can be expressed by the following formulas:

1) LSTM selectively forgets the feature information of the cell state at time $t+i$:

$$f_{t+i} = \sigma(W_f s_{t+i-1} + W_f \bar{h}_{t+i-1} + W_f \bar{c}_{t+i-1} + b_f) \tag{4.11}$$

$$\bar{c}'_{t+i} = f_i \circ \bar{c}_{t+i-1} \tag{4.12}$$

LSTM selectively forgets the feature information with a small contribution in the memory unit c_{i-1} according to the current input $[\bar{h}_{t+i-1}, s_{t+i-1}, \bar{c}_{t+i-1}]$. By multiplying the outputs of the memory unit c_{t+i-1} and the forget gate f_{t+i}, part of the memory information is forgotten.

2) LSTM selects important information from the input features, which is used to update the state cell:

$$\tilde{c}_{t+i} = tanh(W_{\tilde{c}} \bar{h}_{t+i-1} + W_{\tilde{c}} s_{t+i-1} + W_{\tilde{c}} \bar{c}_{t+i-1} + b_{\tilde{c}}) \tag{4.13}$$

$$i_{t+i} = \sigma(W_i \bar{h}_{t+i-1} + W_i x_{t+i-1} + W_i \bar{c}_{t+i-1} + b_i) \tag{4.14}$$

$$c_{t+i} = \bar{c}'_{t+i} + i_{t+i} \circ \tilde{c}_{t+i} \tag{4.15}$$

In the above equations, $\tilde{c}_{t+i}$ represents the initial feature used to update the information of the memory unit c'_i. The function of the input gate i_{t+i} is mainly to assign different weight values to the elements in each dimension of $\tilde{c}_{t+i}$ and to select the important feature information for updating the memory unit $\bar{c}'_{t+i}$.

3) Finally, the LSTM output is determined:

$$o_{t+i} = \sigma(W_o \bar{h}_{t+i-1} + W_o s_{t+i-1} + W_o \bar{c}_{t+i-1} + b_o) \tag{4.16}$$

$$s_{t+i} = W_s(o_{t+i} \circ tanh\,(\bar{c}_{t+i})) \tag{4.17}$$

The output gate o_i is based on the input $[\bar{h}_{t+i-1}, s_{t+i-1}, \bar{c}_{t+i-1}]$ at the current time and selects some important feature information from the memory unit $\bar{c}_{t+i}$ to be output at the current time. The output of the LSTM is s_{t+i}, and we input the results of the calculation into the dynamic spatiotemporal attention layer and fully connected layer to generate the predicted value.

4.2.3.3 Dynamic Spatiotemporal Attention Decoder

According to the above, ridesourcing demand is a spatiotemporal prediction problem; that is, the demand prediction at time $t+i$ in the future is affected by a period of time in the past. The ridesourcing condition at a location is related to the previous observations of itself and its neighbors, and the correlations vary nonlinearly over the time steps. To model these properties, we design an attention mechanism to adaptively model the nonlinear correlations between different time steps, that is, dynamic spatiotemporal attention, as illustrated in Figure 4-3. Note that ridesourcing demand prediction is influenced by both the spatial dimension and time dimension. For example, a ridesourcing demand that occurs during the morning peak hours may affect the ridesourcing demand in the future, or a ridesourcing demand at a certain location may affect the ridesourcing demands of itself and its neighbors. Therefore, we consider both the spatial dimension and time dimension to measure the correlations between different time steps.

Specifically, the dynamic spatiotemporal attention at time step $t+i$ of the decoding stage and the hidden state s_{t+i} output by the LSTM layer of the decoder are first taken as inputs. The goal is then to derive the context vector c_i, which captures related historical spatiotemporal feature information to help predict the ridesourcing demand y_{t+i}. Simply, an attentional hidden state $\tilde{s}_{t+i}$ is generated according to the hidden state s_{t+i} and the context vector c_{t+i}, and then the attentional vector $\tilde{s}_{t+i}$ is fed to the fully connected layer to generate the prediction values. We also add residual connections and layer normalization tricks to the decoder layer to prevent network information loss and internal covariate shift, as shown in the following equations:

$$\tilde{s}_{t+i} = tanh(W_c[c_{t+i}, s_{t+i}]) \tag{4.18}$$

$$y_{t+i} = W_s(\text{LayerNorm}(W_{\tilde{s}}\tilde{s}_{t+i} + W_r s_{t+i-1})) \tag{4.19}$$

The idea of dynamic spatiotemporal attention is to consider all the historical spatiotemporal features of the encoder when deriving the context vector c_{t+i} (Cheng et al., 2021). The alignment weight a_{t+i}, whose size equals the number of input time

steps of the encoder, is derived by comparing the current hidden state s_{t+i} with each spatiotemporal feature h_{t-j}. Formally, the correlation between time steps $t-j$ and $t+i$ is defined as:

$$a_{t+i}(h_{t-j}) = \frac{exp(h_{t-j}^{\mathrm{T}} s_{t+i})}{\sum_{j=t-r+1}^{t} exp(h_{t-j}^{\mathrm{T}} s_{t+i})} \tag{4.20}$$

$$c_{t+i} = a_{t+i}{}^{\mathrm{T}}\{h_{t-r+1}, \ldots, h_{t-j}, \ldots, h_t\} \tag{4.21}$$

With dynamic spatiotemporal attention, at each time step $t+i$, the model infers an aligned weight a_{t+i} dynamically based on the current hidden state s_{t+i} of the decoder output and all historical spatiotemporal features $h = \{h_{t-r+1}, \ldots, h_{t-j}, \ldots, h_t\}$. A context vector c_i is then computed as a weighted sum of a_{t+i} and all the historical spatiotemporal features, and the prediction process has been introduced above.

4.2.3.4 Loss Function

In the O-STEDN model, a loss function is used to measure the degree of inconsistency between the predicted value $\hat{y}$ and the real value y. The loss function is given in (4.22):

$$loss = \sqrt{\frac{\sum_{i=1}^{n}(y_i - \hat{y}_i)^2}{n}} + \frac{\lambda}{2}\|W\|_2^2 \tag{4.22}$$

where n is the length of the predicted sequence, y_i denotes the observed value, $\hat{y}_i$ is the predicted value, λ is the regularization parameter, and W denotes all learnable parameters in the O-STEDN.

4.3 Experiments

4.3.1 Data Description

The study area, Chengdu, is divided into 162 census tracts based on administrative boundaries, which guarantees the integrity of the districts, as shown in Figure 4-5. Ridesourcing order data are obtained from the DiDi platform through the DiDi GAIA Initiative (DiDi Chuxing, 2018b). The dataset includes the complete order data of DiDi Express and DiDi Premier Services in Chengdu, China, from November 1st to November 30th, 2016. The fields of the order dataset are the order ID, start timestamp, end timestamp, and pick-up and drop-off locations. We clean the data and remove outliers such as order data with travel times less than 120 s or greater than 7200 s. Then,

the ridesourcing demand for every 15 min of each census tract can be calculated.

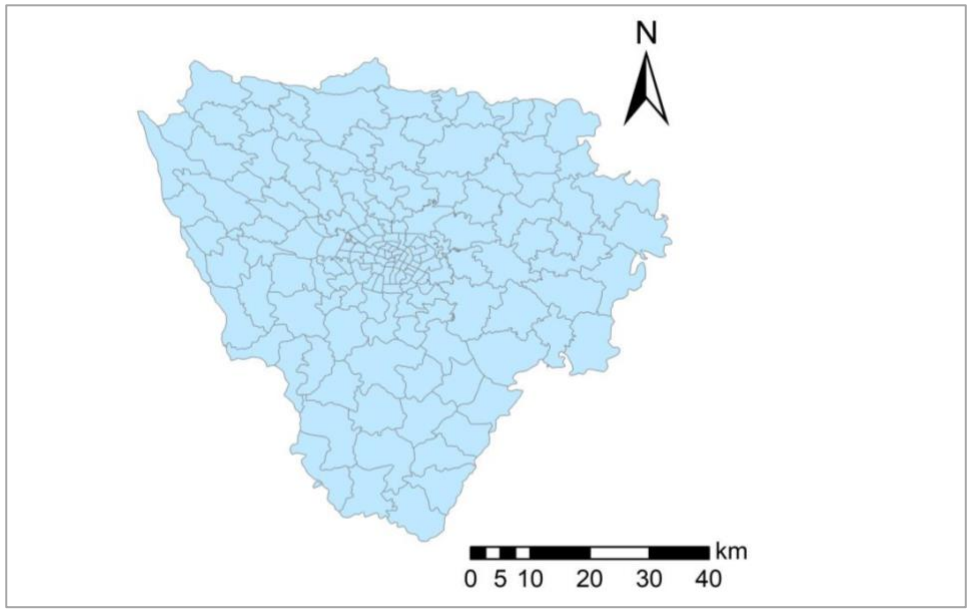

Figure 4-5 Study area

4.3.2 Baselines and Metrics

We compare our model with the following prediction methods:

HA: The HA model uses the average value of the historical data at the same time every day as the predicted value at the same time in the future prediction task (L. Liu et al., 2019).

ARIMA: This is a traditional time series prediction method that combines moving average and autoregressive components to model historical time series data (Williams & Hoel, 2003).

RNN: This network is mainly used to analyze time series data and has achieved good performance in various research fields (Liu & Shoji, 2019).

GRU: This is an extension of an RNN that introduces a gating mechanism to solve the problem of gradient disappearance and is widely used for complex time series prediction tasks, such as short-term wind speed interval prediction (C. Li et al., 2019).

LSTM: This network can learn long-term dependencies by using a gating mechanism to store information; that is, it can be trained to store all relevant information to predict specific future results. LSTM is an advanced sequence learning model that has been used in research on demand forecasting tasks (Kontou et al., 2020; Xu et al., 2017).

DMVST-Net: This network uses LSTM and CNN networks as feature extractors

to model spatial and temporal relationships (Yao et al., 2018).

ST-MGCN: This network encodes the non-Euclidean pairwise correlations among regions into multiple graphs and then uses an RNN and a GCN to model these correlations (Geng et al., 2019).

GCN and RNN (GCN-RNN): This combined approach uses a GCN and an RNN to model spatial and temporal relationships(Lv et al., 2019).

DTCNN: This network contributes a novel dynamic transition-based GCN method that is effective for traffic demand prediction (Du et al., 2020).

MLRNN: This network develops cluster-level and global-level prediction modules to extract intracluster and intercluster features, respectively (C. Zhang et al., 2021).

MultiConvLSTM: This approach uses the ConvLSTM network and considers temporal and spatial correlations to predict future travel demands and on-demand flows (Chu et al., 2019).

ST-ED-RMGC: This network uses RMGC to encode spatially dependent features, uses LSTM to encode temporal features, and finally uses RMGC as a decoder to predict the origin-destination ride-sourcing demand at the next moment (Ke et al., 2021).

To evaluate the prediction performance of the O-STEDN model, we use three metrics to evaluate the difference between the observed values y_i and the prediction values $\hat{y}_i$: the root mean square error (RMSE), mean absolute error (MAE), and coefficient of determination (R^2). High R^2 and low RMSE and MAE values indicate more accurate prediction performance. The experimental metrics are calculated by the following formulas:

$$RMSE(y,\hat{y}) = \sqrt{\frac{1}{T}\sum_{i=1}^{T}(y_i - \hat{y}_i)^2} \tag{4.23}$$

$$MAE(y,\hat{y}) = \frac{1}{T}\sum_{i=1}^{T}|y_i - \hat{y}_i| \tag{4.24}$$

$$\mathrm{R}^2(y,\hat{y}) = 1 - \frac{\sum_i(\hat{y}_i - y_i)^2}{\sum_i(y_i - \bar{y})^2} \tag{4.25}$$

where T is the test set size.

4.3.3 Experimental Settings

4.3.3.1 Training

The hyperparameters in our O-STEDN model are determined during the training

process; that is, the best-performing model is selected according to the RMSE on the validation set. We manually specify the hyperparameter ranges of the learning rate {0.01, 0.005, 0.003, 0.001}, dropout rate {0.0, 0.1, 0.2, 0.3, 0.4, 0.5}, regularization parameter {0.1, 0.01, 0.001, 0.0001} and decay rate {0.99, 0.95, 0.90, 0.85}. For the O-STEDN model, we find that the following settings work well: the dropout is set to 0.5, the decay rate is set to 0.99, the regularization parameter is set to 0.0001 and the learning rate is set to 0.001. When using the comparison models, these settings still work well. We implement the O-STEDN in TensorFlow and train all models using the stochastic gradient descent (SGD) optimizer with a batch size of 32.

4.3.3.2 Evaluation

The validation set used in this chapter is closely related to the training stage, and after each epoch, the RMSE, MAE, and R^2 obtained by the prediction model on the validation set are calculated. Therefore, the optimal model is selected based on the model error calculated on the validation set. The specific process is as follows: for each experiment, the number of epochs is 200. After training for an epoch, we test the trained model on the validation set. If the RMSE of the prediction model on the validation set decreases, we update and save the model parameters. After many parameter adjustments and experiments, when the prediction effect of the prediction model on the validation set is optimal, the training process ends. Finally, the prediction result is obtained by iterating all the samples in the test set. In all experiments, we use an early-stop mechanism; that is, the number of early-stop rounds and the maximum number of epochs are set to 10 and 200, respectively.

4.3.3.3 Model Parameters

After multiple training and evaluation steps, we determine the final model framework parameters. As shown in Table 4-1, the number of layers, number of nodes, output size, and related hyperparameters of the O-STEDN model are listed in detail. The implementation codes of our proposed O-STEDN model and the comparison models are open source; please refer to our personal GitHub homepage (https://github.com/zouguojian/traffic-demand-prediction).

Table 4-1 Model parameters

Layer name	Output Size	Parameters	Values
GCN	128	layer nodes × number of layers layer nodes × number of layers k	128×1 128×1 2
RLSTM	128	layer nodes × number of layers	128×1
LSTM	128	layer nodes × number of layers	128×1
Dynamic Spatiotemporal Attention	128	layer nodes × number of layers	128×1
Feed Forward	128	layer nodes × number of layers	128×1
Fully Connected Layer	128 64 1	layer nodes × number of layers	128×1 64×1 1×1
-	-	Batch size	32
-	-	Dropout	0.5
-	-	Decay rate	0.99
-	-	Learning rate	0.001
-	-	Epoch	200
-	-	λ	0.0001
-	-	Training method	SGD

4.4 Comparative results and discussions

4.4.1 Single step prediction

Table 4-2 lists the 120-15 min ridesourcing prediction performance of our proposed O-STEDN model and the baseline models. The performance of the HA and ARIMA is far inferior to that of other methods, which also reflects the difficulty of ridesourcing demand prediction. The MAEs are 1.674 and 1.159, respectively. The reason why the accuracies of the RNN, GRU and LSTM are better than those of the two traditional methods is that the former approaches have the advantage of extracting time series features and are good at associating input time series features. The MAEs are 0.931, 0.914, and 0.906, respectively. The prediction performance of DMVST-Net is inferior to that of the GCN-RNN, DTCNN and GCN-LSTM, which shows the shortcomings of using a CNN to extract discrete spatial features; that is, it is difficult to extract the spatial correlations of ridesourcing demand data among different regions. The reason for the poor effect achieved by the ST-MGCN model based on the RNN-GCN may be that we use a single graph, that is, a regional position relationship graph, without considering the problem of regional similarity; second, in the process of extracting time series features, the influence of spatial factors is ignored. Therefore, the prediction performance of the GCN-RNN is significantly better than that of the ST-

MGCN model based on an RNN and a GCN, which also verifies our conjecture regarding the poor prediction performance of the ST-MGCN. The performance of the DTCNN, MLRNN, and MultiConvLSTM models is relatively prominent among the baseline models, and the optimal MAE, RMSE, and R^2 values reach 0.863, 1.491, and 0.928, respectively. The disadvantages of MultiConvLSTM are that the model is too complex, a CNN is used as the basis for spatial feature extraction, and the training and inference times are extremely long, which is not suitable for practical applications. The GCN solves the problem faced by the CNN network; that is, it can effectively extract the spatial correlation features of ridesourcing demand data among discrete regions in non-Euclidean space. Therefore, among the baseline models, the DTCNN model based on a GCN and a GRU has the best prediction effect.

Our model takes the spatiotemporal correlation features of ridesourcing demand data among discrete regions, the improvement of the temporal and spatial feature extraction models, the residual connections used to prevent the loss of feature information, and the influence of historical ridesourcing demand data on the prediction periods into account. Therefore, the prediction performance of the GCN-LSTM, GCN-RLSTM-LSTM, GCN-RLSTM-LSTM-Attention, and O-STEDN models we proposed in this chapter is better than that of all baseline models. Moreover, the three metrics (MAE, RMSE, and R^2) have obvious scoring advantages: the MAEs are 0.867, 0.846, 0.807, and 0.794, respectively; the RMSEs are 1.467, 1.445, 1.420, and 1.409, respectively; the R^2 values are 0.930, 0.932, 0.935, and 0.936, respectively. Compared with the best performance among the baseline models, our proposed O-STEDN method exhibits relative improvements of 8.0% (MAE), 5.5% (RMSE), and 0.9% (R^2).

Table 4-2 Performance comparison of all models for the [120-15 min] task

Model	MAE	RMSE	R^2
HA	1.674	2.743	0.791
ARIMA	1.159	1.668	0.862
RNN	0.931	1.543	0.923
GRU	0.914	1.531	0.924
LSTM	0.906	1.535	0.924
DMVST-Net	0.890	1.528	0.924
ST-MGCN	0.899	1.527	0.925
GCN-RNN	0.877	1.498	0.927
DTCNN	0.863	1.491	0.928
MLRNN	0.886	1.525	0.925
MultiConvLSTM	0.879	1.512	0.926
GCN-LSTM	0.867	1.467	0.930
GCN-RLSTM-LSTM	0.846	1.445	0.932
GCN-RLSTM-LSTM-Attention	0.807	1.420	0.935
O-STEDN	**0.794**	**1.409**	**0.936**

4.4.2 Multi-step prediction

The existing demand forecasting research mainly focuses on single-step forecasting for the next time, which may not be sufficient to meet the needs of actual application scenarios. In the introduction section, we introduce the significance of demand forecasting, so the significance of multi-step demand forecasting is self-evident. Table 4-3 lists the multi-step ridesourcing demand predictions for multiple periods in the future. Due to the limitations of the baseline models, we choose several state-of-the-art models with better performance and suitability for multi-step prediction for the experimental comparison. We can see that for multi-step prediction tasks, our proposed O-STEDN model performs best compared with all baseline models. For the multi-step prediction task [120-45 min], compared with the optimal baseline model (DTCNN), the MAE is improved by 8.8%, the RMSE is improved by 8.1%, and the R^2 is improved by 1.3%. For the multi-step prediction task [120-90 min], compared with the optimal baseline model (DTCNN), the MAE is improved by 12.6%, the RMSE is improved by 11.0%, and the R^2 is improved by 2.0%. Although the difficulty of prediction continues to increase with the number of time steps, the error of our proposed O-STEDN model is still smaller than that of all baseline models, and the prediction results are satisfactory.

Table 4-3 Model comparison for the [120-45 min] and [120- 90 min] tasks

Model	[120-45 min]			[120-90 min]		
	MAE	RMSE	R^2	MAE	RMSE	R^2
RNN	0.986	1.658	0.912	1.184	1.966	0.877
GRU	0.977	1.680	0.910	1.173	2.046	0.866
LSTM	0.930	1.623	0.916	1.027	1.807	0.896
DMVST-Net	0.919	1.582	0.920	0.986	1.688	0.909
GCN-RNN	0.907	1.564	0.921	0.971	1.680	0.910
DTCNN	0.904	1.561	0.922	0.969	1.672	0.911
MLRNN	0.933	1.593	0.919	0.986	1.686	0.910
MultiConvLSTM	0.909	1.566	0.921	0.989	1.686	0.909
O-STEDN	**0.824**	**1.435**	**0.934**	**0.847**	**1.488**	**0.929**

Figure 4-6 shows the multistep demand prediction results of the [120-45 min] task obtained using the historical data from 11:15-13:15 to predict the travel demand in the next three time periods, 13:15-13:30, 13:30-13:45, and 13:45-14:00. The multi-step demand prediction results are still accurate compared to the single-step demand prediction results. In general, we can identify hot census tracts with high ridesourcing demand and cold census tracts with low ridesourcing demand. In addition, the

prediction result for the first time period (13:15-13:30) is more accurate than that of the other two time periods.

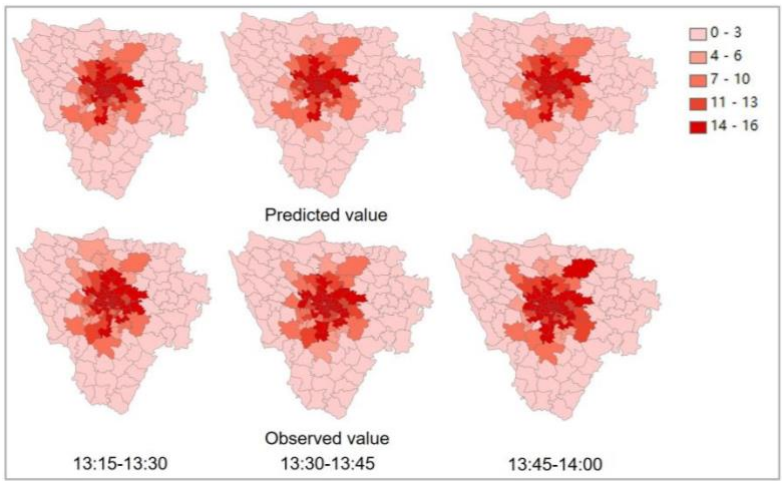

Figure 4-6 The multi-step demand prediction results for the [120-45 min] task.

Figure 4-7 shows the multi-step demand prediction results of the [120-90 min] task obtained using the historical data from 11:15-13:15 to predict the travel demand in the next six time periods, 13:15-13:30, 13:30-13:45, 13:45-14:00, 14:00-14:15, 14:15-14:30, and 14:30-14:45. The prediction accuracy on the [120-90 min] task decreases slightly compared with that on the [120-45 min] task. However, the accuracy is still high in terms of predicting hot census tracts with high ridesourcing demand and cold census tracts with low ridesourcing demand.

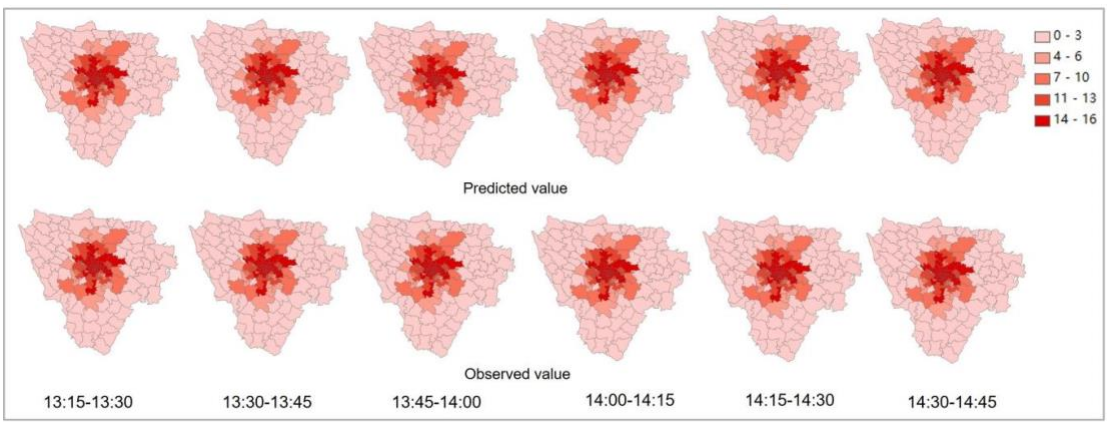

Figure 4-7 The multi-step demand prediction results for the [120-90 min] task.

4.4.3 Discussions

4.4.3.1 Effect of Each Component

As shown in Table 4-2, we compare our proposed O-STEDN model and its variants, GCN-LSTM, GCN-RLSTM-LSTM, and GCN-RLSTM-LSTM-Attention, and we can obtain the following conclusions:

1) First, compared with the optimal baseline model (the DTCNN), GCN-LSTM has better prediction performance. The RMSE improvement is 1.6%, and the R^2 improvement is 0.2%. This shows that the prediction model combining a GCN and LSTM has a better ability to extract spatiotemporal features than a GCN and a GRU.
2) Second, on the basis of GCN-LSTM, we replace the time series feature extractor LSTM in the encoder with RLSTM. As a result, the prediction performance of the model is greatly improved. Compared with DTCNN, the MAE improvement is 2.0%, the RMSE improvement is 3.1%, and the R^2 improvement is 0.4%. The results show that compared with LSTM, the advantage of using RLSTM to extract time series features is more obvious.
3) Third, based on the GCN-RLSTM-LSTM model, GCN-RLSTM-LSTM-Attention uses a global attention mechanism to associate the temporal and spatial features extracted from each moment of GCN-RLSTM with the current prediction value of the decoder. Compared to the DTCNN, the MAE improvement is 6.5%, the RMSE improvement is 4.8%, and the R^2 improvement is 0.8%. The results show that when paying attention to the correlations between the temporal and spatial features of the input data and the current prediction value, that is, considering the impact of historical data on the current prediction, the prediction performance of our proposed model is greatly improved.
4) Finally, we consider the loss of feature information and internal covariate shift on the basis of GCN-RLSTM-LSTM-Attention, so we add residual connections and layer normalization to both the encoder layer and the decoder layer. The experimental results also verify our conjecture, and the prediction performance of the O-STEDN model is improved again. Compared to the DTCNN, the MAE improvement is 8.0%, the RMSE improvement is 5.5%, and the R^2 improvement is 0.9%. This also proves that in the processes of

feature extraction and prediction, the prediction model may lose feature information and incur internal covariate shift problems. Removing and adding effective processing methods in advance can eliminate this phenomenon and can also improve the final prediction accuracy of the model.

Based on the above analysis, we summarize the functions and contributions of each part of the proposed O-STEDN model. Through the comparison, we combine the advantages of all variants, highlighting the predictive performance of the O-STEDN model. Therefore, for the short-term ridesourcing demand prediction task, the proposed O-STEDN model is accurate and plays a positive role.

4.4.3.2 Effects of the GCN Model Parameters

To study the influence of the depth of the regional node in the GCN on the prediction results, we evaluate the O-STEDN model by changing the important hyperparameter k, that is, the number of layers k in the graph convolution. To select the best hyperparameter k, we conduct tests on three tasks: 120-15, 120-45, and 120-90 min. Table 4 shows the performance of the O-STEDN on the three tasks on the test set and gives the values of the three indicators, MAE, RMSE and R^2. We observe that as the number of layers k increases, the error first decreases and then increases, and the coefficient of determination first increases and then decreases. Through observation, we find that when k is equal to 2, the O-STEDN model performs best on each task. To observe the influence of k on the O-STEDN model more intuitively, we use a visual form to demonstrate the performance of the model, as shown in Figure 4-7.

Table 4-4 The comparison of the results obtained on the three tasks with different values of k

k	Target task (min)	MAE	RMSE	R^2
1	[120- 15]	0.837	1.431	0.932
	[120- 45]	0.875	1.470	0.931
	[120- 90]	0.880	1.540	0.924
2	[120- 15]	0.794	1.409	0.936
	[120- 45]	0.824	1.435	0.934
	[120- 90]	0.847	1.488	0.927
3	[120- 15]	0.806	1.417	0.935
	[120- 45]	0.832	1.499	0.932
	[120- 90]	0.939	1.657	0.918
4	[120- 15]	0.806	1.433	0.930
	[120- 45]	0.864	1.536	0.925
	[120- 90]	0.987	1.709	0.907
5	[120- 15]	0.848	1.449	0.930
	[120- 45]	0.935	1.620	0.916
	[120- 90]	1.005	1.712	0.907

From Figure 4-8, we can see that the MAE and RMSE values are minimal when k is equal to 2, and R^2 is maximal when k is equal to 2. A larger number of layers k will enable the O-STEDN model to capture more regional spatial correlation, but it will cause excessive model complexity and overfitting problems. In addition, we can also find that for a 120-15 min prediction task conducted in a short period of time, the error changes with increasing k, and the magnitude of the change is relatively small. Then, for a 120-90 min prediction task conducted in a long period of time, the error increases sharply with increasing k. Combined with the results in Table 4, this also reflects the difficulty of the multi-step prediction task. However, compared with the baseline models, our proposed O-STEDN model still achieves satisfactory performance. This also proves the significance of our O-STEDN model and its value in practical future applications.

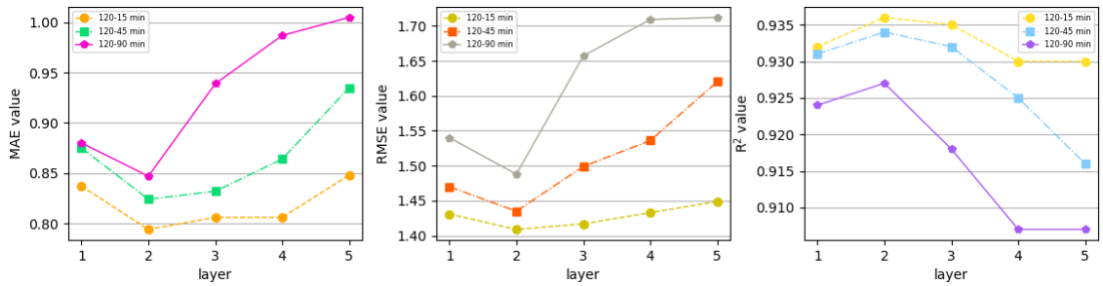

Figure 4-8 The performance of the O-STEDN model as the number of layers k in the graph convolution changes on the 120-15, 120-45, and 120-90 min ridesourcing demand prediction tasks.

4.5 Conclusions

To the best of our knowledge, this is the first time that multi-step ridesourcing demand prediction has been performed based on integral administrative census tracts at the city scale. In this chapter, we propose a new ridesourcing demand prediction framework, the O-STEDN, which implements a novel GCN-RLSTM-LSTM-Attention model. For the encoder layer, we use a combination of a GCN and an RLSTM network as the spatiotemporal feature extractor. The GCN overcomes the shortcomings of a traditional CNN and can deeply extract the spatial correlation features of discrete regions in non-Euclidean space. RLSTM can effectively extract and memorize time-related features. For the decoder layer, we use an LSTM model and a dynamic spatiotemporal attention mechanism to associate historical spatiotemporal features with the current prediction. Furthermore, we add residual connections and layer

normalization tricks in both the encoder layer and the decoder layer to prevent the loss of feature information and internal covariate shift problems.

The experimental results show that the proposed framework outperforms state-of-the-art models for both single-step demand prediction and multi-step prediction. For the single-step prediction task [120-15 min], the prediction performance is greatly improved. Specifically, the MAE is improved by 8%, the RMSE is improved by 5.5%, and the R^2 is improved by 0.9%, even compared with the optimal baseline model (DTCNN). For the multi-step prediction task [120-45 min], compared with the optimal baseline model (DTCNN), the MAE is improved by 8.8%, the RMSE is improved by 8.1%, and the R^2 is improved by 1.3%. For the multi-step prediction task [120-90 min], compared with the optimal baseline model (DTCNN), the MAE is improved by 12.6%, the RMSE is improved by 11.0%, and the R^2 is improved by 2.0%.

The proposed prediction framework can be applied not only to demand prediction problems but also to other spatiotemporal-related problems; it could provide an accurate reference for both transportation network companies and policy makers in advance. Transportation network companies can dispatch vehicles more effectively to improve the occupancy rate and decrease the travel cost of the whole system. Governments can also dynamically manage traffic demand according to demand prediction. In the next chapter, we will further study how to optimize the ridesourcing system with shared autonomous vehicles.

Chapter 5 Optimizing ridesourcing system based on a shareability network

HIGHLIGHTS

1) The percentage of cost savings can be increased from 1.22% up to 18.47%
2) The percentage of shared trips can be increased from 7.85% up to 90.69%
3) The percentage of time savings can reach 25.75% from 2.38%
4) The average delay can be reduced from 9.86 min to 4.76 min
5) Passengers wait less time on average

5.1 Introduction

Ridesourcing is an attractive option for many travelers who do not own a vehicle. However, there are some debates claiming that ridesourcing services result in an estimated 69 percent more climate pollution on average than the trips they displace (Union of Concerned Scientists, 2020). They are threatening the development of public transport services and triggering major market disruption in many countries around the world.

Ridesplitting, a new shared mobility service, is a more sustainable travel mode for improving traffic efficiency and reducing traffic congestion and air pollution problems. Policy makers have realized the benefits of ridesplitting services and encouraged ridesourcing companies to launch ridesplitting services for passengers.

The primary objective of this chapter is to explore the potential opportunity and evaluate the benefits of ridesplitting using an empirical ridesourcing dataset during rush hours in the city of Chengdu, China. More specifically, this chapter includes the following three tasks: First, we calculate the actual level of ridesplitting and analyze its current characteristics of ridesplitting. Second, we compare the potential of ridesplitting under three different objectives to evaluate the benefits of ridesplitting, namely, reduced fleet size, time savings, and cost savings. Third, we analyze the reasons for the gap between the potential of ridesplitting and the actual level of

ridesplitting in the real world.

To our knowledge, most studies have replaced taxi services with ridesplitting services to explore the potential of ridesplitting services. However, taxi services are regarded as premium services. Passengers using taxi services are more concerned about the value of their time and privacy. Therefore, most taxi passengers are not willing to use ridesplitting services. To fill this gap, this chapter aims to evaluate the potential of ridesplitting services on a city scale using empirical ridesourcing data. The proposed ridesplitting service can not only mitigate air pollution but also take passenger delays into consideration to guarantee the ridesplitting service quality. The findings could help ridesourcing companies improve their existing ridesplitting services. Furthermore, this chapter can provide enlightening insights to policy makers to provide a better understanding of the potential of ridesplitting and its related environmental implications to support better planning of low-carbon transport and urban transport management.

The remainder of this chapter is organized as follows. Section 5.2 analyzes the characterization of the present ridesourcing services. A potential ridesplitting identification algorithm based on a shareability network is described in section 5.3. Section 5.4 analyzes the results in detail and further discusses the insights and recommendations on how to increase the adoption of ridesplitting services. Section 5.5 designs a new ridesourcing system with connected and autonomous vehicles based on blockchain for the future urban mobility. The final section 5.6 summarizes the contributions and interesting findings.

5.2 Data and variables

5.2.1 Trip Data

The trip data used in this chapter are from the DiDi GAIA Initiative, DiDi's open data project (DiDi Chuxing, 2018b). The dataset contains the complete order data of DiDi Express and DiDi Premier, two of DiDi Chuxing's core ridesourcing services, in the city of Chengdu, China, from November 1-30, 2016.

According to a previous study (W. Li et al., 2019) on this dataset, 13:00-15:00 is the rush hour for using ridesourcing services. This research only concentrates on rush hours. The extracted order dataset contains over 1.04 million trips, including fields

such as OrderID, start and end timestamps, and pick-up and drop-off locations (sample data are shown in Table 5-1).

Table 5-1 Order Data Structure

Field	Type	Sample	Comment
OrderID	String	mjiwdgkqmonDFvCk3ntBpron5mwfrqvI	Anonymized
Ride Start Timestamp	String	1501581031	Unix timestamp, in seconds
Ride End Timestamp	String	1501582195	Unix timestamp, in seconds
Pick-up Longitude	String	104.11225	GCJ-02 Coordinate System
Pick-up Latitude	String	30.66703	GCJ-02 Coordinate System
Drop-off Longitude	String	104.07403	GCJ-02 Coordinate System
Drop-off Latitude	String	30.6863	GCJ-02 Coordinate System

5.2.2 Map Data

Data from www.openstreetmap.org has been used to reproduce the street network of Chengdu and the central city zone of Chengdu has been chosen as the research area; see Figure 5-1. A network in which nodes are intersections and links are roads connecting those intersections has been built. The network contains 7,783 nodes and 13,087 links. We retain trips with durations of 1 minute to 120 min, thus discarding outliers. After the preprocessing and filtering phase, more than 97% of the trips are kept for further analysis. We match the pick-up and drop-off locations with the intersection nodes from the trip dataset. We compute the travel time between all origins and destinations using the average speed on road segments retrieved from Baidu Map.

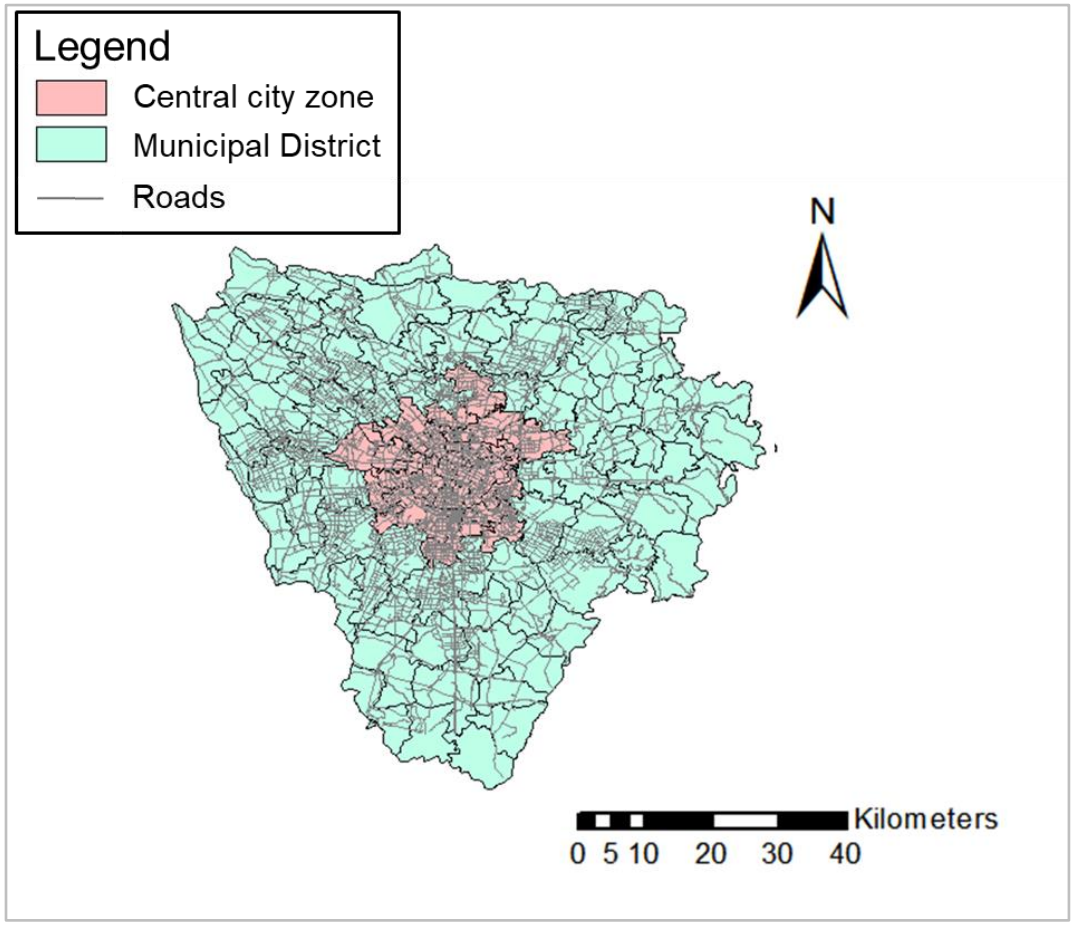

Figure 5-1 Research area in Chengdu

5.2.3 Definitions and Notations

The proposed model has the following assumptions, and the related notations are shown in Table 5-2.

1) All passengers in the ridesourcing data set are willing to choose a ridesplitting service.
2) All vehicles obey to the dispatching schedules completely.
3) More than 90% of ridesplitting trips consist of only two shared rides because of DiDi Chuxing's rule that a driver is only allowed to accept at most two ride requests simultaneously. In addition, the number of passengers for each shared ride is limited to no more than two. Therefore, it is reasonable to assume that at most two trips can be combined in modeling.

Table 5-2 Notations of all variables

Notation	**Comment**
$T = \{T_1, T_2, \ldots, T_n\}$	Trip set
$T_{i,j}$	Shared trips T_i and T_j
$T.o$, $T.d$	Pick-up, drop-off locations of the trip
t_i^s, t_i^e	Desired pick-up, drop-off times of the trip
t_i^o, t_i^d	Actual pick-up, drop-off times for the trip after ridesplitting
$t(i,j)$	Travel time between node i and node j
δ	Time horizon of the search time for ridesplitting
Δ	Maximum tolerable delay for passengers
$L = {}_{i,j\in\{1,2\ldots,n\}}L(T_{i,j})$	Link set that represents feasible ridesplitting
S	Shareability network
M	Matching of the shareability network S
M_{max}	Maximum weighted matching of the shareability network S
S'	Intersection graph
$V = \{V_1, V_2, \ldots, V_n\}$	Node set of intersection graph **S'**
R	Independent set of intersection graph **S'**
R_{max}	Maximum weighted independent set of intersection graph **S'**
$Delay\ (T_i)$	Delay for T_i (min)
$V_{delay\text{-}Ti}$	Value of the delay (T_i)

5.3 Methodology

We build the model based on the shareability network derived from The Senseable City Laboratory of MIT (Santi et al., 2014). We define three performance indicators, which are the percentages of shared trips, time savings and cost savings.

A hybrid iterative local search algorithm based on a variable neighborhood depth search algorithm (ILS-VND), which has the characteristics of fast calculation, good solution quality and high stability, outperforms other heuristic algorithms in relation to the maximum weight independent set problem (Nogueira et al., 2018). Therefore, ILS-VND is used to find the optimal potential ridesplitting solutions under each of the three objectives. We find the best potential ridesplitting solution of the three and quantify the gap between the actual level and potential opportunity. This chapter transforms the ridesplitting assignment problem into a maximum weight independent set problem and solves it with the ILS-VND algorithm. This method is effective in addressing the large-scale dynamic ridesplitting assignment problem through real-time computation.

5.3.1 Model Description

Let $S = (T, L)$ be the shareability network defined as follows. Node set $T = \{T_1, \dots, T_n\}$ corresponds to the set of all trips. If trip nodes T_i and T_j can be combined, the shared trip can be denoted as $T_{i,j}$, and we can add link $L(T_{i,j})$ to connect the two nodes. We define link set $L = {}_{i,j\in\{1,2\dots,n\}}L(T_{i,j})$ as all feasible trips for ridesplitting.

Whether trips T_i and T_j can be combined or not depends on the spatial/temporal properties of the two trips and on an upper bound Δ. If the waiting time and delay time after ridesplitting are both less than the upper bound Δ for passengers, this means that the pick-up times and drop-off times of the 2 trips after ridesplitting are within the given time window, as shown in Figure 5-2 below, and the 2 trips can be regarded as feasible for ridesplitting and be added to the link set.

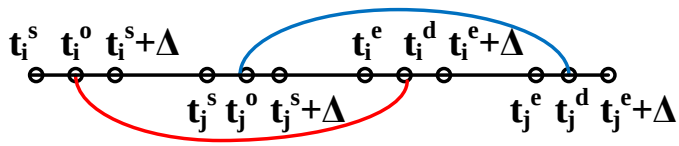

Figure 5-2 Ridesplitting trip example

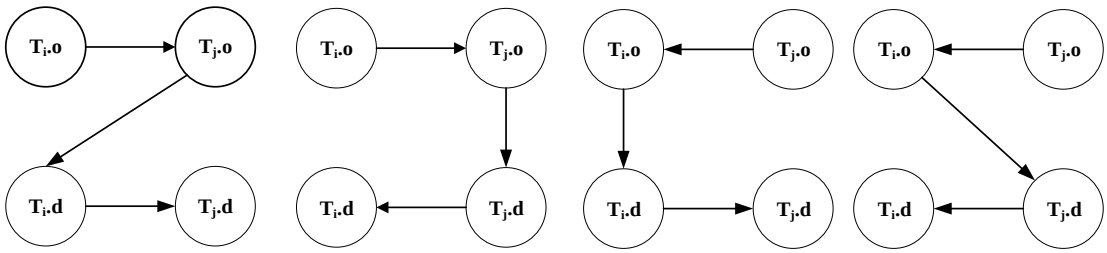

Figure 5-3 Four situations of ridesplitting with two rides

As shown in Figure 5-3, there are 4 situations for ridesplitting with two arbitrary trips, T_i and T_j. If any of the above 4 situations satisfies the time window constraint, T_i and T_j can be combined into $T_{i,j}$. Specifically, the constraints are as follows:

$$t_i^s \le t_i^o \le t_i^s + \Delta \quad (5.1)$$

$$t_i^e \le t_i^d \le t_i^e + \Delta \quad (5.2)$$

$$t_j^s \le t_j^o \le t_j^s + \Delta \quad (5.3)$$

$$t_j^e \le t_j^d \le t_j^e + \Delta \quad (5.4)$$

After deriving the link set L of combinable trips, the shareability network $S = (T, L)$ forms. Given a shareability network $S = (T, L)$, M is a subset of S. If there is no

repeated node on either link of *M*, then *M* is said to be a match of *S*.

For example, given trip T = {T_1, T_2, T_3, T_4, T_5, T_6}, known (T_1, T_2), (T_2, T_3), (T_1, T_5), (T_2, T_6), (T_2, T_4), and (T_5, T_6) are feasible for ridesplitting. Then, shareability network S consists of 6 links: L= {L_1, L_2, L_3, L_4 L_5, L_6}={L($T_{1,2}$), L($T_{2,3}$) L($T_{1,5}$) L($T_{2,6}$) L($T_{2,4}$) L($T_{5,6}$)}, as shown in Figure 5-4.

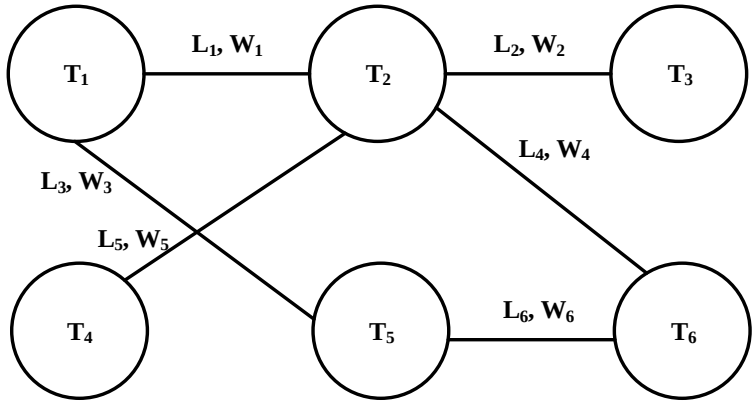

Figure 5-4 Shareability Network

We can give relevant weights to the links according to the optimization objective. Therefore, $\omega(L_i)$, the weight of link $\{T_i, T_j\} \in L$, can be defined as follows:

(1) For the objective of maximizing the number of ridesplitting trips, the weight $\omega(L_i)$ of each edge L_i is defined as the number of trips, which is 2 in all cases in this chapter.

$$\omega(L_i) = 2 \tag{5.5}$$

(2) For the objective of maximizing the total time of all trips, the weight $\omega(L_i)$ of each edge L_i is defined as the time saved by ridesplitting.

$$\omega(L_i) = {}_{i\in\{1,2,\ldots,n\}}\, t\,(T_i) + t\,(T_j) - t\,(T_{i,j}) \tag{5.6}$$

(3) For the objective of maximizing the value saved by ridesplitting, the weight $\omega(L_i)$ of each edge L_i is defined as the value saved by ridesplitting.

$$\omega(L_i) = P_1 * saved\ time + P_2 * saved\ distance - P_3 * delay\ time \tag{5.7}$$

$$\text{Saved time}(T_{i,j}) = t(T_i) + t(T_j) - t(T_{i,j}) \tag{5.8}$$

$$\text{Saved distance}(T_{i,j}) = S(T_i) + S(T_j) - S(T_{i,j}) \quad (5.9)$$

$$Delay\ (T_{i,j}) = Delay\ (T_i) + Delay\ (T_j) = (t_i^d - t_i^e) + (t_j^d - t_j^e) \quad (5.10)$$

$$\omega(L_i) = P_1 * [t(T_i) + t(T_j) - t(T_{i,j})] + P_2 * [S(T_i) + S(T_j) - S(T_{i,j})] - P_3 * (t_i^d - t_i^e + t_j^d - t_j^e) \quad (5.11)$$

where P_1 represents the average price of time, P_2 represents the average price of distance, P_3 represents the value of travel time, and Delay (T_i) represents the delay time for T_i.

Specifically, the average price of time P_1 and the average price of distance P_2 can be calculated by the price of the DiDi ridesourcing service in Chengdu, as shown in Table 5-3. Thus, for the research time interval, P_1 = 0.3 RMB/ minute and P_2 = 1.7 RMB/kilometer.

Table 5-3 Price of the DiDi ridesourcing service in Chengdu

Time	**Fee per kilometer (RMB)**
23:00-07:00	2.4
Other time	1.7
Time	**Fee per minute (RMB)**
7:00-10:00 & 17:00-19:00	0.38
Other time	0.3

Another step is the calculation of the value of the delay time experienced by passengers in Chengdu. Becker (1965) uses the time allocation theory to estimate the value of time and proposes that the value of travel time equals the wage rate. Wardman (1998) states that the hourly wage rate can be used to determine the time value. When using the hourly wage rate method to estimate the value of travel time, it should be multiplied by the reduction factor α for revision since the travel time saved is usually not fully used for work. Miller (1989) proposes a reduction factor close to 60 %. Small et al. (2012) proposes that the reduction factor can be taken as the interval value of 20% to 100%.

$$P_3 = \alpha * \frac{Income}{T} \quad (5.12)$$

where *Income* represents the per capita annual income and T represents the per capita working hours.

According to the Chengdu Statistical Yearbook 2017 compiled by the Chengdu Statistic Bureau, National Bureau of Standards Survey Office in Chengdu, the average wage of fully employed persons in urban units in 2016 was 61330 RMB. The average time spent working per year is 250 days/year * 8 hours/day = 2000 hours/year. The wage rate of people in Chengdu is 61330 /2000 = 30.67 RMB/hour. We set reduction factor α as 0.6. Thus, P_3 = 0.307 RMB/minute.

$$\omega(L_i) = 0.3*[t(T_i) + t(T_j) - t(T_{i,j})] + 1.7*[S(T_i) + S(T_j) - S(T_{i,j})] - 0.307*(t_i^d - t_i^e + t_j^d - t_j^e) \quad (5.13)$$

Ridesourcing companies such as DiDi and Uber must respond to trip requests in real time. Trip requests in a short time window can be known, and we set this window as δ. Passengers need to know whether they will get a shared ride within time window δ. For trips T_i and T_j, only when $|t_i^s - t_j^s| \leq \delta$ can we connect the two trips as a feasible ridesplitting trip. Obviously, if we set a larger δ, there are more sharing opportunities for trips. However, δ should be reasonably small to offer passengers timely service. Therefore, we set δ =1 minute in the model.

5.3.2 Algorithm of the Shareability Network

M with the $Max\{\sum \omega(L_i)\}$ is the maximum weighted matching of the shareability network S, denoted as M_{max}, which corresponds to the optimal ridesplitting solution. The maximum weight matching problem of the shareability network can be solved efficiently by converting the shareability network into the intersection graph. Node V_i of the intersection graph corresponds to link L_i of the shareability network. We add a link if two nodes contain the same trip. The weight of each node $w(V_i)$ in the intersection graph equals the weight of the corresponding link $w(L_i)$. R is a subset of S'. If there is no link between two arbitrary nodes of R, R is said to be an independent set of the intersection graph. The R with the $Max\{\sum \omega(V_i)\}$ is the maximum weight independent set of the intersection graph S', denoted as R_{max}. Obviously, R_{max} equals the corresponding M_{max}. We can transform the shareability network into an intersection graph to solve the maximum weighted matching problem efficiently, as shown in Figure 5-5.

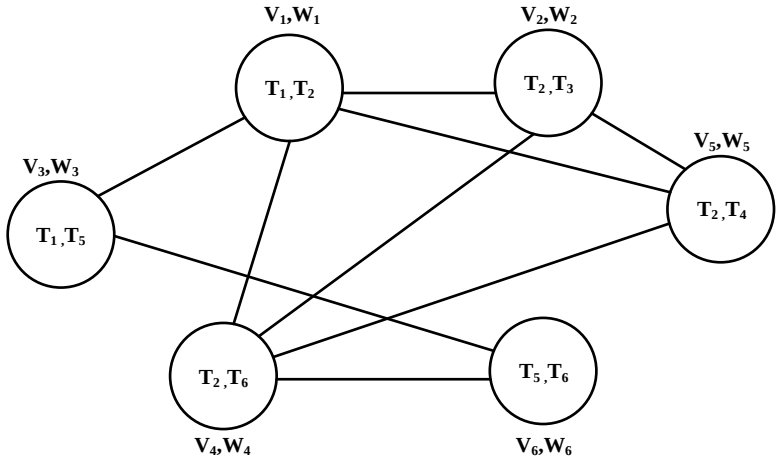

Figure 5-5 Transformation into an Intersection Graph

In this chapter, a hybrid iterative local search algorithm (ILS-VND) based on a variable neighborhood depth search is used to solve the large-scale ridesplitting problem. The specific steps of the algorithm are shown in Table 5-4. The input of the algorithm is the intersection graph G (V, E, W) and the maximum number of iterations, MaxIter. The algorithm follows the standard flow of the local iterative search algorithm. We add disturbance to the local optimal solution obtained by local search to avoid falling into the local optima. The current optimal solution is determined by the total weight of the selected set until the maximum number of iterations is reached.

Table 5-4 Pseudocode under three objectives

Objective: Maximizing shared trips, time savings or cost savings
Input: G(V, E, W), maximum number of iterations MaxIter
Output: The set of selected matching M_{max} , and the total weight of the set ω_{max}
1: $\omega(L_i)$
2: M_0=Initialize(M)
3: **while** iter<= MaxIter **do**
Perturb(M)
LocalSearch(M)
4: **End while**
5:ω_{max}= Weight(M_{max})
6: return M_{max} ,ω_{max}

5.4 Results and discussion

5.4.1 Results Analysis

5.4.1.1 Actual level of Ridesplitting

Based on the ridesplitting trip identification method of a previous study (Li et al., 2019) using this dataset, single and shared rides can be distinguished to obtain the actual current level of DiDi ridesplitting services. As shown in Table 5-5, it can be found that only 7.85% of total ride orders are shared orders. The hours saved by ridesplitting account for 2.4% of the total ride hours. The percentage of cost savings is 1.22%. All of these values are fairly low. In addition, the average delay of actual ridesplitting is 9.86 minutes.

Table 5-5 Actual level of ridesplitting

Item	Number	Percentage
Single ride orders	959,513	92.15%
Shared ride orders	81,694	**7.85%**
Total orders	1,041,207	100%
Single ride hours	365,336.4 h	89.19%
Shared ride hours	44,293.0 h	10.81%
Total ride hours before ridesplitting	409,629.4 h	100%
Single trip hours	365,336.4 h	91.36%
Ridesplitting trip hours	34,548.5 h	8.64%
Total trip hours after ridesplitting	399,884.9 h	100%
Hours saved by ridesplitting*	9,744.5 h	**2.38%**
Total trip cost before ridesplitting	21,300,728.8 RMB	--
Single trip cost after ridesplitting	18,997,492.8 RMB	90.82%
Ridesplitting trip cost after ridesplitting	2,043,811.4 RMB	9.18%
Total trip cost after ridesplitting	21,041,304.2 RMB	100%
Cost saved by ridesplitting*	259,424.6 RMB	**1.22%**

*percentage of saved hours within the total ride hours before ridesplitting

*percentage of cost savings within the total cost before ridesplitting

5.4.1.2 Potential of Ridesplitting

Under the three different objectives, as the maximum tolerable delay increases, the optimal shared trips, time savings and cost savings continue to increase due to more opportunities for ridesplitting. We evaluate the performances of the three different objectives based on three indicators: shared trips, time savings and cost savings.

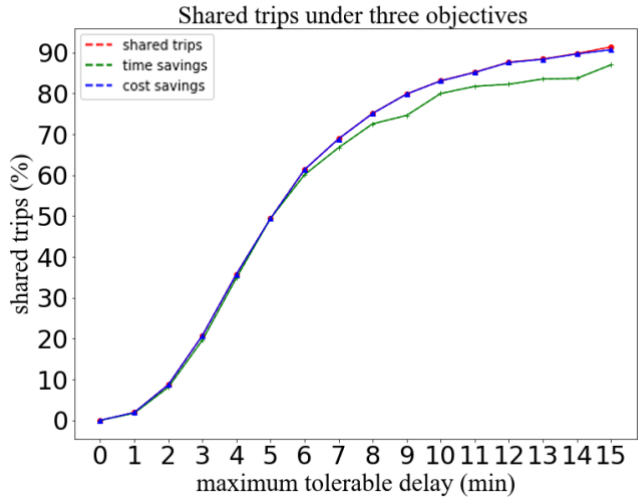

Figure 5-6 Shared trips under the three objectives

For the indicator of shared trips, there is no doubt that the objective of maximizing the number of shared trips has the best performance. As shown in Figure 5-6, the potential opportunity can reach 91.37% with an average delay of 7.27 minutes, while the actual figure is only 7.85%. There is almost no gap between the objectives of maximizing the shared trips and maximizing the cost savings. Under the objective of maximizing cost savings, the percentage of shared trips can reach 90.69%. Under the objective of maximizing the time savings, the percentage of shared trips is a little less than that under the other two objectives, which can reach 86.99%.

For the indicator of time savings, the percentage can reach 25.77% with an average delay of 5.62 minutes under the objective of maximizing the time savings, see Figure 5-7. By contrast, the actual figure is only 2.38%. The percentages of time savings under the objectives of maximizing the time savings and maximizing the cost savings are basically the same. This is because the travel time is also taken into consideration under the objective of maximizing the cost savings, where the percentage of time savings can reach 25.75%. Under the objective of maximizing shared trips, the percentage of time savings is 13.5%, much less than that under the other two objectives. In addition, the percentage of time savings goes down slightly when the maximum tolerable delay is more than 11 minutes. This is because it only considers the number of shared trips rather than the time savings, which can result in longer detours.

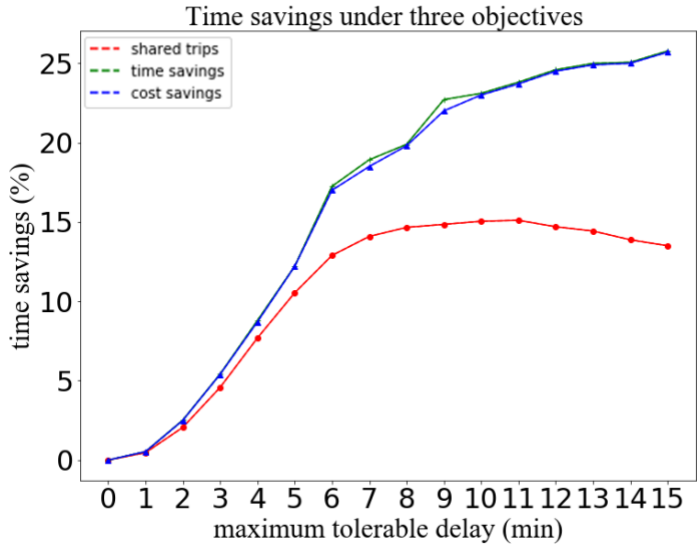

Figure 5-7 Time savings under three objectives

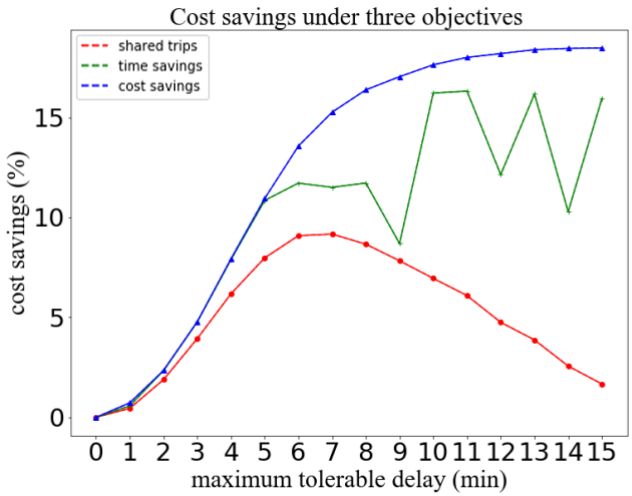

Figure 5-8 Cost savings under the three objectives

For the indicator of cost savings, the percentage of time savings can reach 18.47% with an average delay of 4.76 minutes under the objective of maximizing the cost savings, see Figure 5-8. By contrast, the actual figure is only 1.22%. Under the objective of maximizing the time savings, the percentage of cost savings can reach 16.32% with an average delay of 4.98 minutes. The percentage of cost savings varies between 10% and 15% under the objective of maximizing the time savings. This is because there is no consideration of the delay time of passengers, which can also impact the cost savings. Under the objective of maximizing shared trips, the percentage of cost savings can reach 9.16%. Furthermore, the percentage of cost savings goes

down gradually when the maximum tolerable delay is more than 7 minutes. This is because it only considers the number of shared trips rather than the time savings and delay time of passengers, which can bring about larger costs.

As shown in Table 5-6, the average delay increases with the increase of the maximum tolerable delay. When the maximum tolerable delay increases to 15 minutes, the average delay is 4.76 minutes under the objective of maximizing the cost savings, while the average delay reaches 7.27 minutes and 5.62 minutes under the objectives of maximizing the shared trips and the time savings, respectively. Obviously, the average delays of the potential ridesplitting solutions under the three objectives are all lower than the delay of 9.86 minutes in the real world. Therefore, it can be found that passengers can wait for less time on average when using the ridesplitting algorithm proposed in this chapter. Furthermore, the average delay under the objective of maximizing the cost savings is the lowest of the three objectives.

Table 5-6 Average delay under the three objectives

Maximum Tolerable Delay (min)	Shared Trips	Time Savings	Cost Savings
1	0.48	0.48	0.47
2	1.14	1.12	1.11
3	1.72	1.70	1.68
4	2.34	2.27	2.21
5	2.9	2.78	2.69
6	3.45	3.36	3.12
7	3.98	3.85	3.46
8	4.44	4.32	3.78
9	4.93	4.91	4.03
10	5.4	4.73	4.23
11	5.83	4.98	4.39
12	6.3	5.59	4.53
13	6.66	5.35	4.64
14	6.91	6.13	4.73
15	7.27	5.62	4.76

5.4.2 Discussion

5.4.2.1 Benefits

To evaluate the potential benefits of ridesplitting, we compare the potential of ridesplitting under three objectives with the actual level. We summarize and discuss the main findings in this section.

(i) Ridesplitting has great potential to mitigate congestion and air pollution: under the objective of maximizing cost savings, the percentage of potential shared trips is 90.69%, while the actual scale is 7.85%. The required fleet size can also be reduced considerably by ridesplitting because two shared trips can be served by a single vehicle instead of two vehicles. Therefore, shared trips can be used to reduce the required fleet size to mitigate traffic congestion for society. This also benefits passengers by enhancing their mobility. Zheng et al. (2018) found that ridesplitting in on-demand services can lead to a reduction of 12,327 vehicles in Hangzhou in the future, representing nearly 0.53% of all vehicle ownership in Hangzhou. Furthermore, the potential time savings afforded by ridesplitting can reach 25.75%, whereas this figure is 2.38% in the real world. Sperling (2018) stated that pooling to fill the empty seats in all vehicles is the most important strategy and innovation for achieving sustainable transportation.

(ii) Maximum tolerable delay is a significantly important indicator to maximize benefits. With the increase of the maximum tolerable delay, the percentages of shared trips, time savings and cost savings increase because of there being more opportunities for ridesplitting. However, the average delays also increase due to the increase of maximum tolerable delay. Therefore, trade–off solutions should be proposed to avoid overly long delays and guarantee the travel time reliability for passengers. Specifically, under the objective of maximizing cost savings, the cost savings rise significantly before the maximum tolerable delay increases to 12 minutes. The percentage of cost savings basically maintains the same value when the maximum tolerable delay is more than 12 minutes. Therefore, policy makers and on-demand ridesplitting companies can consider the marginal benefit when setting the maximum delay in matching and routing algorithms.

(iii) According to the results of the above three indicators, it can be found that the objective of maximizing the cost savings has better outcomes than the objectives of maximizing the shared trips or time savings. This is because maximizing the cost savings takes into account not only the value of time savings and saved vehicle miles but also the value of passenger delays. From the perspective of the whole system, we want to minimize the total time and travel distance of all trips. However, from the perspective of individual passengers, the optimal solution for the whole society may not necessarily be optimal for themselves, since the travel time does not include delays caused by detours. This objective also takes the value of the delay experienced by

individual passengers into consideration to guarantee the rights of passengers when using the ridesplitting service. Therefore, the objective is more reasonable than the other two objectives.

5.4.2.2 Recommendations

Upon exploring the actual level and potential of ridesplitting during rush hours, it can be found that there is a large gap between the actual level and potential opportunity. Specific strategies are recommended for ridesplitting companies and policy makers to improve the present ridesplitting service, as follows:

- Ridesplitting companies (e.g., Didi Chuxing) should improve matching and routing algorithms to reduce the extra delays and improve the travel time reliability of the ridesplitting service.
- Ridesplitting companies should establish credit rating systems for both passengers and drivers to discourage tardy behavior. Then the ridesplitting system can operate more efficiently and the travel time reliability can also be improved.
- Ridesplitting companies should subsidize drivers and passengers proportionately to improve their enthusiasm for and participation in ridesplitting. Additionally, transportation management agencies should provide more policy incentives to promote the use of ridesplitting, such as high-occupancy vehicle lanes and waivers for road fees and parking fees.

5.5 The design of new ridesourcing system for the future deployment of connected and autonomous vehicles

In this section, we extensively design the new ridesourcing system for the future deployment of CAVs. It should be noted that it is an initial design in anticipation of applying the previous models and solutions to CAVs. The characterization of shared mobility system reported here is fully representative of an autonomous driving scenario where human operation of vehicles is not necessary, such as constraints on driver availability and maximum operating hours. With the development of CAVs, the research results will be closer to future trends. We assume that all vehicles obey to the dispatching schedules completely in the proposed model. Driver compliance rate may

be different under human-driven vehicles in the reality at present, which illustrates that there is still a lot of room for optimization of current shared mobility services. At the same time, Future urban mobility is envisioned to be reshaped by the emerging CAVs and shared mobility services. Therefore, it is meaningful to design a shared mobility system for the future deployment of connected and autonomous vehicles in urban areas.

Blockchain provides technical conditions that can improve the efficiency and the safety of the shared mobility system. Smart contract makes it possible to finish and record a transaction for CAVs. We propose a ridesourcing system with CAVS based on the blockchain for the future mobility, which has four key components: the car drivers and SAVs, the user-oriented platform (UOP), the location-based service (LBS) and the blockchain system, shown in the Figure 5-9.

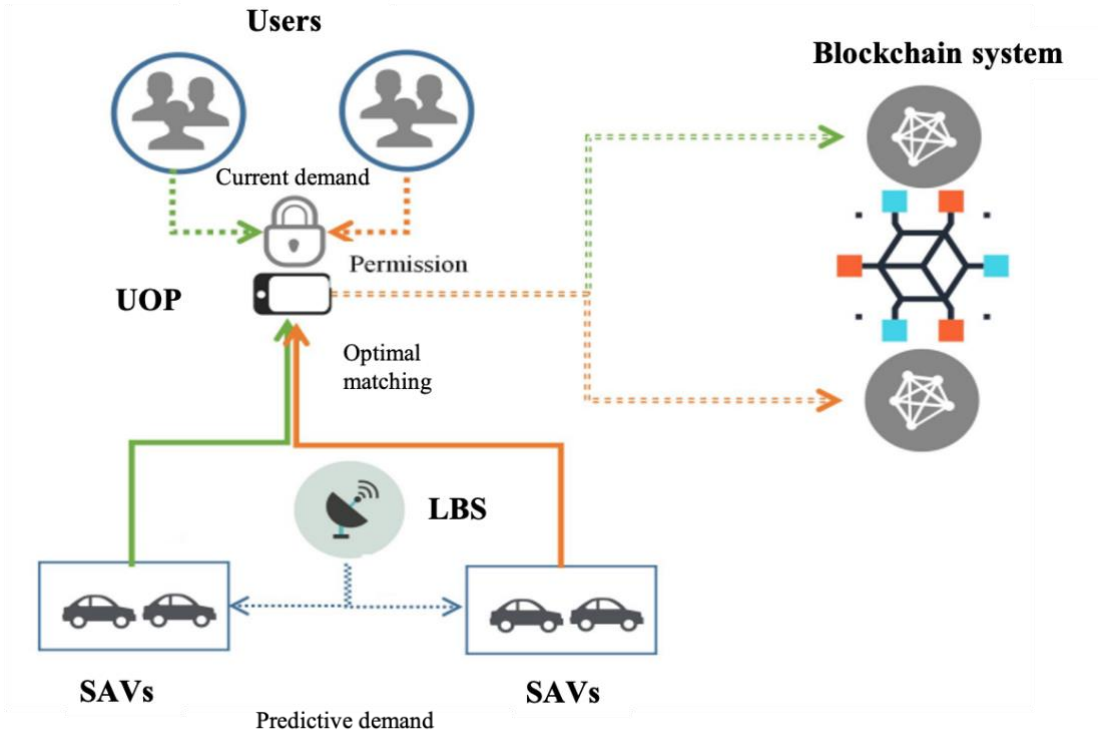

Figure 5-9 Key components of the ridesourcing system with CAVs based on the blockchain

A. Users and SAVs

(i) Users: everyone that downloads the public and private key generator from the UOP platform is already a member of our system. (ii) SAVs: every SAV should have their unique non-fungible tokens to distinguish themselves.

B. The user-oriented platform (UOP)

(i) Authentication: All the identities would be based on public keys and private keys. In order for the blockchain to perform authentication, users use public keys to enter the system. A private key works to protect every transaction's security. (ii) Permission and different tokens: The UOP platform will check every user's permission when they submit any requests. After checking a user's permission, the platform grants different tokens to the user. For example, when a user wants to use the SAV, the UOP platform will check this member's permission and whether the SAV is in use. If the request is successful, the SAV's token will be handed over to this user, which represents that the user has the usufruct of the car.

C. The location-based service (LBS)

Ultra-wide band (UWB) wireless communication technology combined with GPS is recommended to be used to ensure the car's positioning data. First, the SAVs will get the current GPS position information through the Robot Operating System. Then, according to the design of the UWB signal, it will analyse the accurate positioning information, especially when indoors.

D. Blockchain system

Blockchain is a decentralized database that integrates and applies cutting-edge computer technologies such as point-to-point transmission, encryption algorithms, consensus mechanisms, and distributed data storage. In a narrow sense, blockchain is an unalterable and unforgeable distributed ledger guaranteed by cryptography, which forms a chain data structure by sequentially connecting data blocks in chronological order. Broadly speaking, blockchain is a new distributed infrastructure and computing paradigm, which is based on blockchain data structures to verify and store data.

The operation procedures of key components of the ridesourcing system with CAVs based on the blockchain:

Step1: Optimal matching based on the proposed model in this chapter

1. The user sends a driving request to use a SAV.

2. The UOP service makes the SAV run by using a signal.

3. The SAV sends different kinds of data to the blockchain net under the LBS.

4. After optimal computation, the UOP will send the SAV to the place requested by the user.

Step2: Optimal rescheduling of the empty SAVs

1. The area could be divided into hot zones and cold zone based on the proposed predictive demand in chapter 4.

2. The empty SAVs are dispatched to the proper zones to improve the efficiency.

3. The rescheduled SAVs updates the data to the blockchain net under the LBS.

To ensure that the car's situation can be seen in the system and keep the data valid, all the data will be stored both in the blockchain net and UOP database. It should be noted that this is an initial design for the future deployment of CAVs, which need further research about the specific details.

5.6 Conclusions

This chapter aims to improve the ridesplitting service during rush hours using empirical ridesourcing data provided by DiDi Chuxing, which contains complete datasets on ridesourcing orders in the city of Chengdu, China. A ridesplitting trip identification algorithm based on a shareability network is developed to quantify the potential of ridesplitting. We analyze shared trips, time savings and cost savings under three objectives. Furthermore, we evaluate the gap between the potential of ridesplitting and the actual level of ridesplitting. Besides, we make an initial design of the shared mobility system for the future deployment of CAVs. The main findings are as follows:

The percentage of potential cost savings can reach 18.47% with an average delay of 4.76 minutes, whereas the actual percentage is 1.22% with an average delay of 9.86 minutes. Passengers can wait less time on average when using the proposed ridesplitting algorithm. The percentage of shared trips can be increased from 7.85% to 90.69%, and the percentage of time savings can reach 25.75% from 2.38%.

To our knowledge, this is one of the first investigations of the gap between the actual and the potential of ridesplitting on a city scale. The findings of this chapter can help reveal the great potential of ridesplitting. The quantitative benefits could encourage governments to take more action to improve the present ridesplitting services such as by providing high-occupancy vehicle lanes and waivers for road fees and parking fees. The comparative evaluation between the potential and actual level of ridesplitting provides policy implications for improving existing ridesplitting services. The ridesplitting companies should establish credit rating systems to improve the efficiency of ridesplitting services. Furthermore, the maximum tolerable delay should be set properly for policy makers to obtain more benefits for low-carbon urban transport and guarantee the ridesplitting service quality at the same time.

The characterization of shared mobility system reported in this study is fully

representative of an autonomous driving scenario where human operation of vehicles is not necessary, such as constraints on driver availability and maximum operating hours. At the same time, Future urban mobility is envisioned to be reshaped by the emerging CAVs and shared mobility services. Therefore, the research results will be closer to future trends. This chapter makes the initial investigation on the potential of CAVs on ridesplitting services in perfect condition. In the next chapter, we will explore the impacts of cyberattacks on CAVs in adverse condition.

Chapter 6 A resilient and robust control strategy for connected and autonomous vehicles to mitigate the threat of cyberattacks

HIGHLIGHTS

1) An architecture with three layers to investigate the impacts of cyberattacks is proposed
2) Collusive attacks have the greatest adverse impact on a CAV platoon in mixed traffic
3) A resilient and robust control strategy to mitigate the threat of cyberattacks is proposed
4) The stability of the proposed strategy for mitigating cyberattacks is demonstrated

6.1 Introduction

Internet, mobile communication, big data, artificial intelligence and other new technologies accelerate breakthroughs and continue to evolve, promoting the rapid development of mobile Internet and automated driving technology. Connected and automated vehicles which can realize "safe, efficient, comfortable and energy-saving" driving will also emerge as the times require. CAVs are expected to improve the characteristics of traditional traffic flow from the micro vehicle level, and then provide an effective way to solve the problems of traffic congestion, traffic efficiency and traffic pollution. Scholars have also carried out some researches to demonstrate the potential benefits of CAVs (Li et al., 2013; Rios-Torres & Malikopoulos, 2016; Sukuvaara & Nurmi, 2009; Van Arem et al., 2006; Zhao & Sun, 2013). However, with the help of diverse and advanced communication technology, the "intelligent" information exchange between vehicles and the surrounding environment/world is realized all the time. So, such an open-access communication environment system increases the risk of vehicles being exposed to cyberattacks, which is an urgent and

critical challenge to be solved.

Although some studies investigated the impact of cyberattacks and put forward the corresponding strategies, there are two important issues to be addressed: firstly, it's an important problem to build a vehicle dynamics model for CAVs in a mixed traffic flow considering cyberattacks. Secondly, some of the existing cyberattacks response strategies are formulated from the perspective of intrusion detection, privacy protection, etc., so when the cyberattacks have reached the vehicle level and produced negative effects, it will be an urgent problem to formulate the control strategy from the perspective of vehicle dynamics to resist the harmful threat brought by the cyberattacks.

To fill this gap, this chapter proposes a CAV mixed flow car-following model considering cyberattacks based on Intelligent Driver Model (IDM). On this basis, an acceleration control switch is designed as a Robust and Resilient Control Strategy (RRCS) against cyberattacks, which can help traffic flow to restore stability and enhance security. Finally, the influence of cyberattacks on the evolution of mixed traffic flow and the role of RRCS in combating cyberattacks are revealed by numerical simulations.

The remainder of this chapter is organized as follows. Section 6.2 establishes a car-following model of CAV mixed flow under cyberattacks. Section 6.3 proposes the Robust and Resilient Control Strategy against cyberattacks. In Section 6.4, numerical simulations are carried out to reveal the impact of cyberattacks on the evolution of mixed traffic flow, and the feasibility of the RRCS is verified by comparative experiments. Finally, section 6.5 gives a general conclusion about this work.

6.2 The modeling of cyber-attacks on CAVs

6.2.1 General assumption

The schematic diagram of the research scenario is shown below (Figure 6-1), covering the following three assumptions:

1) The CAV mixed traffic flow refers to different types of connected and automated vehicles, rather than the existence of non-connected and automated vehicles;
2) Only the longitudinal car following behavior is considered, and the lane changing behavior and overtaking behavior are not considered;

3) Cyberattacks may appear in every vehicle in the CAV platoon.
4) Each vehicle only has access to its own position and velocity data and has a communication device. No other sensors or information sources are available (no RADAR, cameras, LiDAR …). In this case, the communication mean is seen as a remote sensor.

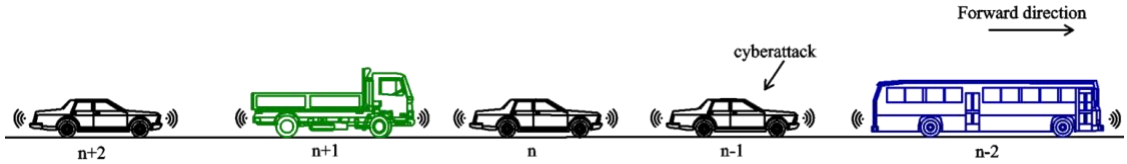

Figure 6-1 Schematic diagram of mixed CAV flow for multiple types of vehicles.

6.2.2 Cyberattacks types and vehicle types

According to different research needs, previous scholars have made different classifications of cyberattacks (Cui et al., 2019; Khattak et al., 2018; Raya & Hubaux, 2007; Zeadally et al., 2012). Considering that we only evaluate the impact of cyberattacks on traffic flow from the perspective of vehicle dynamics, we summarize the cyberattacks as affecting the vehicle's position, velocity and acceleration as shown in Table 6-1. Besides, we classify vehicles into small vehicles, medium vehicles and large vehicles according to the vehicle length. Referring to the characteristic description of different vehicle types in the existing literature (Liu et al., 2016; Ngoduy, 2015) we make reasonable assumption that the larger the vehicle is, the larger the safety headway is, and the smaller the maximum acceleration, maximum deceleration and maximum velocity are.

Table 6-1 Cyberattack classification

Category	**Description**	**Attack consequences**
Bogus messages	These attacks could transmit bogus messages such as erroneous velocity or position through masquerading a legal vehicle or tampering a piece of messages	Tampering with velocity information
		Tampering with location information
Replay/delay	Due to the jammed communication channel or being injected with a replay virus, the communication data is fraudulently repeated or delayed	Delayed transmission information
		Repeat transmission information
Collusion attacks	Two or more vehicles are attacked simultaneously by cooperatively adversaries	Superposition of single attacks

6.2.3 Car following model of CAV mixed traffic flow with cyberattacks

Previous scholars have proposed many classical car following models considering different actual traffic factors (Bando et al., 1995; Jiang et al., 2001; Pipes, 1953; Treiber et al., 2000). In recent years, the car following model in the connected and automated environment has also developed rapidly (Jin & Orosz, 2014; Milanés & Shladover, 2014; Qian et al., 2017; Xie et al., 2018; Ye et al., 2019). The general description of the model is as follows,

$$\begin{aligned} \dot{v}_n(t) &= f\left(v_n(t), s_n(t), \Delta v_n(t)\right) \\ s_n(t) &= x_{n-1} - x_n - l_{n-1} \end{aligned} \tag{6.1}$$

where

$\dot{v}_n(t)$ = the acceleration of vehicle n ;

$v_n(t)$ = the velocity of vehicle n;

$\Delta v_n(t)$ = velocity difference between vehicle n and vehicle $n-1$;

x_n = the position of vehicle n;

l_{n-1} = the length of vehicle $n-1$; and

$s_n(t)$ = the gap between the front of the vehicle n and the rear of the vehicle $n-1$.

The IDM is widely employed in car following modeling for CAVs (Hu et al., 2020; Sharma et al., 2019; Xiao et al., 2018), which was proposed by Treiber et al. (2000). The main advantage of this model is to describe the acceleration and deceleration behavior and retain complex macroscopic traffic phenomenon. In addition, P. Wang et al. (2020) adopted IDM as the basic vehicle dynamics model when exploring the impact of cyberattacks on CAV traffic flow. Therefore, we also refer to and continue to select IDM, and its specific expression is as follows:

$$\dot{v}_n(t) = a\left[1-\left(\frac{v_n(t)}{v_0}\right)^4-\left(\frac{s^*\left(v_n(t),\Delta v_n(t)\right)}{s_n(t)}\right)^2\right]$$
$$s^*\left(v_n(t),\Delta v_n(t)\right) = s_0 + Tv_n(t) + \frac{v_n(t)\Delta v_n(t)}{2\sqrt{ab}} \tag{6.2}$$

where

a = maximum acceleration;

v_0 = desired velocity;

$s^*\left(v_n(t),\Delta v_n(t)\right)$ = desired headway in the current state;

s_0 = minimum gap;

T = safe time headway; and

b = desired deceleration.

Combining the cyberattacks types and vehicle types described above, we develop the extended model, and the specific expression is as follows,

$$\dot{v}_n(t) = a_n^m\left[1-\left(\frac{v_n^m(t)}{v_0^m}\right)^4-\left(\frac{s_n^{m*}\left(v_n^m(t),\Delta\ddot{v}_n^m\left(t-\ddot{\tau}_n^m\right)\right)}{\ddot{s}_n^m\left(t-\ddot{\tau}_n^m\right)}\right)^2\right]$$
$$s_n^{m*}\left(v_n^m(t),\Delta\ddot{v}_n^m\left(t-\ddot{\tau}_n^m\right)\right) = s_0^m + T_n^m v_n^m(t) + \frac{v_n^m(t)\Delta\ddot{v}_n^m\left(t-\ddot{\tau}_n^m\right)}{2\sqrt{a_n^m b_n^m}} \tag{6.3}$$

$$m = \begin{cases} 1 & \textit{vehicle n is small vehicle} \\ 2 & \textit{vehicle n is medium vehicle} \\ 3 & \textit{vehicle n is large vehicle} \end{cases} \tag{6.4}$$

And different types of vehicle n correspond to different parameter values.
where

a_n^m = maximum acceleration;

v_0^m = desired velocity;

s_0^m = minimum gap;

T_n^m = safe time headway; and

b_n^m = desired deceleration.

$\tilde{\tau}_n^m$ = the delay under cyberattacks;

$\Delta\tilde{v}_n^m\left(t-\tilde{\tau}_n^m\right)$ = the velocity difference under cyberattacks;

$s_n^{m*}\left(v_n^m(t),\Delta\tilde{v}_n^m\left(t-\tilde{\tau}_n^m\right)\right)$ = desired headway in the current state under cyberattacks;

$\tilde{s}_n^m\left(t-\tilde{\tau}_n^m\right)$ = the gap under cyberattacks;

6.3 The robust and resilient control strategy (RRCS) against cyberattacks

In order to mitigate and resist the harmful impact of cyberattacks on traffic flow, an acceleration control switch is designed as the RRCS against cyberattacks in this section. The specific control form is as follows:

$$\text{Acceleration controller}=\begin{cases} Controller-A & if \quad \dfrac{\Delta x_n(t)}{v_n(t)}<T_g \\ Controller-IDM & if \ T_g\le\dfrac{\Delta x_n(t)}{v_n(t)}\le T_u \\ Controller-B & if \quad \dfrac{\Delta x_n(t)}{v_n(t)}>T_u \end{cases} \tag{6.5}$$

where

$Controller-A$ = the control strategy in the state of "*too close vehicle gap*";

$Controller-IDM$ = the control strategy based on Intelligent Driver Model;

$Controller-B$ = the control strategy in the state of "*too far vehicle gap*";

T_g = vehicle time headway threshold when triggering and switching to *Controller-A*; and

T_u = vehicle time headway threshold when triggering and switching to *Controller-B*.

The core idea of this strategy mainly has two objectives. The first is to keep the safe distance between vehicles under cyberattacks, and the second is to make the vehicle dynamically adjust the acceleration and gradually restore the stability of the traffic flow. When the vehicle returns to the steady-state position, its velocity shall also reach the steady-state to realize seamless switching with IDM controller. Taking *Controller-A* as an example, its design motivation and design steps are as follows.

First of all, we aim that the vehicles affected by the cyberattacks will return to the equilibrium position as soon as possible after implementing the strategy. At this time, the vehicle velocity is greater steady-state velocity, and the headway is less than the steady-state headway. Therefore, from the perspective of kinematics, the vehicle needs to decelerate first and then accelerate, resulting in the displacement difference with the steady-state, so as to achieve the established steady-state goal, in which a velocity node $v_n(t) = kv_e$ needs to be set to connect deceleration and acceleration, k is the proportional coefficient (After preliminary simulation and verification, considering the control efficiency, we set $k = 5/6$, which can be optimized in the future). The acceleration solution process is as follows. Firstly, the basic kinematic equation is given as follows:

$$\begin{aligned} x_0 &= v_e t \\ v_e - v_n(t) &= a_n(t) \cdot t \\ v_e^2 - v_n^2(t) &= 2a_n(t)x \end{aligned} \tag{6.6}$$

where

t = time required to reach steady-state speed;

x =displacement required to reach steady-state speed;

x_0 =displacement of vehicle running at steady-state velocity in time t;

Construct $x - x_0$, combined with Eq. (6.6),

$$2a_n(t)(x - x_0) = 2a_n(t)x - 2a_n(t)v_e t = 2a_n(t)x - 2a_n(t)v_e \cdot \frac{v_e - v_n(t)}{a_n(t)} \tag{6.7}$$

Besides, the displacement difference is equal to the gap difference, that is:

$$x_0 - x = s_n^e - s_n(t) \tag{6.8}$$

Thus, the acceleration is:

$$a_n(t) = \frac{(v_e - v_n)^2}{2(s_n^e - s_n(t))} \tag{6.9}$$

Similarly, *Controller-B* controls the vehicle to accelerate first and then decelerate to restore the steady state, and the specific expressions of the two acceleration control strategies are as follows:

$$Controller-A:$$

$$\dot{v}_n(t)=\begin{cases} d_{e\max} & until \quad v_n(t)=\dfrac{5}{6}v_e \\ \dfrac{\left(v_e-v_n\right)^2}{2\left(s_n^e-s_n(t)\right)} & when \quad \dfrac{5}{6}v_e \le v_n(t) \le v_e \end{cases} \tag{6.10}$$

$$Controller-B:$$

$$\dot{v}_n(t)=\begin{cases} a_{c\max} & until \quad v_n(t)=\dfrac{6}{5}v_e \\ \dfrac{\left(v_e-v_n\right)^2}{2\left(s_n^e-s_n(t)\right)} & when \quad v_e \le v_n(t) \le \dfrac{6}{5}v_e \end{cases} \tag{6.11}$$

where

v_e = steady-state velocity;

s_n^e = steady-state gap;

$d_{e\max}$ = maximum deceleration; and

$a_{c\max}$ = maximum acceleration.

As shown in Figure 6-2, we design an architecture with three layers to investigate the impacts of cyberattacks and RRCS of mixed CAV flow. In the first modeling building layer, we propose a car following model considering different cyberattack types for mixed CAV flow based on IDM. RRCS is proposed to mitigate the bad effects of cyberattacks on mixed CAV flow in the strategy construction layer. Finally, in the numerical simulation layer, we compare spatiotemporal evolution diagrams of mixed CAV flow under cyberattacks in two cases with and without RRCS. Besides, sensitivity analyses are conducted in different platoon compositions, vehicle distribution and cyberattack intensities.

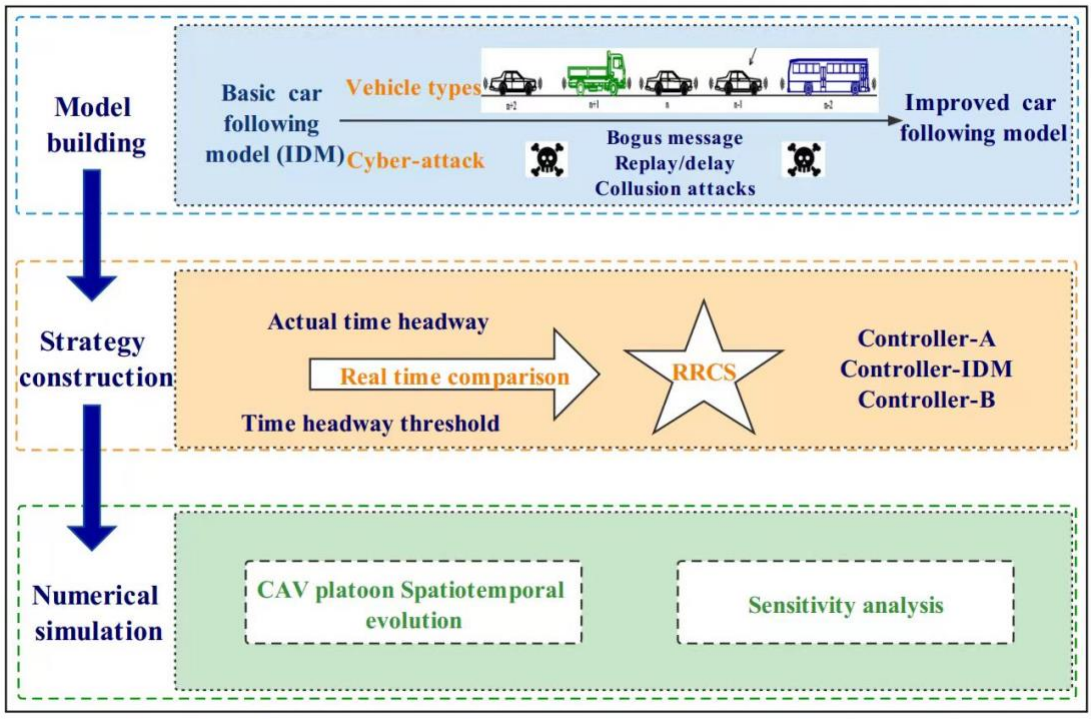

Figure 6-2 Architecture for exploring the impacts of RRCS on mixed CAV flow

6.4 Numerical simulations and Results

6.4.1 Evolution of traffic flow under different cyberattack scenarios with or without RRCS

In order to analyze the impact of cyberattacks on the evolution of mixed traffic flow and the feasibility of RRCS applying, this section selects some typical scenarios according to the previous classification of cyberattacks for numerical simulations, and makes a comparative analysis of the evolution results with and without RRCS. We set up ten vehicles to form a CAV platoon. The number of large vehicles, medium vehicles and small vehicles can be controlled according to the set proportion, and the vehicle distribution is randomly generated. The vehicle type ratio we set in this part of the simulation is 2 large vehicles, 2 medium vehicles and 6 small vehicles. The initial velocity of all vehicles is *12 m/s*, and the same type of vehicle has the same initial headway. Table 6-2 summarizes the parameters of three kinds of vehicle adopted from the existing research works and makes appropriate adjustments (Sharma et al., 2019; P. Wang et al., 2020; Xie et al., 2018). It is worth noting that IDM variables are regarded as constants in this chapter for the consideration of sensitivity analysis of cyberattack

related parameters in the section 6.4.2.

Table 6-2 Parameter values of different types of vehicles

Parameter	l	v_0	a	b	T	τ	s_0	T_g	T_u	$a_{c\max}$	$d_{e\max}$
Unit	m	m/s	m/s^2	m/s^2	s	s	m	s	s	m/s^2	m/s^2
Small vehicle	5	33	2.5	3	1.3	0.1	4	1.3	3.5	2.5	4
Medium vehicle	8	27	2	2	1.6	0.15	6	1.6	3.8	2	3
Large vehicle	11	22	1.5	1	2	0.2	8	2	4	1.5	2

6.4.1.1 Bogus velocity messages

Overestimate velocity

In this scenario, the fourth vehicle was attacked from $t = 40s$ to $t = 60s$, and the velocity information transmitted to the fifth vehicle is tampered. This velocity value is put to 1.5 times the actual velocity of the current vehicle (4th vehicle). That is to say, the rear vehicle overestimates the velocity of the front car. Figure 6-3(a)-(c) describes the evolution of mixed traffic flow under bogus velocity messages attack when there is no RRCS. Due to the random distribution, the leading and sixth vehicles are medium vehicles, and the seventh and eighth vehicles are large vehicles. It can be seen from Figure 6-3(a) that during $t = 40s$ to $t = 60s$, the fifth vehicle received a false message, and it kept accelerating to approach the vehicle in front, causing potential safety hazards. In the $t = 60s$, the cyberattack ended and the traffic flow slowly returned to the steady state. Figure 6-3(b) and Figure 6-3(c) show the evolution of velocity and headway respectively, which corresponds to Figure 6-3(a). What is depicted in Figure 6-3(d)-(f) is mixed traffic flow evolution diagrams under the overestimated velocity with RRCS. We can clearly find that in the case of cyberattacks, the vehicle still keeps a certain distance from the vehicle in front, which ensures the driving safety. It can also be seen from the Figure 6-3(f) that the headway (platoon state with inter-distances and vehicle positioning from the leader) has been kept in a small range under cyberattack, and the platoon can still restore stability under this control strategy when attacks disappear, which proves that this strategy can play an effective role in the process of resistance overestimate velocity attack.

Without RRCS

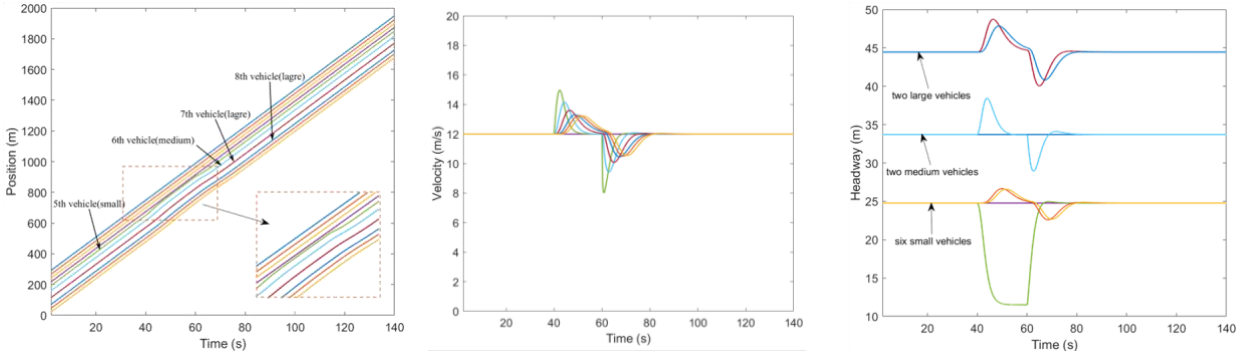

(a) Position evolution (b) Velocity evolution (c) Headway evolution

With RRCS

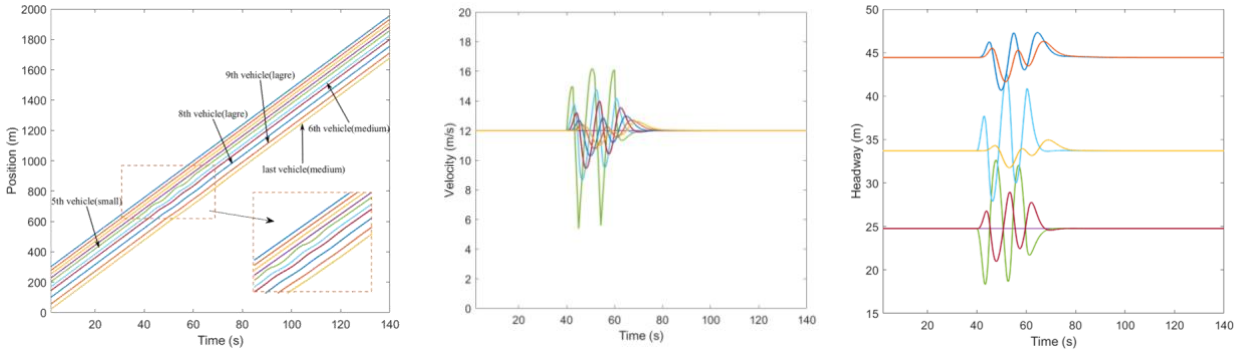

(d) Position evolution (e) Velocity evolution (f) Headway evolution

Figure 6-3 Mixed traffic flow evolution diagrams under the overestimated velocity with/without RRCS.

Underestimate velocity

Contrary to overestimating velocity, here, the velocity information of the fourth vehicle is tampered with a lower velocity (40% of the actual value). This attack is applied in the time *t=40 s* and then transmitted to the rear vehicle, resulting in the underestimation of the velocity of the rear vehicle to the front vehicle, which lasts 20 seconds and ends in *t=60 s*. The distribution of randomly generated vehicles is that the sixth and seventh vehicles are medium vehicles, and the ninth and last vehicle are large vehicles. Figure 6-4(a) shows the running track of the CAV platoon. The fifth vehicle mistakenly continues to decelerate, resulting in a large headway, which can also be directly reflected in Figure 6-4(b) and Figure 6-4(c).

Comparatively speaking, the impact of this kind of cyberattack is less critical than that of overestimating velocity attack, which will not cause vehicle collision, but it will produce unnecessary vehicle spacing, which leads to the loss and waste of road resources.

Figure 6-4(d)-(f) depicts the impact of the underestimated velocity attack on traffic flow evolution under RRCS, which can be used for comparative analysis without RRCS. It can be found that in the case of attack, the vehicle velocity still keeps a small fluctuation, and the vehicle headway is also maintained in a good state, and the stability and safety of the fleet are guaranteed. Therefore, we have arguments to explain the feasibility and superiority of this RRCS.

Without RRCS

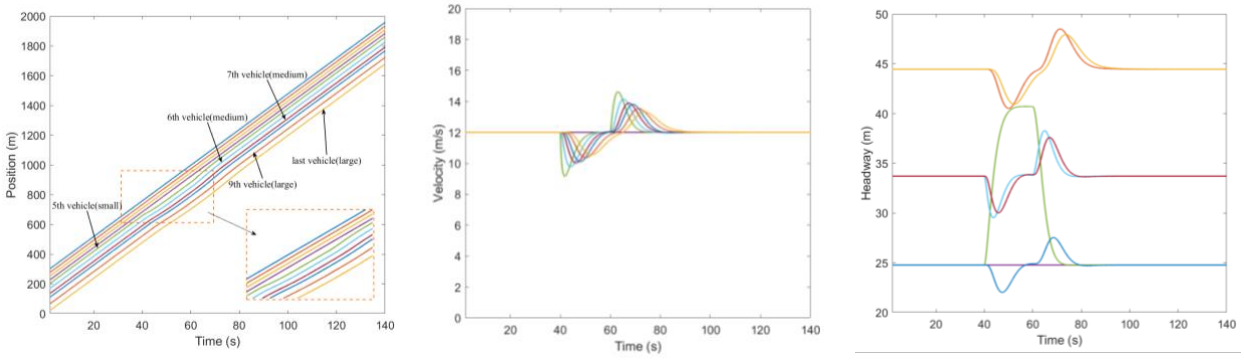

(a) Position evolution (b) Velocity evolution (c) Headway evolution

With RRCS

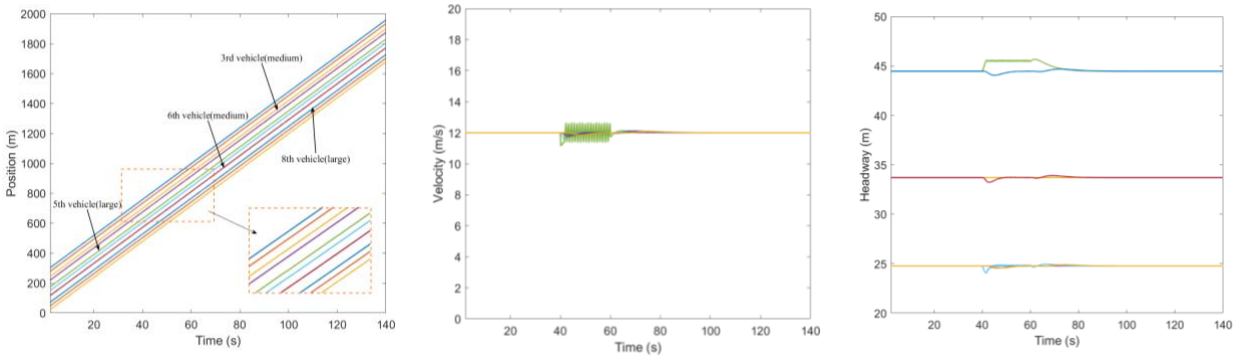

(d) Position evolution (e) Velocity evolution (f) Headway evolution

Figure 6-4 Mixed traffic flow evolution diagrams under the underestimated velocity with/without RRCS

6.4.1.2 Bogus position messages

Overestimate position

The cyberattack set here is that the position information transmitted to the rear vehicle by the third vehicle is 15 meters further than the actual position, which causes the rear vehicle to overestimate the position of the front vehicle, and the attack lasts for 20 seconds, starting from the $t=40\ s$ to $t=60\ s$.

Figure6-5(a)-(c) depicts the evolution of the position, velocity and headway of the

CAV platoon under overestimated position message attack without RRCS. In Figure 6-5(a) and Figure 6-5(c), when the cyberattack occurs, the fourth vehicle represented by the purple line begins to approach the third vehicle, resulting in too small headway. While in Figure 6-5(d) and Figure 6-5(f), under the attack of false position information, the vehicle is also dynamically adjusted, and there will be no scene of trolley headway. Comparing the evolution diagram of vehicle velocity under the influence of overestimating position with or without the RRCS in Figure 6-5(b) and Figure 6-5(e), we can find when there is no RRCS, the velocity of the fourth cheated vehicle changes suddenly when the cyberattack occurs in *t=40 s* and returns to normal at the end of the cyberattack in *t=60 s*. When there is RRCS, the velocity is dynamically adjusted to maintain an appropriate headway. However, there is also a disadvantage that acceleration and deceleration are more frequent, which will have an adverse impact from the perspective of passenger comfort. Overall, the RRCS can play a positive role in dealing with the cyberattack of overestimating position information.

Without RRCS

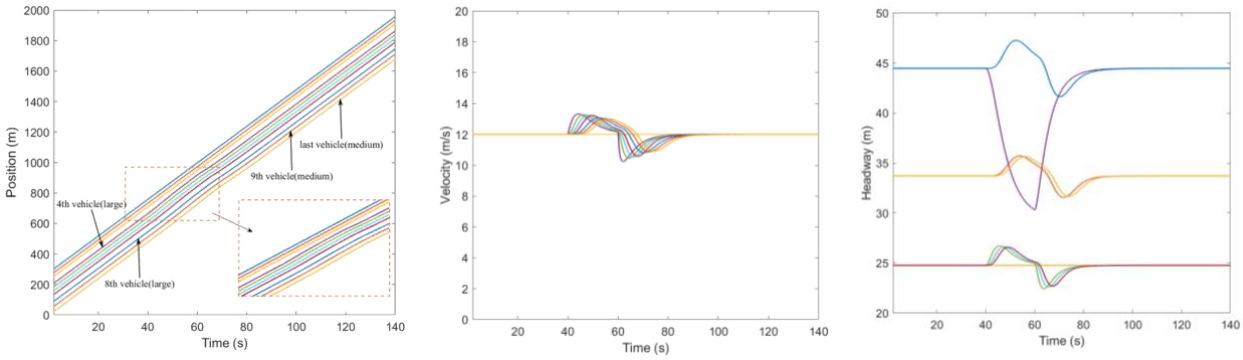

(a) Position evolution (b) Velocity evolution (c) Headway evolution

With RRCS

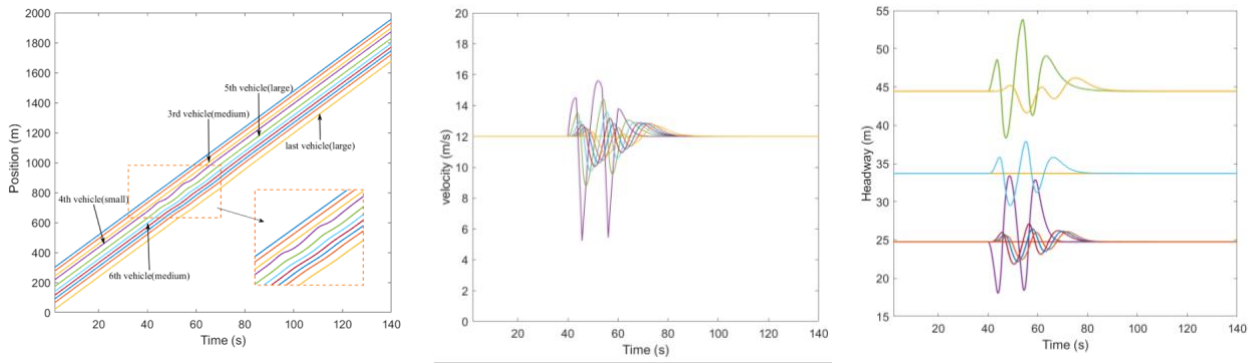

(d) Position evolution (e) Velocity evolution (f) Headway evolution

Figure 6-5 Mixed traffic flow evolution diagrams under the overestimated position with/without RRCS

Underestimate position

Similarly, we set up an attack of underestimated position, tampering with the position information of the third vehicle in the 40th second, so that the position information transmitted to the fourth car is 15 meters closer than the actual position. Figure 6-6(a) shows the position evolution of vehicles under the influence of cyberattacks when there is no strategy. The purple line represents the fourth vehicle cheated by the false information of the vehicle in the front, which is a small car.

Without RRCS

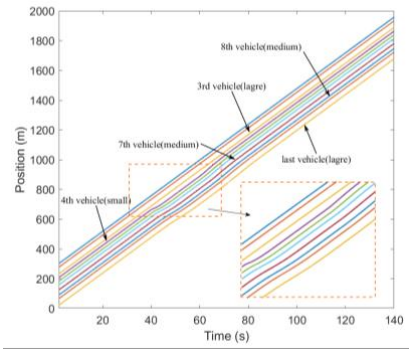

(a) Position evolution

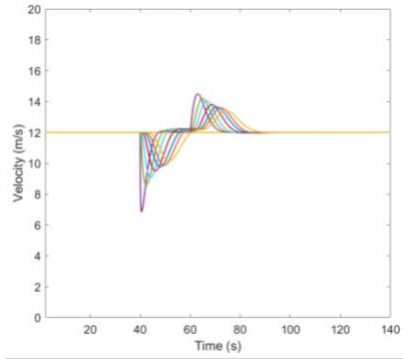

(b) Velocity evolution

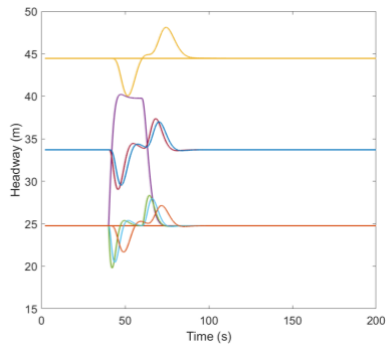

(c) Headway evolution

With RRCS

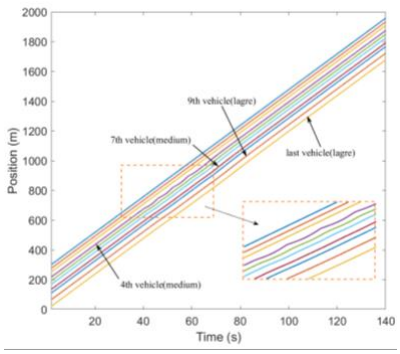

(d) Position evolution

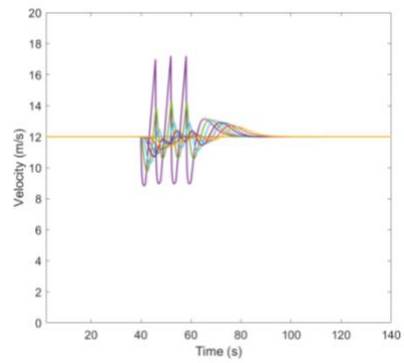

(e) Velocity evolution

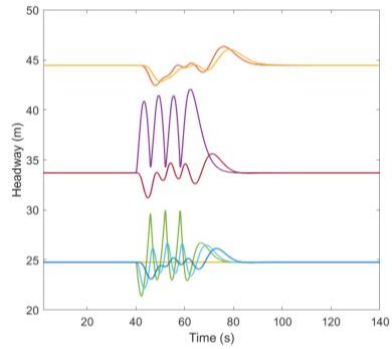

(f) Headway evolution

Figure 6-6 Mixed traffic flow evolution diagrams under the underestimated position with/without RRCS

It can be seen from Figure 6-6(b) and Figure 6-6(c) that the velocity of the fourth vehicle decelerates from the steady-state velocity of *12m/s* to *8.7m/s* in the 40th second, and the headway increases from the steady-state headway to 40 meters, which has a negative impact on the whole traffic flow system. Figure 6-6(d)-(f) is the evolution diagram of position, velocity and headway under the RRCS. Figure 6-6(d) shows that the fourth vehicle is a medium-sized vehicle, and the wave line with minimal amplitude means the process of the vehicle resisting the cyberattack under the influence of the

control strategy. In the process of the application of the RRCS, the velocity appears more frequent acceleration and deceleration fluctuations, but it can ensure that under the influence of cyberattacks, the headway can be ensured in a stable and safe range, which can be revealed from Figure 6-6(e) and Figure 6-6(f).

Replay messages attack- Replay old acceleration

After randomly generating a platoon of three types of vehicles, we make all vehicles start to drive at a uniform constant speed of *12 m/s*. At $t = 30s$, the leading vehicle started to accelerate at an acceleration of $0.5m/s^2$ and lasted for 10 seconds. Then the leading vehicle remains its velocity. At $t = 45s$, the attacker recorded the acceleration message of the subject vehicle and replayed the message to it and its followers. The attack lasted 13 seconds and ended at $t = 58s$.

Without RRCS

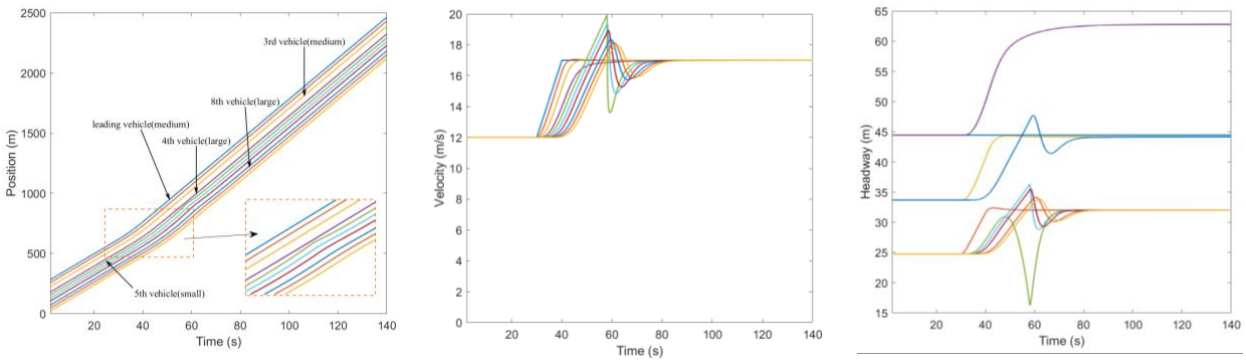

(a) Position evolution (b) Velocity evolution (c) Headway evolution

With RRCS

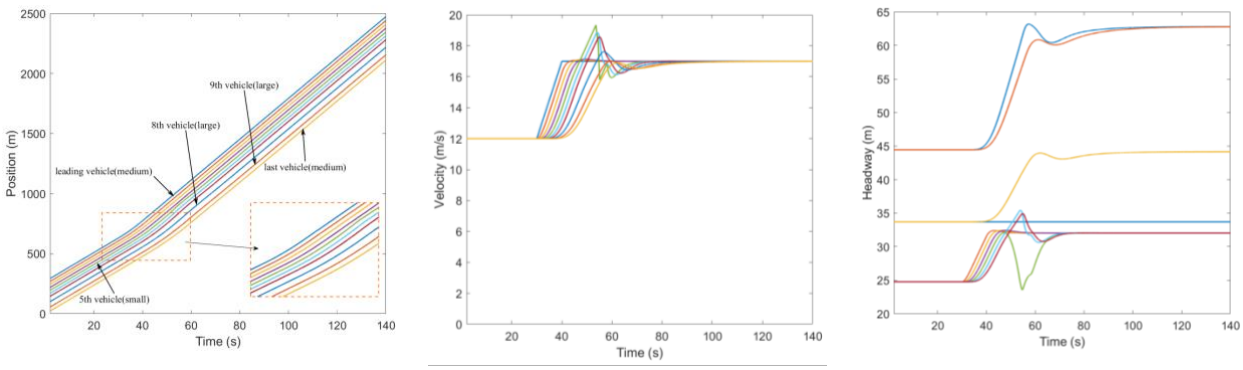

(d) Position evolution (e) Velocity evolution (f) Headway evolution

Figure 6-7 Mixed traffic flow evolution diagrams under replay acceleration attacks with/without RRCS

Figure 6-7 described the mixed traffic flow evolution under replay acceleration attacks with/without RRCS. In Figure 6-7(a), the purple line and the green line corresponding to the fourth vehicle and the fifth vehicle are very close to each other from $t = 45s$ to $t = 58s$ when they are attacked, so the stability is poor and the risk is high. In Figure 6-7(b) and Figure 6-7(c), the speed of the fifth car reached *19.7m/s*, and the headway was shortened to *16.2 m*. After the RRCS is added, the evolution of position, velocity and headway (vehicle position states in the platoon from the leader position) is improved, as shown in Figure 6-7(d)-(f). For example, in Figure 6-7(f), under the influence of replay acceleration attacks, the fifth vehicle will not always approach the front vehicle or even rear end, but still maintain a suitable headway, and under this acceleration control strategy, the vehicle can return to the steady velocity and steady headway, showing the superiority of the RRCS.

6.4.1.3 Collusion attack

Overestimate the velocity of two different vehicles simultaneously (Type I)

The actual scenario corresponding to this part is that the attacker forges messages from multiple vehicles at the same time to mislead the subject vehicle. Firstly, the first kind of collusion attack (Type I) means that the velocity information of two different vehicles is tampered with simultaneously. The specific setting here is that the velocity messages issued by the third vehicle and the seventh vehicle from *t=40 s* to *t=60 s* are tampered with 1.5 times of the actual velocity respectively, so the network information received by the fourth vehicle and the eighth vehicle are wrong.

Figure 6-8 shows the evolution of traffic flow under the influence of collusion attacks with/without the RRCS. Compared with the close proximity of the fourth vehicle and the third vehicle, the eighth vehicle and the seventh vehicle in Figure 6-8(a), the evolution of driving position between the vehicles in Figure 6-8(d) has been better improved, which is the role of RRCS in the cyberattack stage. In Figure 6-8(c), the fourth vehicle is a small vehicle, and the eighth vehicle is a medium vehicle. The headway of each vehicle decreases from its constant-state headway to *11.5 m* and *14.0 m* respectively, which causes adverse interference and impact on the safety and stability of the CAV platoon. Compared with bogus information attacks, collusion attacks generate more serious traffic risks.

Figure 6-8(d)-(f) shows the evolution of traffic flow under the influence of collusion attack when the RRCS is added, which reveals that RRCS can still play a

positive role under collusion attack. However, there is also an adverse phenomenon here, that is, the frequent velocity fluctuations in the process of resisting cyberattacks, resulting in the decline of passenger comfort.

Without RRCS

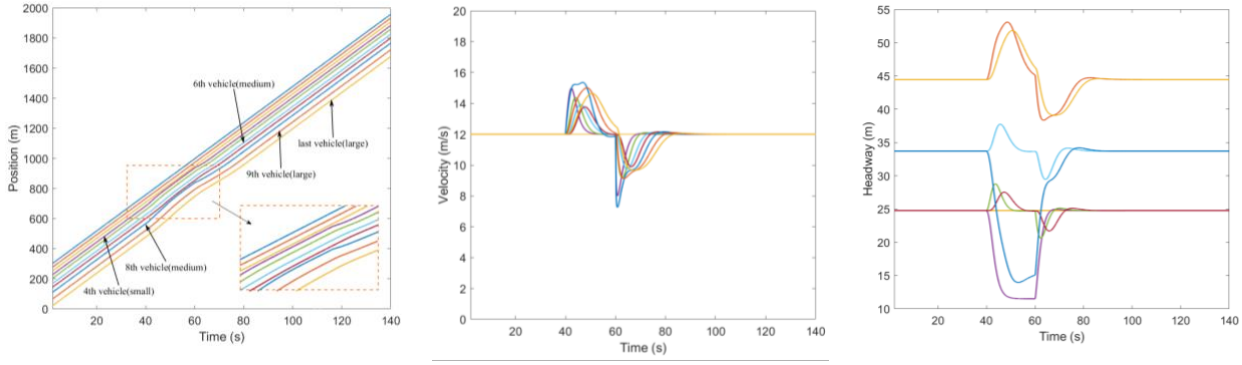

(a) Position evolution (b) Velocity evolution (c) Headway evolution

With RRCS

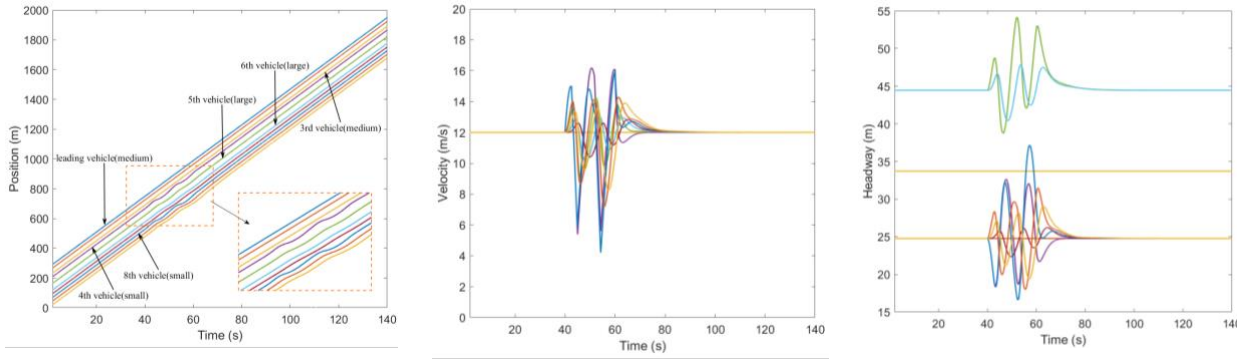

(d) Position evolution (e) Velocity evolution (f) Headway evolution

Figure 6-8 Mixed traffic flow evolution diagrams under collusion attacks (Type I) with/without RRCS

Overestimate the velocity of one vehicle and the position of another vehicle simultaneously (Type II)

Another type of collusion attack we have tested is called Type II, which means that the velocity information of one vehicle and the position information of another vehicle are tampered simultaneously. Specifically, the velocity information of the third vehicle is tampered with 1.5 times the actual velocity and transmitted to the fourth vehicle, and the location information of the seventh vehicle is tampered with to be 17 meters farther than the actual distance and transmitted to the eighth vehicle. The whole collusion attack lasted 20 seconds, from $t=40\ s$ to $t=60\ s$. Comprehensive comparative analysis

of Figure 6-9 shows that the application of RRCS can play the following three roles when vehicles are attacked: the first is to make fewer vehicles have a greater impact on velocity fluctuations; the second is to make the attacked vehicles keep a reasonable headway; the third is to make the CAV platoon return to a stable state faster. Therefore, this also shows that the RRCS can also deal with different forms of collusion attacks.

Without RRCS

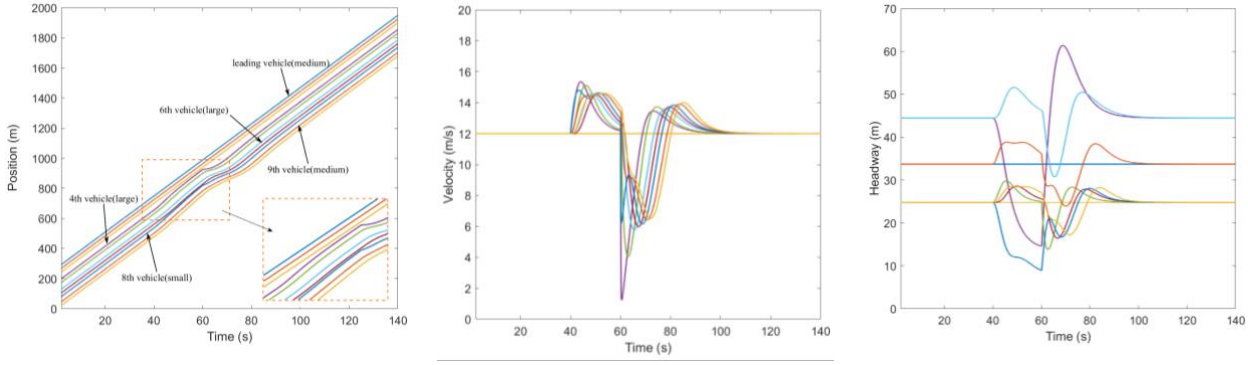

(a) Position evolution (b) Velocity evolution (c) Headway evolution

With RRCS

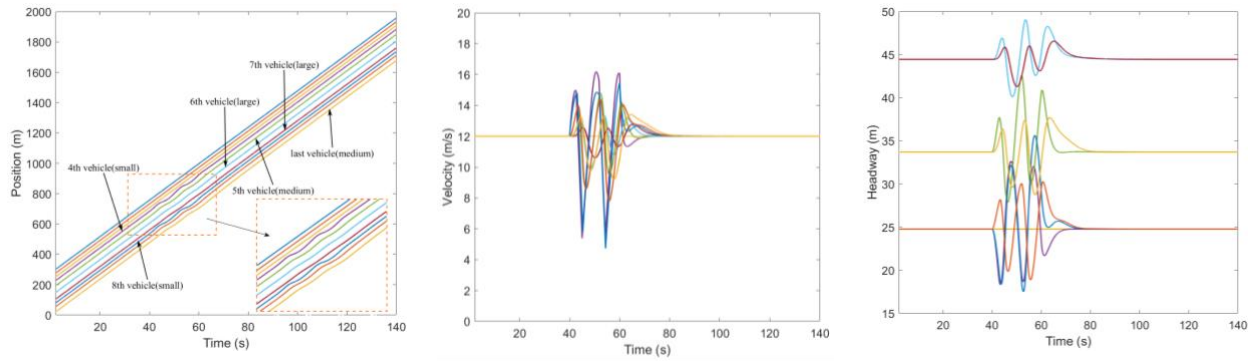

(d) Position evolution (e) Velocity evolution (f) Headway evolution

Figure 6-9 Mixed traffic flow evolution diagrams under collusion attacks (Type II) with/without RRCS

6.4.2 Sensitivity analysis for RRCS

In order to study the effect of RRCS on traffic flow stabilization when vehicles are subjected to cyberattacks, we observe and analyze the distribution of headway of all vehicles with or without RRCS over time. It is worth noting that considering the different steady-state headway of different vehicle types, it is unreasonable to directly calculate the variance of all headway at all times for analysis. Therefore, we first calculate the deviation between the headway of all vehicles at all times and their own

steady-state headway, and then analyze the variance of this deviation as an indicator. The specific expression is as follows,

$$\begin{aligned}
&\Delta x_n^e(t) = s_n^e(t) + l_n(t) \\
&\Delta x_n^{dev}(t) = \Delta x_n(t) - \Delta x_n^e(t) \\
&c_1 = \frac{t_1}{\Delta t} \\
&c_2 = \frac{t_2}{\Delta t} \\
&\Delta x_{mean}^{dev} = \frac{\sum_{k=c_1}^{c_2}\sum_{n=1}^{10}\Delta x_n^{dev}(k)}{10*(c_2 - c_1)} \\
&\mathrm{VAR} = \frac{\sum_{k=c_1}^{c_2}\sum_{n=1}^{10}\left(\Delta x_n^{dev}(k) - \Delta x_{mean}^{dev}\right)^2}{10*(c_2 - c_1) - 1}
\end{aligned} \tag{6.7}$$

where

$\Delta x_n^e(t)$ = steady-state headway;

$\Delta x_n^{dev}(t)$ = the deviation between actual headway and steady headway;

c_1 = count start position;

c_2 = count end position;

t_1 = the start time of the evolution phase used to calculate the variance, $t_1 = 40s$;

t_2 = the end time of the evolution phase used to calculate the variance, $t_2 = 60s$;

k = number of discrete time steps;

Δt = time step, 0.01s for each step;

Δx_{mean}^{dev} = average of all deviations;

VAR = variance.

6.4.2.1 Sensitivity analysis of different platoon compositions

Furthermore, due to the necessity of exploring the universality of RRCS to deal with cyberattacks in different scenarios, we carried out numerical simulation covering more generally applicable traffic flow composition scenarios, mainly including different vehicle distribution types and proportions.

Firstly, our simulation object is still a platoon composed of 10 vehicles, then 25 different proportion combinations are randomly generated by Gaussian mixture distribution for the proportion composition of large, medium and small vehicles, and then 4 vehicle distribution types are randomly generated for each proportion combination. Therefore, 100 different platoon compositions scenarios are randomly generated here, as shown in Table 6-3. In addition, the seven cyberattack types and

specific forms are also consistent with the cyberattacks in the simulation in Section 6.4.1.

Table 6-3 CAV platoon composition types (100 in total)

Vehicle proportion (small:medium:large)	*Vehicle distribution*
7:1:2	S-S-S-L-S-S-L-S-S-M
	S-S-S-S-L-S-L-S-S-M
	S-S-S-S-S-S-M-S-L-L
	S-M-S-S-S-S-L-S-S-L
2:6:2	M-M-M-M-M-S-M-S-L-L
	S-L-S-L-M-M-M-M-M-M
	M-M-M-S-M-M-M-L-L-S
	M-M-L-M-L-S-M-S-M-M
5:1:4	L-S-S-S-S-L-S-L-L-M
	S-L-S-S-S-L-S-L-L-M
	S-L-L-S-S-L-L-S-S-M
	L-M-S-L-L-L-S-S-S-S
. . .	. . .
6:3:1	S-M-S-S-M-L-S-M-S-S
	M-S-M-S-M-S-S-L-S-S
	S-M-M-S-S-L-S-S-S-M
	M-S-S-S-S-M-S-S-M-L

*S means the small vehicle, M means the medium vehicle, L means the large vehicle

In the case of 100 randomly generated platoon composition, we calculate the variance of headway deviation value with or without RRCS in different cyberattack scenarios, and drew the results into the box plot that can directly reflect the distribution characteristics of all variances shown in Figure 6-9 for comparative analysis. The relevant result data are shown in Table 6-4 below.

Figure 6-10(a)-(d) shows the box plot of variance distribution of headway deviation value in 100 traffic flow scenarios with or without RRCS under bogus messages attack. The attack type in Figure 6-10(a) is overestimated velocity information. In the absence of RRCS, the upper quartile and median of variance distribution are *52.44* and *24.95* respectively, while in the presence of RRCS, the upper quartile and median decreased to *28.09* and *16.87* respectively. Looking at Figure 6-10(b), the simulated cyberattack form is overestimated position information attack. The upper quartile and median of variance with RRCS are *19.78* and *3.48* respectively, which is also obviously lower than that without RRCS. Figure 6-10(c) represents the cyberattack scenario corresponding to underestimated velocity information. Compared

with the upper quartile and median of *18.38* and *15.55* without RRCS, the presence of RRCS significantly reduces the upper quartile and median to *17.64* and *10.85* respectively. The comparison in Figure 6-10(d) describing the cyberattack scenario of underestimating position information is significant, and the upper quartile and median of variance decrease from *21.80* and *19.23* without RRCS to *3.96* and *3.59* with RRCS. In addition, the more prominent and interesting findings are as follows: first, in the cyberattack scenario with overestimated position information, in the case of 100 different traffic flow compositions randomly generated, RRCS will play a negative role in coping with cyberattack in a few cases; Second, the effect of RRCS in the attack scenario of underestimating velocity information and underestimating position information is better than the other two scenarios of overestimating vehicle information. Overall, the above four figures reflect the positive role of RRCS proposed in this chapter in dealing with the cyberattack type of bogus messages, that is, RRCS can resist the damage of cyberattack to the stability of traffic flow and help the traffic flow develop in a stable direction.

Secondly, we discuss the impact of RRCS on traffic flow stability under cyberattack scenarios of replay old acceleration information. The box diagram on the left in Figure 6-10(e) shows the variance distribution of headway deviation without RRCS, and its upper quartile and median are *28.42* and *24.76* respectively, while the box diagram on the right is obtained after RRCS plays a role when the vehicle platoon is attacked by the network, and its upper quartile and median are reduced to *25.42* and *20.13* respectively. Although the improvement effect is not very significant in terms of variance distribution, it also means that RRCS can also play a favorable role in resisting the cyberattack of replay old acceleration and promote the stability of the platoon.

The cyberattack scenarios corresponding to Figure 6-10(f) and Figure 6-10(g) are two types of collusion attacks described in section 6.4.1. In Figure 6-10(f), the upper quartile and median of the left box graph without RRCS are *68.98* and *42.14* respectively, which are higher than *36.48* and *23.71* of the right box diagram with RRCS. The overall trend of Figure 6-10(g) is similar to that of Figure 6-10(f). Compared with the case without RRCS, the upper quartile and median of variance distribution with RRCS are reduced from *43.80* and *36.54* to *41.57* and *33.24*. The results of the above two figures confirm the feasibility of the RRCS proposed in this chapter in resisting collusion attacks and improving the resilience and robustness of vehicle platoon.

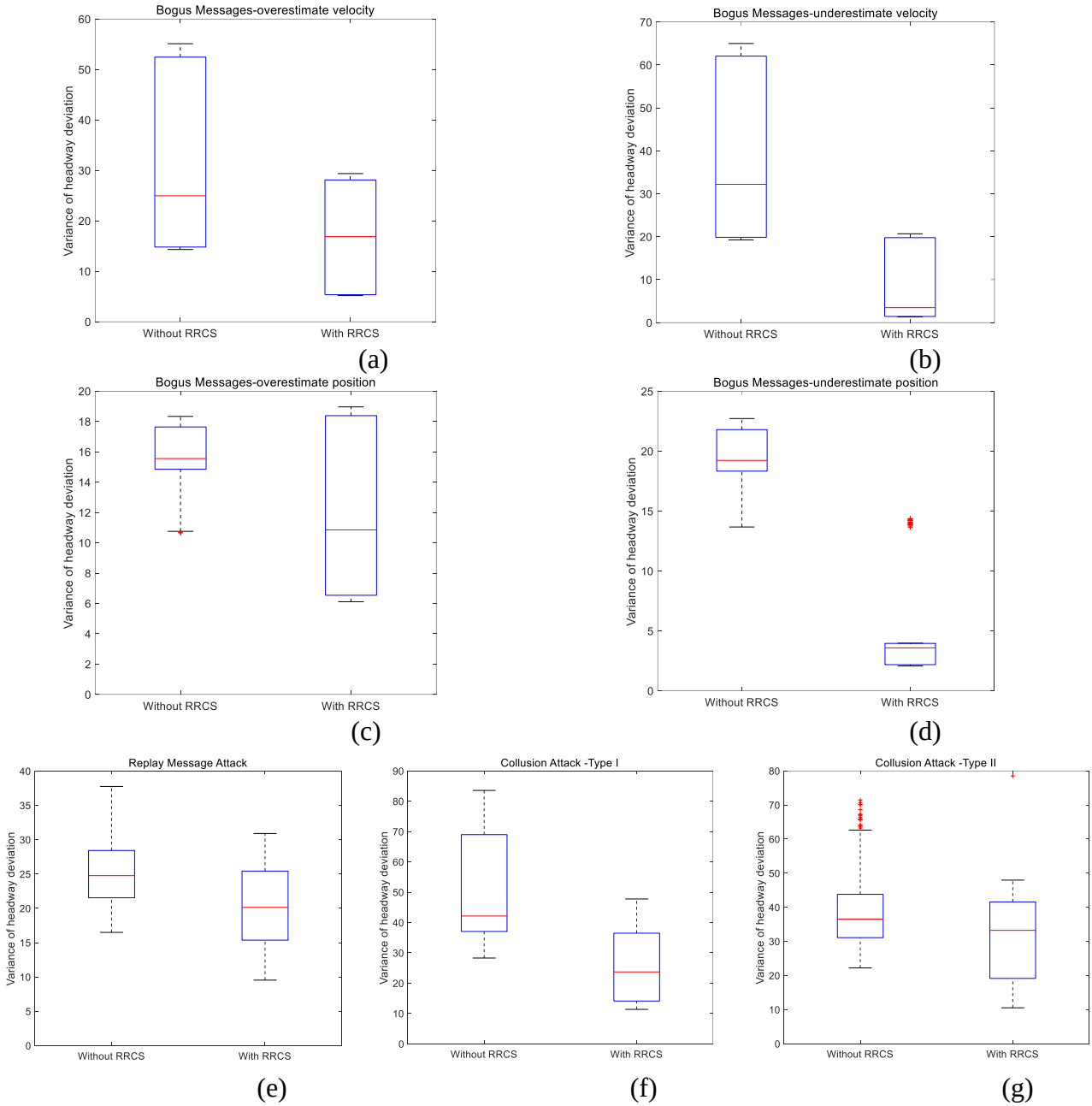

Figure 6-10 Variance distribution of headway deviation under different cyberattacks scenarios with different vehicle proportion and distribution

Table 6-4 Box plot data of variance distribution of headway deviation with or without RRCS under different vehicle proportion and vehicle distribution

Cyberattack type	*RRCS*	*Upper quartile*	*Median*	*U-IV*	*M-IV*	*U-IP*	*M-IP*
Overestimate velocity	Y	28.09	16.87	24.35	8.08	46.43%	32.38%
	N	52.44	24.95				
Underestimate velocity	Y	19.78	3.48	42.26	28.71	68.12%	89.19%
	N	62.04	32.19				
Overestimate position	Y	17.64	10.85	0.74	4.7	4.03%	30.23%
	N	18.38	15.55				

Underestimate position	Y	3.96	3.59	17.84	15.73	81.83%	81.80%
	N	21.80	19.23				
Replay old acceleration	Y	25.42	20.13	3.00	4.63	10.56%	18.70%
	N	28.42	24.76				
collusion attack - Type I	Y	36.48	23.71	32.50	18.43	47.12%	43.74%
	N	68.98	42.14				
collusion attack - Type II	Y	41.57	33.24	2.23	3.30	5.09%	9.03%
	N	43.80	36.54				

**Y* indicates the presence of RRCS, *N* indicates the absence of RRCS, *U-IV* means Upper quartile improvement value, *M-IV* means Median improvement value, *U-IP* means Upper quartile improvement percentage, *M-IP* means Median improvement percentage.

6.4.2.2 Sensitivity analysis of different attack intensity

In the above numerical simulation, the respective cyberattack intensity under different cyber- attack scenarios considered is a fixed value, such as overestimated velocity attack of 1.5 times the actual velocity and underestimated velocity attack of 0.4 times the actual velocity. In this section, we further explore the variance distribution of headway deviation under different cyberattack scenarios when the cyberattack intensity follows the linear distribution, so as to verify that the effectiveness of the RRCS proposed in this chapter in resisting cyberattacks is not accidental in individual attack intensity scenarios. The cyberattack intensity of different attack types subject to linear distribution is shown in Table 6-5 Table 6-5below.

Table 6-5 Linearly distributed cyberattack intensity in different cyberattacks scenarios

Cyberattack type	*Specific distribution of cyberattack intensity*
Overestimate velocity	Actual Velocity * (1.1~3.5)
Underestimate velocity	Actual Velocity * (0.1~0.9)
Overestimate position	Actual Position + (5~45)
Underestimate position	Actual Position - (5~25)
Replay old acceleration	Replay lasts for (1s~10s)
collusion attack -Type I	Actual Velocity * (1.1~3.1) and Actual Velocity * (1.1~3.1)
collusion attack -Type II	Actual Velocity * (1.1~3.1) and Actual Position + (5~30)

Here, we set the composition of the platoon as two large vehicles, two medium vehicles and six small vehicles, and the vehicle distribution is randomly formed. Figure 6-11 is a set of variance distribution box diagrams of headway deviation obtained by

setting different cyberattack intensities under different cyberattack scenarios. Table 6-6 shows the specific data of the box diagram corresponding to Figure 6-11and some intuitive comparison data, including the improvement value and improvement proportion of the upper quartile value and median value in the box diagram.

On the premise that the multiple of overestimated velocity attack obeys the linear distribution of *1.1* to *3.5* times, Figure 6-11(a) shows the box diagram of variance distribution of headway deviation with or without RRCS. An important discovery is that the upper quartile values of the two box graphs are equal, which actually means that when the attack velocity reaches a certain multiple, RRCS will not continue to play a role, which will need further research. Nevertheless, the median with RRCS is still *22.81%* lower than that without RRCS, which shows the positive role of RRCS in overestimated velocity attack to a certain extent. Figure 6-11(b) is the box diagram drawn by setting a group of linearly distributed underestimated velocity attacks. Obviously, the upper quartile of the right box graph is even smaller than the lower quartile of the left box plot, which conveys the universal effectiveness of RRCS in resisting cyberattacks under the scenario of underestimated velocity attacks. Then we focus on Figure 6-11(c) and Figure 6-11(d). These two box charts correspond to overestimated position attack and underestimated position attack respectively. The overestimated position satisfies the linear distribution of 5 meters to 45 meters away from the actual position, and the underestimated position satisfies the linear distribution of 5 meters to 25 meters closer to the actual position. In Figure 6-11(c), compared with the case without RRCS to resist cyberattacks, the upper quartile and median of the box chart on the right when RRCS plays a role are reduced to *5.81* and *5.03* respectively, which significantly enhances the stability. In Figure 6-11(d), the upper quantile and median of the box graph without RRCS are 20.07 and 10.89, which are significantly higher than the indicators of the box graph with RRCS, showing that RRCS can enhance the stability of the platoon when underestimated position attack occurs.

Then, we move to the cyberattack scenario of replay old acceleration and the replay duration is determined to obey the linear distribution of 1 second to 10 seconds, the box diagram is shown in Figure 6-11(e). After RRCS played a role, the upper quartile and median of the variance distribution of headway deviation decreased by *60.53%* and *61.46%* respectively, which shows that RRCS can slow down the negative impact of replay old acceleration cyberattack on the platoon.

Next, we analyze the variance distribution of the headway deviation with or without RRCS when the collusion attack obeys the linear distribution. The collusion attack corresponding to Figure 6-11(f) is that the overestimated multiple of the overestimated velocity attack suffered by two vehicles follows a linear distribution of 1.1 to 3.1 times the actual velocity. It is worth noting that by comparing the left and right box graphs in Figure 6-11(f), we can find that RRCS can't play a positive role in the scenario of few attacks, but from the two indicators of the upper quartile and median, RRCS can resist collusive attacks (Type I) as a whole. Finally, the premise of drawing Figure 6-11(g) is to meet the collusion attack that the velocity attack multiple obeys the linear distribution of 1.1-3.1 times and the position attack information obeys the linear distribution of 5-30 meters away from the actual position. By observing and comparing the Figure 6-11, it can be seen that the upper quartile decreased from 58.48 without RRCs to 13.87 with RRCS, and the median decreased from 39.16 to 10.61, down 76.28% and 72.91% respectively, which significantly shows that RRCS can maintain good stability when the platoon is subjected to collusive attacks (Type II).

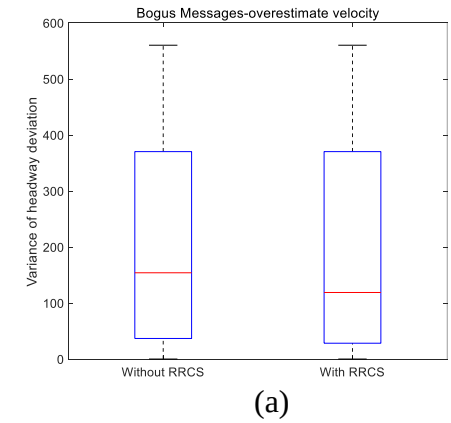

(a)

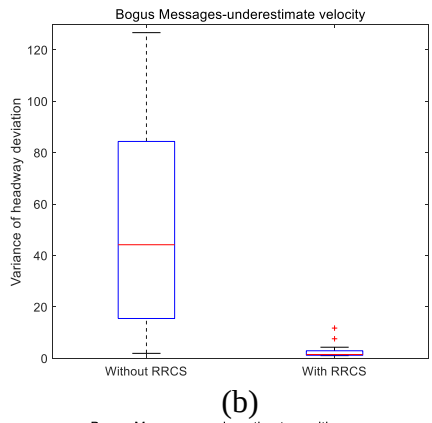

(b)

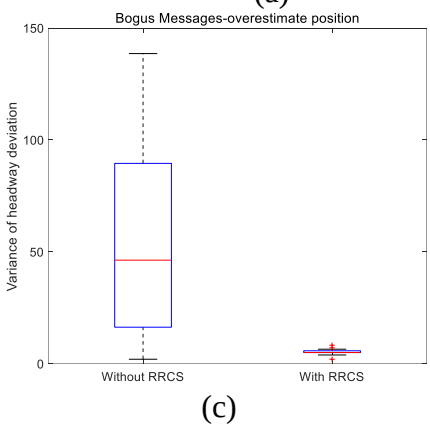

(c)

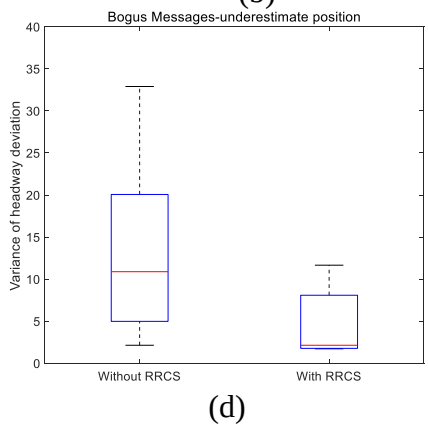

(d)

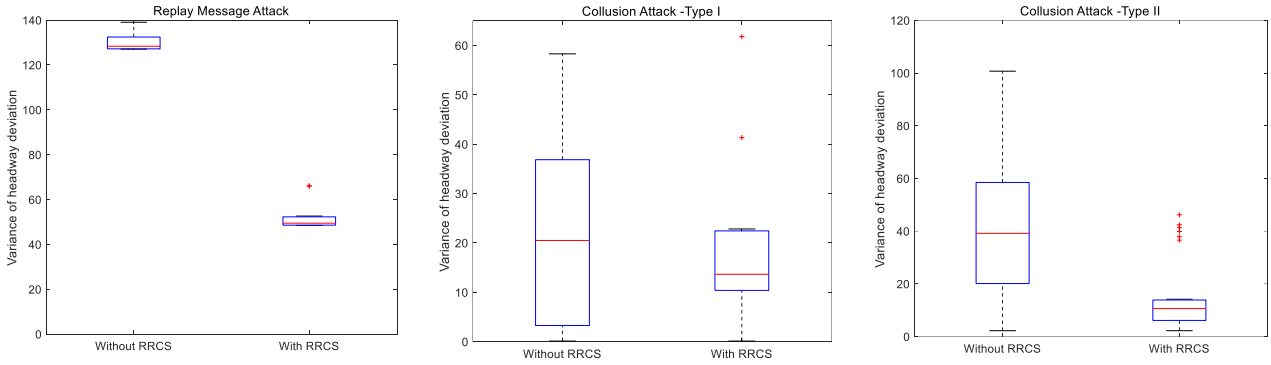

(e) (f) (g)

Figure 6-11 Variance distribution of headway deviation under different cyberattacks scenarios with different cyberattack intensities

Table 6-6 Box plot data of variance distribution of headway deviation with or without RRCS under different cyberattack intensities

Cyberattack type	*RRCS*	*Upper quartile*	*Median*	*U-IV*	*M-IV*	*U-IP*	*M-IP*
Overestimate velocity	Y	370.38	118.96	0	35.18	0%	22.82%
	N	370.38	154.14				
Underestimate velocity	Y	2.95	1.49	81.42	42.71	96.50%	96.63%
	N	84.37	44.20				
Overestimate position	Y	5.81	5.03	83.73	41.27	93.51%	89.14%
	N	89.54	46.30				
Underestimate position	Y	8.09	2.14	11.98	8.75	59.69%	80.35%
	N	20.07	10.89				
Replay old acceleration	Y	52.28	49.46	80.18	78.89	60.53%	61.46%
	N	132.46	128.35				
collusion attack - Type I	Y	22.44	13.65	14.42	6.85	39.12%	33.41%
	N	36.86	20.50				
collusion attack - Type II	Y	13.87	10.61	44.61	28.55	76.28%	72.91%
	N	58.48	39.16				

**Y* indicates the presence of RRCS, *N* indicates the absence of RRCS, *U-IV* means Upper quartile improvement value, *M-IV* means Median improvement value, *U-IP* means Upper quartile improvement percentage, *M-IP* means Median improvement percentage.

One-way Analysis of Variance (ANOVA) was carried out to further test whether there is significant difference in the variance distribution of headway deviation with or without RRCS as shown in the Table 6-7 below. In most scenarios, the p-values are less than 0.05, which shows that there is significant difference in the variance distribution of headway deviation with or without RRCS under the simulation premise that the cyberattack intensity follows the linear distribution. It proves that RRCS could effectively alleviate the threat brought by cyberattacks in most scenarios with different

cyberattack intensities. Besides, the p-values of overestimate velocity attack scenario and collusion attack-Type I scenario are *0.9234* and *0.7215* respectively, which indicates that there is no significant difference in the deviation distribution of headway with or without RRCS in different cyberattack intensities. RRCS could not mitigate the negative impacts of cyberattacks in some cases of these two scenarios. More complementary strategies need to be further explored in the future.

Table 6-7 One-way ANOVA with or without RRCS under different cyberattacks scenarios

Scenarios	*Source*	*SS*	*df*	*MS*	*F*	*p-value*
Overestimate velocity	Columns	212.1	1	212.1	0.01	0.9234
	Error	538997.7	24	22458.2		
	Total	539209.8	25			
Underestimate velocity	Columns	20369.7	1	20369.7	24.49	2.30386e-5
	Error	26612.2	32	831.6		
	Total	46981.9	33			
Overestimate position	Columns	25993.6	1	25993.6	27.4	5.58769e-6
	Error	37942.6	40	948.6		
	Total	63936.2	41			
Underestimate position	Columns	295.68	1	295.683	4.93	0.0434
	Error	839.2	14	59.943		
	Total	1134.88	15			
Replay old acceleration	Columns	33146.9	1	33146.9	1065.52	8.0089e-19
	Error	622.2	20	31.1		
	Total	33769.1	21			
collusion attack -Type I	Columns	49.23	1	49.23	0.13	0.7215
	Error	5982.45	16	373.903		
	Total	6031.68	17			
collusion attack -Type II	Columns	8345.4	1	8345.39	21.05	2.8538e-5
	Error	20612.5	52	396.39		
	Total	28957.9	53			

6.5 Conclusions

It is an initial exploration to study the impact of cyberattacks on the mixed traffic. It should be noted that how cyberattack impacts the travel demand, traffic efficiency and energy consumption of the shared mobility system would be explored in the next stage. Under the background of possible cyberattacks in the future connected and automated vehicles environment, this chapter first builds a CAV mixed traffic flow car-following model considering cyberattacks. This will help us understand the evolution characteristics of CAV mixed traffic flow under cyberattacks. Furthermore, we design an acceleration control switcher as a Robust and Resilient Control Strategy, so that the vehicle can switch the lower layer control strategy according to the current state under

the cyberattack scenario. Finally, traffic simulation experiments are carried out to study the impact of cyberattacks on the evolution of CAV mixed traffic flow with or without RRCS, and to verify the feasibility of the RRCS proposed in this chapter. The conclusion mainly includes the following five points:

- The threat of cyberattacks to CAV mixed traffic flow is significant, and the stability and security of the CAV platoon are adversely affected;
- Different forms of cyberattacks will cause different forms and different degrees of harmful effects. For example, vehicles will suddenly accelerate or brake, resulting in too small or too large headways between vehicles, and may even lead to vehicle collisions;
- Collusive attacks have the greatest adverse impact on the CAV platoon, as they involve multiple vehicle attacks;
- The RRCS proposed in this chapter is feasible. It can not only dynamically switch the acceleration control strategy when the vehicle is under cyberattacks, so as to maintain a safe and appropriate headway, but also ensure that the CAV platoon can gradually return to a stable state after being attacked.
- The results of the sensitivity analyses indicate that RRCS could effectively alleviate the threat brought by cyberattacks in most scenarios with different platoon compositions, vehicle distribution and most different cyberattack intensities, which shows a strong robustness.

Chapter 7 Summary

7.1 Conclusions

Vehicular traffic congestion and air pollution during rush hours are two difficult problems for urban areas worldwide. Shared mobility service and CAVs, two new revolutions in transportation, provide a major historical opportunity to solve the above problems for the rise of new cities. The motivation of this study is to propose an optimization framework for the shared mobility system (SMS). The research results could provide the decision makers with policy implication for a low-carbon transport and help the society better understand how the shared mobility services including potential CAVs will develop in the future.

In this dissertation, we propose an optimization framework for the shared mobility system applicable to CAVs. The shared mobility system is made up of **users** who use/interact/cooperate with **city infrastructures** and **CAVs technologies** on **ridesourcing system** to move efficiently and optimally according to 3 main criteria (efficiency/energy-consumption/safety) for personal or economic goals (see from Figure 7-1). There are four research domains for the shared mobility system with CAVs: city infrastructures, users, shared mobility system and CAVs technologies. Critical results and conclusions can be summarized into the following four aspects:

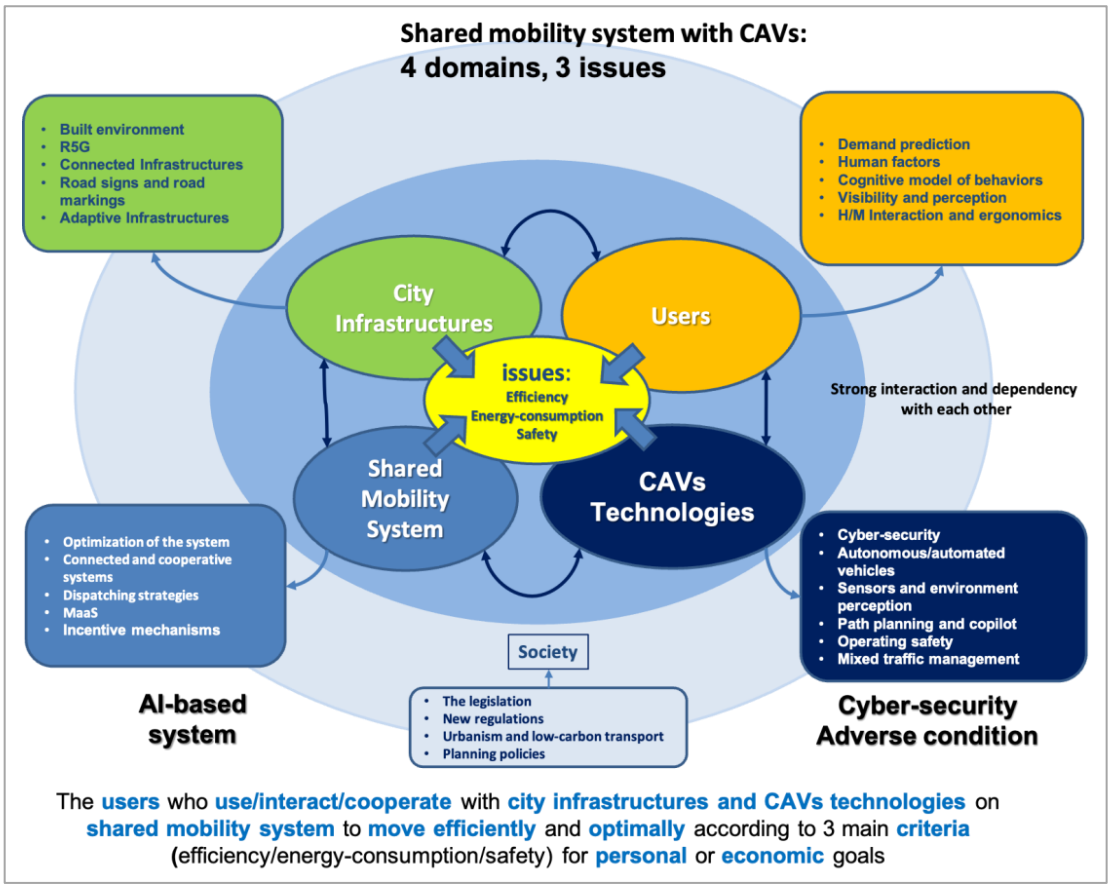

Figure 7-1 A diagram illustration of shared mobility system with CAVs
[Source: modified from (Gruyer et al., 2021) in Gustave Eiffel University]

1) Domain 1: City infrastructures

Research topic: Exploring nonlinear effects of the built environment on ridesplitting service

Ridesplitting, a form of ridesourcing services that matches riders with similar routes to the same driver, is a high occupancy travel mode that can bring considerable benefits. However, the current ratio of ridesplitting in the ridesourcing services is relatively low and its influencing factors remain unrevealed. Therefore, we use a machine learning method, gradient boosting decision tree model, to identify the impacts of the built environment on the origin-destination ridesplitting ratio. The results show that most built environment features have a strong nonlinear effect on the ridesplitting ratio. Distance to city center, land use diversity and road density are the key explanatory variables impacting the ridesplitting ratio. The non-linear thresholds of built environment factors are found based on partial dependence plots, which could provide policy implications for the government and transportation network companies to promote the ridesplitting.

2) Domain 2: Users

Research topic: Improving the demand prediction of ridesourcing services with an Optimized Spatiotemporal Encoder-Decoder Neural Network

Ridesourcing services will be the first application scenario of shared autonomous vehicles with the development of automated technology and the shard economy. The enhancement of spatiotemporal ridesourcing demand prediction performance is important for dispatching shared autonomous vehicles, as this can reduce the idle times of vehicles on streets, which aggravate traffic congestion and air pollution. However, the existing studies focus on single-step prediction, which not only limits the practical application value of the resultant model but also presents the problem of insufficient prediction ability. To fill this gap, we propose a novel ridesourcing demand prediction framework, the optimized spatiotemporal encoder-decoder neural network (O-STEDN). For the encoder layer, we use a combination of a graph convolutional network (GCN) and a read-first long short-term memory (RLSTM) network to better extract spatial and temporal features simultaneously. For the decoder layer, we use an LSTM model and a dynamic spatiotemporal attention mechanism to adaptively associate historical spatiotemporal features with the current prediction. Furthermore, we add residual connections and layer normalization tricks in both the encoder layer and the decoder layer to prevent the loss of feature information and internal covariate shift problems. The experimental results show that the proposed framework outperforms state-of-the-art models for both single-step demand prediction and multi-step prediction. Our method can not only help transportation network companies improve their ridesourcing services but also help policy makers implement traffic demand management measures dynamically. Ridesourcing demand prediction is the first step for the shared mobility system to match the demand and supply and dispatch shared autonomous vehicles appropriately. This capability will be very useful for an optimal dispatching of automated/autonomous vehicles.

3) Domain 3: Ridesourcing system

Research topic: Optimizing ridesourcing system based on a shareability network

Ridesourcing services play a crucial role in metropolitan transportation systems and aggravate urban traffic congestion and air pollution. Ridesplitting is one possible way to reduce these adverse effects and improve the transport efficiency, especially during rush hours. We explore the potential of ridesplitting during peak hours using

empirical ridesourcing data provided by DiDi Chuxing, which contains complete datasets of ridesourcing orders in the city of Chengdu, China. A ridesplitting trip identification algorithm based on a shareability network is developed to quantify the potential of ridesplitting. Then, we evaluate the gap between the potential and actual scales of ridesplitting. The results show that the percentage of potential cost savings can reach 18.47% with an average delay of 4.76 minutes, whereas the actual percentage is 1.22% with an average delay of 9.86 minutes. The percentage of shared trips can be increased from 7.85% to 90.69%, and the percentage of time savings can reach 25.75% from 2.38%. This is the first investigation of the gap between the actual level and the potential of ridesplitting on a city scale. The proposed ridesplitting algorithm can not only bring benefits on a city level but also take passenger delays into consideration. The quantitative benefits could encourage transportation management agencies and transportation network companies to develop sensible policies to improve the existing ridesplitting services. This chapter could be seen as a work which explores the potential of connected and autonomous vehicles on ridesourcing services in perfect condition.

4) Domain 4: CAVs technologies

Research topic: Proposing a resilient and robust control strategy for connected and autonomous vehicles to resist the threat of cyber-attacks

CAVs present significant potentials for improving road safety and mitigating traffic congestion for the future mobility system. However, cooperative driving vehicles are more vulnerable to cyberattacks when communicating with each other, which will introduce a new threat to the transportation system. In order to guarantee safety aspects, it is also necessary to ensure a high level of information quality for CAV. To the best of our knowledge, this is one of the first investigations on the impacts of cyberattacks on CAV in mixed traffic (large vehicles, medium vehicles, and small vehicles) from the perspective of vehicle dynamics. The research part aims to explore the influence of cyberattacks on the evolution of CAV mixed traffic flow and propose a resilient and robust control strategy (RRCS) to alleviate the threat of cyberattacks. First, we propose a CAV mixed traffic car-following model considering cyberattacks based on Intelligent Driver Model (IDM). Furthermore, a RRCS for cyberattacks is developed by setting the acceleration control switch and its impacts on the mixed traffic flow are explored in different cyberattack types. Finally, sensitivity analyses are conducted in different platoon compositions, vehicle distribution and cyberattack

intensities. The results show that the proposed RRCS of cyberattacks is robust and can resist the negative threats of cyberattacks on the CAV platoon, thereby providing a theoretical basis for restoring the stability and improving the safety of the CAV.

7.2 Perspectives

The perspectives for the shared mobility services involving the deployment of CAVs can be summarized as follows:

1) Domain 1: City infrastructures

Research perspectives in the proposed topic: Exploring nonlinear effects of the built environment on ridesplitting service

This study uses the GBDT model to explore the nonlinear relationship between the built environment features and ridesplitting ratio, which can provide a more reasonable explanations without hypothesizing a prior function. However, this study has some limitations, which could be improved by further research in the future. In this study, we use ridesourcing data for only one city and only one month. The proposed method can be easily applied to other cities. We need more data from other cities and other time durations to compare and validate the relationship between the features of the built environment and the ridesplitting ratio. Furthermore, we consider only the effects of the built environment features, demographic factors and travel time on ridesplitting, while more travel impedance variables such as delays and detours, travel behaviors over a week (weekdays and weekends), and travel behaviors during one day (peak and nonpeak hours), may also have impacts on the ridesplitting ratio; therefore, these variables need to be explored. In addition, we divide Chengdu into 162 census tracts based on the administrative boundaries. We can investigate the results of the different scaling cells to explore the impacts of the scaling method. This study uses the modeling method to explore the relationship between ridesplitting and built environment. It should be noted that there are some qualitative approaches, such as deductive and inductive, which could also be used for research on the built environment.

Other research directions in this domain: R5G, connected infrastructures, road signs and road markings, adaptive infrastructures, etc.

It is worth exploring that the safety and efficiency impacts on CAVs of connected

and adaptive infrastructures, such as communication facilities (R5G) and road infrastructures (road signs, road markings). It is also recommended that the impacts on pedestrians and conventional human-driven vehicles of connected and adaptive infrastructures.

Another study could be to identify the traffic bottlenecks due to the infrastructure and to propose adapted or new infrastructure allowing an efficient ridesourcing with connected and autonomous vehicles. This remark lead to the following research direction about R5G and new infrastructure concepts like LOSAD (Level Of Service for Automated Driving) and ISAD (Infrastructure Services for Autonomous Driving).

2) Domain 2: Users

Research perspectives in the proposed topic: Improving the demand prediction of ridesourcing services with an Optimized Spatiotemporal Encoder-Decoder Neural Network

One possible direction for future work is to further study how to develop a real-time dispatching and trajectory planning scheme for shared autonomous vehicles according to the demand prediction results of ridesourcing services. And it is worth studying how to set the time windows for the demand prediction to optimize the whole shared mobility system.

Other research directions in this domain: human factors, transportation equity, cognitive model of behaviors visibility and perception, H/M Interaction and ergonomics, etc.

There are still some directions which could be further explored in the future: human factors involved in the shared mobility services with CAVs such as personalized preferences of users. It is worth considering how to guarantee the equity of shared mobility services with CAVs such as elderly or disabled people.

3) Domain 3: Ridesourcing system

Research perspectives in the proposed topic: Optimizing ridesourcing system based on a shareability network with connected and autonomous vehicles

There are some limitations to the current study, which can motivate a few future research directions. First, it assumes that all the passengers using the ridesourcing service are willing to use a ridesplitting service. In fact, the percentage of passengers who choose ridesplitting services is related to the quality of the ridesplitting service

such as the delay time. Second, a constant speed is used to compute the travel time. The speed should be dynamic according to the road segments and time sequences in a follow-up study. Finally, the density of vehicles can also impact the results. The proposed ridesplitting algorithm can be used in different cities to make a comparison.

Other research directions in this domain: MaaS (Mobility as a Service), incentive mechanisms, optimization of the system, connected and cooperative systems, dispatching strategies, etc.

It is worth exploring the MaaS framework, integration the ridesourcing service using CAVs with the public transportation services. Ridesourcing services with CAVS will increase the number of trips for its convenience in the long run. It is more energy-efficient for integrating the ridesourcing services using CAVs with the subway., which can help build a low-carbon transportation. It is also meaningful to explore incentive mechanism for shared mobility vehicles rather than private and conventional vehicles, such as high-occupancy vehicle lanes and waivers for road fees and parking fees.

4) Domain 4: CAVs technologies

Research perspectives in the proposed topic: Proposing a resilient and robust control strategy for connected and autonomous vehicles to resist the threat of cyber-attacks

Of course, there are still some deficiencies in this research part and the following aspects could be further explored in the future: First, how cyberattack impacts the travel demand, traffic efficiency and energy consumption of the shared mobility system would be explored in the next stage. Secondly, there are common lane changing and overtaking behaviors in real traffic scenarios, which should be considered in the vehicle dynamics model to better describe the characteristics of traffic flow. Thirdly, some parameters like safe headway could vary rather than a fixed value, which will help to improve the universality and persuasion of the model and strategy. Last but not least, more sensor data could be considered such as LIDAR and camera. In this way it could be possible to merge the proposed approach (RRCS) with the perception outputs and a risk assessment system.

Other research directions in this domain: autonomous/automated vehicles, sensors and environment perception, path planning and copilot, operating safety, mixed traffic management, etc.

There are several more directions that can be explored for further study. It is worth exploring the path planning strategy for shared mobility services with electric CAVs. How to set the location and number of charging piles is really an interesting research

direction. It is also meaningful to design a feasible shared mobility services with CAVs based on the blockchain to improve the efficiency and safety of the whole system.

References

Accenture. (2016). *Car sharing service outlook in China*.

Accorsi, L., Lodi, A., & Vigo, D. (2022). Guidelines for the computational testing of machine learning approaches to vehicle routing problems. *Operations Research Letters*, *50*(2), 229-234.

Alemi, F., Circella, G., Handy, S., & Mokhtarian, P. (2018). What influences travelers to use Uber? Exploring the factors affecting the adoption of on-demand ride services in California. *Travel Behaviour and Society*, *13*, 88-104.

Alexander, L. P., & González, M. C. (2015). Assessing the impact of real-time ridesharing on urban traffic using mobile phone data. *Proc. UrbComp*, *15*, 1-9.

Alipour-Fanid, A., Dabaghchian, M., Zhang, H., & Zeng, K. (2017). String stability analysis of cooperative adaptive cruise control under jamming attacks. 2017 IEEE 18th International Symposium on High Assurance Systems Engineering (HASE),

Aliwa, E., Rana, O., Perera, C., & Burnap, P. (2021). Cyberattacks and countermeasures for in-vehicle networks. *ACM Computing Surveys (CSUR)*, *54*(1), 1-37.

Alonso-Mora, J., Samaranayake, S., Wallar, A., Frazzoli, E., & Rus, D. (2017). On-demand high-capacity ride-sharing via dynamic trip-vehicle assignment. *Proceedings of the National Academy of Sciences*, *114*(3), 462-467.

Anderson, J. M., Nidhi, K., Stanley, K. D., Sorensen, P., Samaras, C., & Oluwatola, O. A. (2014). *Autonomous vehicle technology: A guide for policymakers*. Rand Corporation.

Angrist, J. D., Caldwell, S., & Hall, J. V. (2021). Uber versus taxi: A driver's eye view. *American Economic Journal: Applied Economics*, *13*(3), 272-308.

Asuquo, P., Cruickshank, H., Morley, J., Ogah, C. P. A., Lei, A., Hathal, W., Bao, S., & Sun, Z. (2018). Security and privacy in location-based services for vehicular and mobile communications: an overview, challenges, and countermeasures. *IEEE Internet of Things Journal*, *5*(6), 4778-4802.

Audenhove, F.-J. V., Ali, S., & Salem, J. (2020). *Rethinking on-demand mobility*. https://www.adlittle.com/en/rethinking-demand-mobility

Ba, J. L., Kiros, J. R., & Hinton, G. E. (2016). Layer normalization. *arXiv preprint arXiv:1607.06450*.

Baker, B. M., & Ayechew, M. (2003). A genetic algorithm for the vehicle routing problem. *Computers & Operations Research*, *30*(5), 787-800.

Bando, M., Hasebe, K., Nakayama, A., Shibata, A., & Sugiyama, Y. (1995). Dynamical model of traffic congestion and numerical simulation. *Physical review E*, *51*(2), 1035.

Bates, J., & Leibling, D. (2012). Spaced Out: Perspectives on parking policy.

Becker, G. S. (1965). A Theory of the Allocation of Time. *The economic journal*,

75(299), 493-517.

Braekers, K., Caris, A., & Janssens, G. K. (2014). Exact and meta-heuristic approach for a general heterogeneous dial-a-ride problem with multiple depots. *Transportation Research Part B: Methodological*, *67*, 166-186.

Brunsdon, C., Fotheringham, A. S., & Charlton, M. E. (1996). Geographically weighted regression: a method for exploring spatial nonstationarity. *Geographical analysis*, *28*(4), 281-298.

Casprini, E., Di Minin, A., & Paraboschi, A. (2019). How do companies organize nascent markets? The BlaBlaCar case in the inter-city shared mobility market. *Technological Forecasting and Social Change*, *144*, 270-281.

Castro-Neto, M., Jeong, Y.-S., Jeong, M.-K., & Han, L. D. (2009). Online-SVR for short-term traffic flow prediction under typical and atypical traffic conditions. *Expert systems with applications*, *36*(3), 6164-6173.

Cervero, R., & Kockelman, K. (1997). Travel demand and the 3Ds: Density, diversity, and design. *Transportation research part D: Transport and environment*, *2*(3), 199-219.

Chakour, V., & Eluru, N. (2016). Examining the influence of stop level infrastructure and built environment on bus ridership in Montreal. *Journal of Transport Geography*, *51*, 205-217.

Chan, N. D., & Shaheen, S. A. (2012). Ridesharing in North America: Past, present, and future. *Transport reviews*, *32*(1), 93-112.

Chen, G., Wu, J., Yang, W., Bashir, A. K., Li, G., & Hammoudeh, M. (2021). Leveraging graph convolutional-LSTM for energy-efficient caching in blockchain-based green IoT. *IEEE Transactions on Green Communications and Networking*, *5*(3), 1154-1164.

Chen, K., Zhao, T., Yang, M., Liu, L., Tamura, A., Wang, R., Utiyama, M., & Sumita, E. (2017). A neural approach to source dependence based context model for statistical machine translation. *IEEE/ACM Transactions on Audio, Speech, and Language Processing*, *26*(2), 266-280.

Chen, L., Wu, L., Hong, R., Zhang, K., & Wang, M. (2020). Revisiting graph based collaborative filtering: A linear residual graph convolutional network approach. *Proceedings of the AAAI conference on artificial intelligence*, *34*(01), 27-34.

Chen, M. K., Rossi, P. E., Chevalier, J. A., & Oehlsen, E. (2019). The value of flexible work: Evidence from Uber drivers. *Journal of political economy*, *127*(6), 2735-2794.

Chen, X., Zheng, H., Wang, Z., & Chen, X. (2021). Exploring impacts of on-demand ridesplitting on mobility via real-world ridesourcing data and questionnaires. *Transportation*, *48*(4), 1541-1561.

Chen, X. M., Zahiri, M., & Zhang, S. (2017). Understanding ridesplitting behavior of on-demand ride services: An ensemble learning approach. *Transportation Research Part C: Emerging Technologies*, *76*, 51-70.

Chen, Y., Gonder, J., Young, S., & Wood, E. (2019). Quantifying autonomous

vehicles national fuel consumption impacts: A data-rich approach. *Transportation Research Part A: Policy and Practice*, *122*, 134-145.

Cheng, L., Shi, Y., Zhang, K., Wang, X., & Chen, Z. (2021). GGATB-LSTM: Grouping and Global Attention-based Time-aware Bidirectional LSTM Medical Treatment Behavior Prediction. *ACM Transactions on Knowledge Discovery from Data (TKDD)*, *15*(3), 1-16.

Chengdu Bureau of Statistics. (2020). *Statistical report on the national economic and social evelopment of Chengdu*.

Cho, K., Courville, A., & Bengio, Y. (2015). Describing multimedia content using attention-based encoder-decoder networks. *IEEE Transactions on Multimedia*, *17*(11), 1875-1886.

Choudhury, C. F., Yang, L., e Silva, J. d. A., & Ben-Akiva, M. (2018). Modelling preferences for smart modes and services: A case study in Lisbon. *Transportation Research Part A: Policy and Practice*, *115*, 15-31.

Chu, K.-F., Lam, A. Y., & Li, V. O. (2019). Deep multi-scale convolutional LSTM network for travel demand and origin-destination predictions. *IEEE Transactions on Intelligent Transportation Systems*, *21*(8), 3219-3232.

Clarke, G., & Wright, J. W. (1964). Scheduling of vehicles from a central depot to a number of delivery points. *Operations research*, *12*(4), 568-581.

Clements, L. M., & Kockelman, K. M. (2017). Economic effects of automated vehicles. *Transportation research record*, *2606*(1), 106-114.

Conti, J., Holtberg, P., Diefenderfer, J., LaRose, A., Turnure, J. T., & Westfall, L. (2016). *International energy outlook 2016 with projections to 2040*.

Cortés, C. E., Matamala, M., & Contardo, C. (2010). The pickup and delivery problem with transfers: Formulation and a branch-and-cut solution method. *European Journal of Operational Research*, *200*(3), 711-724.

Cui, J., Liew, L. S., Sabaliauskaite, G., & Zhou, F. (2019). A review on safety failures, security attacks, and available countermeasures for autonomous vehicles. *Ad Hoc Networks*, *90*, 101823.

Davidson, P., & Spinoulas, A. (2016). Driving alone versus riding together-How shared autonomous vehicles can change the way we drive. *Road & Transport Research: A Journal of Australian and New Zealand Research and Practice*, *25*(3), 51-66.

Defferrard, M., Bresson, X., & Vandergheynst, P. (2016). Convolutional neural networks on graphs with fast localized spectral filtering. *Advances in neural information processing systems*, *29*.

DiDi Chuxing. (2018a). *Daily rides of DiDi ExpressPool exceed 2.4 million*. Retrieved May 16th, 2018 from http://www.DiDichuxing.com/en/press-news/j3km2785.html

DiDi Chuxing. (2018b). *What does the GAIA Initiative provide in the first phase?* Retrieved February 5th, 2018 from

Didi Chuxing. (2020). *White Paper of Green Travel on Didi Platform*.

DiDi Chuxing. (2021). *Index to Consolidated Financial Statements*. D. G. Inc.

Ding, C., Cao, X., & Liu, C. (2019). How does the station-area built environment influence Metrorail ridership? Using gradient boosting decision trees to identify non-linear thresholds. *Journal of Transport Geography*, *77*, 70-78.

Ding, C., Cao, X. J., & Næss, P. (2018). Applying gradient boosting decision trees to examine non-linear effects of the built environment on driving distance in Oslo. *Transportation Research Part A: Policy and Practice*, *110*, 107-117.

Dong, C., Wang, H., Ni, D., Liu, Y., & Chen, Q. (2020). Impact evaluation of cyber-attacks on traffic flow of connected and automated vehicles. *IEEE Access*, *8*, 86824-86835.

Dorigo, M., Birattari, M., & Stutzle, T. (2006). Ant colony optimization. *IEEE computational intelligence magazine*, *1*(4), 28-39.

Du, B., Hu, X., Sun, L., Liu, J., Qiao, Y., & Lv, W. (2020). Traffic demand prediction based on dynamic transition convolutional neural network. *IEEE Transactions on Intelligent Transportation Systems*, *22*(2), 1237-1247.

Duncan, M. (2011). The cost saving potential of carsharing in a US context. *Transportation*, *38*(2), 363-382.

Durning, M., & Townsend, C. (2015). Direct ridership model of rail rapid transit systems in Canada. *Transportation research record*, *2537*(1), 96-102.

El-Assi, W., Salah Mahmoud, M., & Nurul Habib, K. (2017). Effects of built environment and weather on bike sharing demand: a station level analysis of commercial bike sharing in Toronto. *Transportation*, *44*(3), 589-613.

Ewing, R., & Cervero, R. (2001). Travel and the built environment: a synthesis. *Transportation research record*, *1780*(1), 87-114.

Ewing, R., & Cervero, R. (2010). Travel and the built environment: A meta-analysis. *Journal of the American planning association*, *76*(3), 265-294.

Fagnant, D. J., & Kockelman, K. M. (2014). The travel and environmental implications of shared autonomous vehicles, using agent-based model scenarios. *Transportation Research Part C: Emerging Technologies*, *40*, 1-13.

Firnkorn, J., & Müller, M. (2011). What will be the environmental effects of new free-floating car-sharing systems? The case of car2go in Ulm. *Ecological economics*, *70*(8), 1519-1528.

Fisher, M. L., & Jaikumar, R. (1981). A generalized assignment heuristic for vehicle routing. *Networks*, *11*(2), 109-124.

Friedman, J. H. (2001). Greedy function approximation: a gradient boosting machine. *Annals of statistics*, 1189-1232.

Fukasawa, R., Longo, H., Lysgaard, J., Aragão, M. P. d., Reis, M., Uchoa, E., & Werneck, R. F. (2006). Robust branch-and-cut-and-price for the capacitated vehicle routing problem. *Mathematical programming*, *106*(3), 491-511.

Gan, Z., Yang, M., Feng, T., & Timmermans, H. J. (2020). Examining the relationship between built environment and metro ridership at station-to-station level. *Transportation research part D: Transport and environment*, *82*, 102332.

Geng, X., Li, Y., Wang, L., Zhang, L., Yang, Q., Ye, J., & Liu, Y. (2019).

Spatiotemporal multi-graph convolution network for ride-hailing demand forecasting. *Proceedings of the AAAI conference on artificial intelligence*, *33*(01), 3656-3663.

Gillett, B. E., & Miller, L. R. (1974). A heuristic algorithm for the vehicle-dispatch problem. *Operations research*, *22*(2), 340-349.

Greenblatt, J. B., & Shaheen, S. (2015). Automated vehicles, on-demand mobility, and environmental impacts. *Current sustainable/renewable energy reports*, *2*(3), 74-81.

Groër, C., Golden, B., & Wasil, E. (2010). A library of local search heuristics for the vehicle routing problem. *Mathematical Programming Computation*, *2*(2), 79-101.

Gruyer, D., Orfila, O., Glaser, S., Hedhli, A., Hautière, N., & Rakotonirainy, A. (2021). Are connected and automated vehicles the silver bullet for future transportation challenges? Benefits and weaknesses on safety, consumption, and traffic congestion. *Frontiers in Sustainable Cities*, 63.

Guan, H., Chen, J., & Cao, W. (2013). Empirical study on the relationship between carbon emission and urbanization. *China Population, Resources and Environment*, *23*(4), 111-116.

Guo, K., Hu, Y., Qian, Z., Liu, H., Zhang, K., Sun, Y., Gao, J., & Yin, B. (2020). Optimized graph convolution recurrent neural network for traffic prediction. *IEEE Transactions on Intelligent Transportation Systems*, *22*(2), 1138-1149.

Guo, Z., Li, X., Huang, H., Guo, N., & Li, Q. (2019). Deep learning-based image segmentation on multimodal medical imaging. *IEEE Transactions on Radiation and Plasma Medical Sciences*, *3*(2), 162-169.

Hall, J. D., Palsson, C., & Price, J. (2018). Is Uber a substitute or complement for public transit? *Journal of urban economics*, *108*, 36-50.

Handke, V., & Jonuschat, H. (2012). *Flexible ridesharing: new opportunities and service concepts for sustainable mobility*. Springer Science & Business Media.

Hara Associates Inc. (2013). *Taxi User Surveys*. S. F. M. T. Agency. https://www.sfmta.com/sites/default/files/Draft%20SF%20UserSurvey%2055%20WEB%20version04042013.pdf

Hastie, T., Tibshirani, R., Friedman, J. H., & Friedman, J. H. (2009). *The elements of statistical learning: data mining, inference, and prediction* (Vol. 2). Springer.

Hawkins, J., & Nurul Habib, K. (2019). Integrated models of land use and transportation for the autonomous vehicle revolution. *Transport reviews*, *39*(1), 66-83.

He, K., Zhang, X., Ren, S., & Sun, J. (2016). Deep residual learning for image recognition. *Proceedings of the IEEE conference on computer vision and pattern recognition*, 770-778.

Hochreiter, S., & Schmidhuber, J. (1997). Long short-term memory. *Neural computation*, *9*(8), 1735-1780.

Hu, G., Wang, F., Lu, W., Kwembe, T. A., & Whalin, R. W. (2020). Cooperative bypassing algorithm for connected and autonomous vehicles in mixed traffic. *IET Intelligent Transport Systems*, *14*(8), 915-923.

Hughes, R., & MacKenzie, D. (2016). Transportation network company wait

times in Greater Seattle, and relationship to socioeconomic indicators. *Journal of Transport Geography*, *56*, 36-44.

Idir, Y. M., Orfila, O., Judalet, V., Sagot, B., & Chatellier, P. (2021). Mapping Urban Air Quality from Mobile Sensors Using Spatio-Temporal Geostatistics. *Sensors*, *21*(14), 4717.

IEA, I. (2015). *CO2 Emissions from fuel combustion highlights 2014*.

Ignall, E., & Schrage, L. (1965). Application of the branch and bound technique to some flow-shop scheduling problems. *Operations research*, *13*(3), 400-412.

Ioffe, S., & Szegedy, C. (2015). Batch normalization: Accelerating deep network training by reducing internal covariate shift. *International conference on machine learning*, 448-456.

Iqbal, M. (2022a). *Lyft Revenue and Usage Statistics*. Business of Apps. Retrieved March 30th, 2022 from https://www.businessofapps.com/data/lyft-statistics/

Iqbal, M. (2022b). *Uber Revenue and Usage Statistics*. Business of Apps. Retrieved March 30th, 2022 from https://www.businessofapps.com/data/uber-statistics/

Jiang, R., Wu, Q., & Zhu, Z. (2001). Full velocity difference model for a car-following theory. *Physical review E*, *64*(1), 017101.

Jin, I. G., & Orosz, G. (2014). Dynamics of connected vehicle systems with delayed acceleration feedback. *Transportation Research Part C: Emerging Technologies*, *46*, 46-64.

Jin, S. T., Kong, H., Wu, R., & Sui, D. Z. (2018). Ridesourcing, the sharing economy, and the future of cities. *Cities*, *76*, 96-104.

Katragadda, S., Darby, P. J., Roche, A., & Gottumukkala, R. (2020). Detecting low-rate replay-based injection attacks on in-vehicle networks. *IEEE Access*, *8*, 54979-54993.

Ke, J., Qin, X., Yang, H., Zheng, Z., Zhu, Z., & Ye, J. (2021). Predicting origin-destination ride-sourcing demand with a spatio-temporal encoder-decoder residual multi-graph convolutional network. *Transportation Research Part C: Emerging Technologies*, *122*, 102858.

Ke, J., Yang, H., Zheng, H., Chen, X., Jia, Y., Gong, P., & Ye, J. (2018). Hexagon-based convolutional neural network for supply-demand forecasting of ride-sourcing services. *IEEE Transactions on Intelligent Transportation Systems*, *20*(11), 4160-4173.

Kent, J. L. (2014). Carsharing as active transport: What are the potential health benefits? *Journal of Transport & Health*, *1*(1), 54-62.

Khan, S. K., Shiwakoti, N., Stasinopoulos, P., & Chen, Y. (2020). Cyber-attacks in the next-generation cars, mitigation techniques, anticipated readiness and future directions. *Accident Analysis & Prevention*, *148*, 105837.

Khattak, Z. H., Park, H., Hong, S., Boateng, R. A., & Smith, B. L. (2018). Investigating cybersecurity issues in active traffic management systems. *Transportation research record*, *2672*(19), 79-90.

Khattak, Z. H., Smith, B. L., & Fontaine, M. D. (2021). Impact of cyberattacks

on safety and stability of connected and automated vehicle platoons under lane changes. *Accident Analysis & Prevention*, *150*, 105861.

King, D. A., & Saldarriaga, J. F. (2017). Access to taxicabs for unbanked households: An exploratory analysis in New York City. *Journal of Public Transportation*, *20*(1), 1.

Kipf, T. N., & Welling, M. (2016). Semi-supervised classification with graph convolutional networks. *arXiv preprint arXiv:1609.02907*.

Kirchler, D., & Calvo, R. W. (2013). A granular tabu search algorithm for the dial-a-ride problem. *Transportation Research Part B: Methodological*, *56*, 120-135.

Kleiner, A., Nebel, B., & Ziparo, V. A. (2011). A mechanism for dynamic ride sharing based on parallel auctions. *Twenty-second international joint conference on artificial intelligence*.

Kontou, E., Garikapati, V., & Hou, Y. (2020). Reducing ridesourcing empty vehicle travel with future travel demand prediction. *Transportation Research Part C: Emerging Technologies*, *121*, 102826.

Krueger, R., Rashidi, T. H., & Rose, J. M. (2016). Preferences for shared autonomous vehicles. *Transportation Research Part C: Emerging Technologies*, *69*, 343-355.

Laporte, G. (1992). The vehicle routing problem: An overview of exact and approximate algorithms. *European Journal of Operational Research*, *59*(3), 345-358.

Li, B., Krushinsky, D., Van Woensel, T., & Reijers, H. A. (2016). An adaptive large neighborhood search heuristic for the share-a-ride problem. *Computers & Operations Research*, *66*, 170-180.

Li, C., Tang, G., Xue, X., Saeed, A., & Hu, X. (2019). Short-term wind speed interval prediction based on ensemble GRU model. *IEEE transactions on sustainable energy*, *11*(3), 1370-1380.

Li, J., Sun, A., Han, J., & Li, C. (2020). A survey on deep learning for named entity recognition. *IEEE Transactions on Knowledge and Data Engineering*, *34*(1), 50-70.

Li, L., Wen, D., & Yao, D. (2013). A survey of traffic control with vehicular communications. *IEEE Transactions on Intelligent Transportation Systems*, *15*(1), 425-432.

Li, W., Li, Y., Fan, J., & Deng, H. (2017). Siting of carsharing stations based on spatial multi-criteria evaluation: A case study of Shanghai EVCARD. *Sustainability*, *9*(1), 152.

Li, W., Pu, Z., Li, Y., & Ban, X. J. (2019). Characterization of ridesplitting based on observed data: A case study of Chengdu, China. *Transportation Research Part C: Emerging Technologies*, *100*, 330-353.

Li, Y., Tu, Y., Fan, Q., Dong, C., & Wang, W. (2018). Influence of cyber-attacks on longitudinal safety of connected and automated vehicles. *Accident Analysis & Prevention*, *121*, 148-156.

Li, Z., Xiong, G., Tian, Y., Lv, Y., Chen, Y., Hui, P., & Su, X. (2020). A multi-

stream feature fusion approach for traffic prediction. *IEEE Transactions on Intelligent Transportation Systems*.

Liu, J., Zhang, S., Sun, W., & Shi, Y. (2017). In-vehicle network attacks and countermeasures: Challenges and future directions. *IEEE Network*, *31*(5), 50-58.

Liu, L., Qiu, Z., Li, G., Wang, Q., Ouyang, W., & Lin, L. (2019). Contextualized spatial–temporal network for taxi origin-destination demand prediction. *IEEE Transactions on Intelligent Transportation Systems*, *20*(10), 3875-3887.

Liu, L., Zhu, L., & Yang, D. (2016). Modeling and simulation of the car-truck heterogeneous traffic flow based on a nonlinear car-following model. *Applied Mathematics and Computation*, *273*, 706-717.

Liu, W., & Shoji, Y. (2019). DeepVM: RNN-based vehicle mobility prediction to support intelligent vehicle applications. *IEEE Transactions on Industrial Informatics*, *16*(6), 3997-4006.

Liu, Y., Lyu, C., Khadka, A., Zhang, W., & Liu, Z. (2019). Spatio-temporal ensemble method for car-hailing demand prediction. *IEEE Transactions on Intelligent Transportation Systems*, *21*(12), 5328-5333.

Luo, X., Dong, L., Dou, Y., Li, Y., Liu, K., Ren, J., Liang, H., & Mai, X. (2017). Factor decomposition analysis and causal mechanism investigation on urban transport CO2 emissions: Comparative study on Shanghai and Tokyo. *Energy Policy*, *107*, 658-668.

Luong, M.-T., Pham, H., & Manning, C. D. (2015). Effective approaches to attention-based neural machine translation. *arXiv preprint arXiv:1508.04025*.

Lv, X., Wang, Z.-L., Ren, Y., Yang, D.-Z., Feng, Q., Sun, B., & Liu, D. (2019). Traffic network resilience analysis based on the GCN-RNN prediction model. *2019 International Conference on Quality, Reliability, Risk, Maintenance, and Safety Engineering (QR2MSE)*, 96-103.

Ma, S., Zheng, Y., & Wolfson, O. (2013). T-share: A large-scale dynamic taxi ridesharing service. *2013 IEEE 29th International Conference on Data Engineering (ICDE)*, 410-421.

Maciejewski, M., & Bischoff, J. (2016). Congestion effects of autonomous taxi fleets.

Mackenzie, J., Roddick, J. F., & Zito, R. (2018). An evaluation of HTM and LSTM for short-term arterial traffic flow prediction. *IEEE Transactions on Intelligent Transportation Systems*, *20*(5), 1847-1857.

Milanés, V., & Shladover, S. E. (2014). Modeling cooperative and autonomous adaptive cruise control dynamic responses using experimental data. *Transportation Research Part C: Emerging Technologies*, *48*, 285-300.

Miller, T. R. (1989). The value of time and the benefit of time saving: A literature synthesis and recommendations on values.

Minaee, S., Boykov, Y. Y., Porikli, F., Plaza, A. J., Kehtarnavaz, N., & Terzopoulos, D. (2021). Image segmentation using deep learning: A survey. *IEEE transactions on pattern analysis and machine intelligence*.

Mousavinejad, E., Yang, F., Han, Q.-L., Ge, X., & Vlacic, L. (2019). Distributed cyber attacks detection and recovery mechanism for vehicle platooning. *IEEE Transactions on Intelligent Transportation Systems*, *21*(9), 3821-3834.

Nakamura, K., & Hayashi, Y. (2013). Strategies and instruments for low-carbon urban transport: An international review on trends and effects. *Transport Policy*, *29*, 264-274.

National ICV, & China SAE. (2021). *Guidelines for the Development of Connected and Automated Vehicles in Cities*.

Nazari, F., Noruzoliaee, M., & Mohammadian, A. (2018). *Shared mobility versus private car ownership: A multivariate analysis of public interest in autonomous vehicles*.

Ngoduy, D. (2015). Effect of the car-following combinations on the instability of heterogeneous traffic flow. *Transportmetrica B: transport dynamics*, *3*(1), 44-58.

Nielsen, J. R., Hovmøller, H., Blyth, P.-L., & Sovacool, B. K. (2015). Of "white crows" and "cash savers:" A qualitative study of travel behavior and perceptions of ridesharing in Denmark. *Transportation Research Part A: Policy and Practice*, *78*, 113-123.

Niepert, M., Ahmed, M., & Kutzkov, K. (2016). Learning convolutional neural networks for graphs. *International conference on machine learning*, 2014-2023.

Noei, S., Parvizimosaed, M., & Noei, M. (2021). Longitudinal Control for Connected and Automated Vehicles in Contested Environments. *Electronics*, *10*(16), 1994.

Nogueira, B., Pinheiro, R. G., & Subramanian, A. (2018). A hybrid iterated local search heuristic for the maximum weight independent set problem. *Optimization Letters*, *12*(3), 567-583.

Osman, I. H. (1993). Metastrategy simulated annealing and tabu search algorithms for the vehicle routing problem. *Annals of operations research*, *41*(4), 421-451.

Palomar, E., de Fuentes, J. M., González-Tablas, A. I., & Alcaide, A. (2012). Hindering false event dissemination in VANETs with proof-of-work mechanisms. *Transportation Research Part C: Emerging Technologies*, *23*, 85-97.

Parragh, S. N., Doerner, K. F., & Hartl, R. F. (2010). Variable neighborhood search for the dial-a-ride problem. *Computers & Operations Research*, *37*(6), 1129-1138.

Penna, P. H. V., Subramanian, A., & Ochi, L. S. (2013). An iterated local search heuristic for the heterogeneous fleet vehicle routing problem. *Journal of Heuristics*, *19*(2), 201-232.

Pipes, L. A. (1953). An operational analysis of traffic dynamics. *Journal of applied physics*, *24*(3), 274-281.

Qian, Z. S., Li, J., Li, X., Zhang, M., & Wang, H. (2017). Modeling heterogeneous traffic flow: A pragmatic approach. *Transportation Research Part B: Methodological*, *99*, 183-204.

Raya, M., & Hubaux, J.-P. (2007). Securing vehicular ad hoc networks. *Journal*

of computer security, *15*(1), 39-68.

Rayle, L., Dai, D., Chan, N., Cervero, R., & Shaheen, S. (2016). Just a better taxi? A survey-based comparison of taxis, transit, and ridesourcing services in San Francisco. *Transport Policy*, *45*, 168-178.

Rayle, L., Shaheen, S., Chan, N., Dai, D., & Cervero, R. (2014). App-based, on-demand ride services: Comparing taxi and ridesourcing trips and user characteristics in san francisco university of california transportation center (uctc). *University of California: Berkeley, CA, USA*.

Renaud, J., Boctor, F. F., & Laporte, G. (1996). An improved petal heuristic for the vehicle routeing problem. *Journal of the operational Research Society*, *47*(2), 329-336.

Rios-Torres, J., & Malikopoulos, A. A. (2016). A survey on the coordination of connected and automated vehicles at intersections and merging at highway on-ramps. *IEEE Transactions on Intelligent Transportation Systems*, *18*(5), 1066-1077.

Ropke, S., Cordeau, J. F., & Laporte, G. (2007). Models and branch‐and‐cut algorithms for pickup and delivery problems with time windows. *Networks: An International Journal*, *49*(4), 258-272.

Roskilly, A., Palacin, R., & Yan, J. (2015). Novel technologies and strategies for clean transport systems. *Applied Energy*, *100*(157), 563-566.

Sabouri, S., Park, K., Smith, A., Tian, G., & Ewing, R. (2020). Exploring the influence of built environment on Uber demand. *Transportation research part D: Transport and environment*, *81*, 102296.

Santi, P., Resta, G., Szell, M., Sobolevsky, S., Strogatz, S. H., & Ratti, C. (2014). Quantifying the benefits of vehicle pooling with shareability networks. *Proceedings of the National Academy of Sciences*, *111*(37), 13290-13294.

Santos, A., McGuckin, N., Nakamoto, H. Y., Gray, D., & Liss, S. (2011). *Summary of travel trends: 2009 national household travel survey*.

Santos, L. d. C., & Mariani, V. C. (2006). Particle swarm optimization with quasi-Newton local search for solving economic dispatch problem. *2006 IEEE International Conference on Systems, Man and Cybernetics*, *4*, 3109-3113.

Sapankevych, N. I., & Sankar, R. (2009). Time series prediction using support vector machines: a survey. *IEEE computational intelligence magazine*, *4*(2), 24-38.

Schrank, D., Eisele, B., & Lomax, T. (2012). TTI's 2012 urban mobility report. *Texas A&M Transportation Institute. The Texas A&M University System*, *4*.

Shaheen, S., Chan, N., Bansal, A., & Cohen, A. (2015). Shared mobility: Definitions, industry developments, and early understanding. *Transportation Sustainability Research Center, Innovative Mobility Research*.

Shaheen, S., Cohen, A., & Zohdy, I. (2016). *Shared mobility: current practices and guiding principles*.

Shaheen, S. A., Chan, N. D., & Gaynor, T. (2016). Casual carpooling in the San Francisco Bay Area: Understanding user characteristics, behaviors, and motivations. *Transport Policy*, *51*, 165-173.

Shams, S. R., Jahani, A., Kalantary, S., Moeinaddini, M., & Khorasani, N. (2021). Artificial intelligence accuracy assessment in NO2 concentration forecasting of metropolises air. *Scientific Reports*, *11*(1), 1-9.

Sharma, A., Zheng, Z., Bhaskar, A., & Haque, M. M. (2019). Modelling car-following behaviour of connected vehicles with a focus on driver compliance. *Transportation Research Part B: Methodological*, *126*, 256-279.

Shi, X., Wong, Y. D., Li, M. Z.-F., Palanisamy, C., & Chai, C. (2019). A feature learning approach based on XGBoost for driving assessment and risk prediction. *Accident Analysis & Prevention*, *129*, 170-179.

Shu, P., Sun, Y., Zhao, Y., & Xu, G. (2020). Spatial-temporal taxi demand prediction using LSTM-CNN. *2020 IEEE 16th International Conference on Automation Science and Engineering (CASE)*, 1226-1230.

Simonetto, A., Monteil, J., & Gambella, C. (2019). Real-time city-scale ridesharing via linear assignment problems. *Transportation Research Part C: Emerging Technologies*, *101*, 208-232.

Small, K. A., Winston, C., & Evans, C. A. (2012). *Road work: A new highway pricing and investment policy*. Brookings Institution Press.

Song, Y., Wang, X., Wright, G., Thatcher, D., Wu, P., & Felix, P. (2018). Traffic volume prediction with segment-based regression kriging and its implementation in assessing the impact of heavy vehicles. *IEEE Transactions on Intelligent Transportation Systems*, *20*(1), 232-243.

Sperling, D. (2018). *Three revolutions: Steering automated, shared, and electric vehicles to a better future*. Island Press.

Sukuvaara, T., & Nurmi, P. (2009). Wireless traffic service platform for combined vehicle-to-vehicle and vehicle-to-infrastructure communications. *IEEE Wireless Communications*, *16*(6), 54-61.

Tang, X., Qin, Z., Zhang, F., Wang, Z., Xu, Z., Ma, Y., Zhu, H., & Ye, J. (2019). A deep value-network based approach for multi-driver order dispatching. *Proceedings of the 25th ACM SIGKDD international conference on knowledge discovery & data mining*, 1780-1790.

Tao, T., Wang, J., & Cao, X. (2020). Exploring the non-linear associations between spatial attributes and walking distance to transit. *Journal of Transport Geography*, *82*, 102560.

Tariq, S., Lee, S., Kim, H. K., & Woo, S. S. (2020). CAN-ADF: The controller area network attack detection framework. *Computers & Security*, *94*, 101857.

Taylor, A., Leblanc, S., & Japkowicz, N. (2018). Probing the limits of anomaly detectors for automobiles with a cyberattack framework. *IEEE Intelligent Systems*, *33*(2), 54-62.

The Ministry of Public Security of China. (2022). *The number of new energy vehicles in 2021 increased by 59.25% over 2020*. Retrieved March 30th, 2022 from https://www.mps.gov.cn/n2254314/n6409334/c8322353/content.html

TheWhiteHouse. (2021). *Leaders Summit on Climate Summary of Proceedings*.

Retrieved APRIL 23 from https://www.whitehouse.gov/briefing-room/statements-releases/2021/04/23/leaders-summit-on-climate-summary-of-proceedings/

Torun, A. Ö., Göçer, K., Yeşiltepe, D., & Argın, G. (2020). Understanding the role of urban form in explaining transportation and recreational walking among children in a logistic GWR model: A spatial analysis in Istanbul, Turkey. *Journal of Transport Geography*, *82*, 102617.

Treiber, M., Hennecke, A., & Helbing, D. (2000). Congested traffic states in empirical observations and microscopic simulations. *Physical review E*, *62*(2), 1805.

Tu, M., Li, W., Orfila, O., Li, Y., & Gruyer, D. (2021). Exploring nonlinear effects of the built environment on ridesplitting: Evidence from Chengdu. *Transportation research part D: Transport and environment*, *93*, 102776.

Tu, M., Li, Y., Li, W., Tu, M., Orfila, O., & Gruyer, D. (2019). Improving ridesplitting services using optimization procedures on a shareability network: A case study of Chengdu. *Technological Forecasting and Social Change*, *149*, 119733.

Uber Estimator. (2022). *Uber cities*. Retrieved March 30th, 2022 from https://uberestimator.com/cities

Union of Concerned Scientists. (2020). *Ride-Hailing's Climate Risks*.

Van Arem, B., Van Driel, C. J., & Visser, R. (2006). The impact of cooperative adaptive cruise control on traffic-flow characteristics. *IEEE Transactions on Intelligent Transportation Systems*, *7*(4), 429-436.

Vazifeh, M. M., Santi, P., Resta, G., Strogatz, S. H., & Ratti, C. (2018). Addressing the minimum fleet problem in on-demand urban mobility. *Nature*, *557*(7706), 534-538.

Vosooghi, R., Puchinger, J., Jankovic, M., & Vouillon, A. (2019). Shared autonomous vehicle simulation and service design. *Transportation Research Part C: Emerging Technologies*, *107*, 15-33.

Wang, G., Ye, J. C., Mueller, K., & Fessler, J. A. (2018). Image reconstruction is a new frontier of machine learning. *IEEE transactions on medical imaging*, *37*(6), 1289-1296.

Wang, H., Guo, X.-H., Jia, Z.-W., Li, H.-K., Liang, Z.-G., Li, K.-C., & He, Q. (2010). Multilevel binomial logistic prediction model for malignant pulmonary nodules based on texture features of CT image. *European journal of radiology*, *74*(1), 124-129.

Wang, H., & Yang, H. (2019). Ridesourcing systems: A framework and review. *Transportation Research Part B: Methodological*, *129*, 122-155.

Wang, P., Wu, X., & He, X. (2020). Modeling and analyzing cyberattack effects on connected automated vehicular platoons. *Transportation Research Part C: Emerging Technologies*, *115*, 102625.

Wang, P., Yu, G., Wu, X., Qin, H., & Wang, Y. (2018). An extended car-following model to describe connected traffic dynamics under cyberattacks. *Physica A: Statistical Mechanics and its Applications*, *496*, 351-370.

Wang, Z., Su, X., & Ding, Z. (2020). Long-term traffic prediction based on lstm encoder-decoder architecture. *IEEE Transactions on Intelligent Transportation*

Systems, *22*(10), 6561-6571.

Wardman, M. (1998). The value of travel time: a review of British evidence. *Journal of transport economics and policy*, 285-316.

Wen, F., Zhang, G., Sun, L., Wang, X., & Xu, X. (2019). A hybrid temporal association rules mining method for traffic congestion prediction. *Computers & Industrial Engineering*, *130*, 779-787.

Williams, B. M., & Hoel, L. A. (2003). Modeling and forecasting vehicular traffic flow as a seasonal ARIMA process: Theoretical basis and empirical results. *Journal of transportation engineering*, *129*(6), 664-672.

Wu, W., Xia, Y., & Jin, W. (2020). Predicting bus passenger flow and prioritizing influential factors using multi-source data: Scaled stacking gradient boosting decision trees. *IEEE Transactions on Intelligent Transportation Systems*, *22*(4), 2510-2523.

Wu, Z., Pan, S., Chen, F., Long, G., Zhang, C., & Philip, S. Y. (2020). A comprehensive survey on graph neural networks. *IEEE transactions on neural networks and learning systems*, *32*(1), 4-24.

Xiao, X., Jiang, M., Wen, J., & Wu, C. (2018). A novel car-following model considering conditional heteroskedasticity of acceleration fluctuation and driving force. *Journal of Intelligent & Fuzzy Systems*, *34*(4), 2301-2311.

Xie, D.-F., Zhao, X.-M., & He, Z. (2018). Heterogeneous traffic mixing regular and connected vehicles: Modeling and stabilization. *IEEE Transactions on Intelligent Transportation Systems*, *20*(6), 2060-2071.

Xu, J., Rahmatizadeh, R., Bölöni, L., & Turgut, D. (2017). Real-time prediction of taxi demand using recurrent neural networks. *IEEE Transactions on Intelligent Transportation Systems*, *19*(8), 2572-2581.

Yan, L. (2010). Low carbon Eco-city——The Strategic Choice of Global City for Sustainable Development in the Future under the Influence of Climate Change [J]. *Urban Studies*, *5*, 35-41.

Yan, X., Liu, X., & Zhao, X. (2020). Using machine learning for direct demand modeling of ridesourcing services in Chicago. *Journal of Transport Geography*, *83*, 102661.

Yang, H. (2021). Smart Mobility Management in the Era of Smart Transportation. International Symposium on Transportation Data and Modelling, Virtual.

Yao, H., Wu, F., Ke, J., Tang, X., Jia, Y., Lu, S., Gong, P., Ye, J., & Li, Z. (2018). Deep multi-view spatial-temporal network for taxi demand prediction. *Proceedings of the AAAI Conference on Artificial Intelligence*, *32*(1).

Ye, Y., Zhang, X., & Sun, J. (2019). Automated vehicle's behavior decision making using deep reinforcement learning and high-fidelity simulation environment. *Transportation Research Part C: Emerging Technologies*, *107*, 155-170.

Yoshizaki, H. T. Y. (2009). Scatter search for a real-life heterogeneous fleet vehicle routing problem with time windows and split deliveries in Brazil. *European Journal of Operational Research*, *199*(3), 750-758.

Yu, B., Lee, Y., & Sohn, K. (2020). Forecasting road traffic speeds by considering

area-wide spatio-temporal dependencies based on a graph convolutional neural network (GCN). *Transportation Research Part C: Emerging Technologies*, *114*, 189-204.

Yu, H., & Peng, Z.-R. (2019). Exploring the spatial variation of ridesourcing demand and its relationship to built environment and socioeconomic factors with the geographically weighted Poisson regression. *Journal of Transport Geography*, *75*, 147-163.

Yu, W., & Gao, B. (2011). Comprehensive Development of Tianfu Square in Chengdu City. *Urban Rapid Rail Transit*.

Zaki, J. F., Ali-Eldin, A., Hussein, S. E., Saraya, S. F., & Areed, F. F. (2020). Traffic congestion prediction based on Hidden Markov Models and contrast measure. *Ain Shams Engineering Journal*, *11*(3), 535-551.

Zeadally, S., Hunt, R., Chen, Y.-S., Irwin, A., & Hassan, A. (2012). Vehicular ad hoc networks (VANETS): status, results, and challenges. *Telecommunication Systems*, *50*(4), 217-241.

Zhai, C., & Wu, W. (2021). Designing continuous delay feedback control for lattice hydrodynamic model under cyber-attacks and connected vehicle environment. *Communications in Nonlinear Science and Numerical Simulation*, *95*, 105667.

Zhang, B., Zou, G., Qin, D., Lu, Y., Jin, Y., & Wang, H. (2021). A novel Encoder-Decoder model based on read-first LSTM for air pollutant prediction. *Science of the Total Environment*, *765*, 144507.

Zhang, C., Zhu, F., Lv, Y., Ye, P., & Wang, F.-Y. (2021). MLRNN: Taxi demand prediction based on multi-level deep learning and regional heterogeneity analysis. *IEEE Transactions on Intelligent Transportation Systems*.

Zhang, Y., & Haghani, A. (2015). A gradient boosting method to improve travel time prediction. *Transportation Research Part C: Emerging Technologies*, *58*, 308-324.

Zhang, Y., & Zhang, Y. (2018). Exploring the relationship between ridesharing and public transit use in the United States. *International journal of environmental research and public health*, *15*(8), 1763.

Zhang, Z., Cui, P., & Zhu, W. (2020). Deep learning on graphs: A survey. *IEEE Transactions on Knowledge and Data Engineering*.

Zhang, Z., Li, M., Lin, X., Wang, Y., & He, F. (2019). Multistep speed prediction on traffic networks: A deep learning approach considering spatio-temporal dependencies. *Transportation Research Part C: Emerging Technologies*, *105*, 297-322.

Zhao, L., Song, Y., Zhang, C., Liu, Y., Wang, P., Lin, T., Deng, M., & Li, H. (2019). T-gcn: A temporal graph convolutional network for traffic prediction. *IEEE Transactions on Intelligent Transportation Systems*, *21*(9), 3848-3858.

Zhao, L., & Sun, J. (2013). Simulation framework for vehicle platooning and car-following behaviors under connected-vehicle environment. *Procedia-Social and Behavioral Sciences*, *96*, 914-924.

Zhu, L., Yu, F. R., Wang, Y., Ning, B., & Tang, T. (2018). Big data analytics in intelligent transportation systems: A survey. *IEEE Transactions on Intelligent*

Transportation Systems, *20*(1), 383-398.

Acknowledgement

I sincerely extend my gratitude and appreciation to my advisors, Prof. Ye LI, Prof. Dominique Gruyer, and Prof. Olivier Orfila, for their support, guidance, and encouragement throughout my research work at Tongji University and Paris-Saclay University. They play an essential role in my research journey. It was a great privilege and honor to work and study under their guidance. I am really grateful for their confidence in capabilities, which always make me have motivation and inspirations to finish my research work. I also want to acknowledge the support of the other committee members, Dr. Shiyi Chen, Dr. Andry Rakotonirainy, Dr Xiaohong Chen, Dr Jianhong Ye, Dr. Mahdi Zargayouna, Dr. Lydie Nouvelière, Dr. Ouafae El Ganaoui-Mourlan, Dr Haihao Sun, for their insightful comments and immense knowledge.

My special appreciation to all the members of the transportation lab in Tongji University and the PICS lab in Gustave Eiffel University (Former IFSTTAR), for their accompany and integral help. I have special thanks to my collegues, Xiao Luo, Yuao Wei, Ji Fan, Zhiyong Shen, Wenxiang LI, Lei BAO, Qing He, Hanyu Shu, Mi Wang, Zhongzhong Yang, Yinpei Liu, Hongyong Huang, Guojian Zou, Ting Wang, Zhefeng Wang, Jingjue Bao, Ziliang Lai, Xinghua Liu, Wei Xu, Mohamed Yacine Idir, Jeremy Leroy, Rémi Sainct, Eric Dumont , Karima Hamdi.

I also need to express my gratitude to my parents and my brother, for their love, support and caring. Without their encouragement and love, I could achieve nothing.

Finally, I would like to thank all my colleagues, friends, and professors I met, for being part of my research journey.

Biography

Education background

Female, 1995.08
2013.09-2017.06 Beijing Jiaotong University, Transportation Engineering, Bachelor
2017.09-until now, Tongji University, Transportation Engineering, PhD
2018.12-until now, Paris Saclay University (global 13th in ARWU ranking in 2021), Automatic, PhD

Main awards:

2019-2021 CSC Sino-French Cai Yuanpei Scholarship (中法蔡元培奖学金)
2022 Shanghai Leading Talents (Overseas) Project (上海市海外领军人才计划)
2022 Shanghai Talent Acquisition Program （上海市高等教育人才拦蓄计划）

Publications：

[1] **Tu M.,** Li W.*, Orfila O., Li Y., & Gruyer D. Exploring nonlinear effects of the built environment on ridesplitting: Evidence from Chengdu. Transportation Research Part D: Transport and Environment, 2021, 93, 102776. **(SCI, Q1, IF= 5.495)**

[2] **Tu M.,** Li Y*, Li W, Orfila O., & Gruyer D. Improving ridesplitting services using optimization procedures on a shareability network: A case study of Chengdu [J]. Technological Forecasting and Social Change, 2019, 149: 119733. **(SCI, Q1, IF= 8.593, Top)**

[3] **Tu M.,** Li Y, Bao L*, Wei Y., Orfila O., & Gruyer D. Logarithmic Mean Divisia Index Decomposition of CO2 Emissions from Urban Passenger Transport: An Empirical Study of Global Cities from 1960–2001[J]. Sustainability, 2019, 11(16): 4310. **(SCI, Q2, IF= 3.251)**

[4] **Tu M.,** Li Y*, Li W, Orfila O., & Gruyer D. Improving Ridesplitting Service Using Optimization Procedures on Shareability Network: A Case Study of Chengdu, China. IEEE Intelligent Transportation Systems Conference (ITSC), 2019, 10: 4506-4511. (EI)

[5] Li, Y., **Tu, M.*,** & Wang, J. Layout Study of the Variable Message Signs on Urban Road Networks. CICTP 2019. 2019. 4306-4317. (EI)

[6] Li W., Pu Z., Li Y., & **Tu M**. How does ridesplitting reduce emissions from ridesourcing? A spatiotemporal analysis in Chengdu, China. Transportation Research Part D: Transport and Environment, 2021, 95, 102885. **(SCI, Q1, IF= 5.495)**

[7] Li, H., Ou, D., Rasheed, I., & **Tu, M.,** A Software-Defined Networking Roadside Unit Cloud Resource Management Framework for Vehicle Ad Hoc Networks. Journal of Advanced Transportation, 2022. **(SCI, Q2, IF= 2.93)**

[8] Shen, Z., Shen, Z., Luo, X., **Tu, M.**, & Liu, X. Human-Scale Quantitative Analysis on Urban Road Intersections. In CICTP 2021 (pp. 1152-1160).

[9] Lai Z, Liu X, Li W, …, **Tu, M.,** Corrigendum: Exploring the Spatial Heterogeneity of Residents' Marginal Willingness to Pay for Clean Air in Shanghai[J]. Frontiers in Public Health, 2022, 10.

Research projects:

[1] 2017.09-2020.09 Theoretical Research on Urban Traffic Governance Modernization, Key Project of National Natural Science Foundation of China

[2] 2017.09-2020.12 Big Data-driven Shared Traffic Management and Decision-making Paradigm Shift, Major Research Program of National Natural Science Foundation of China

International conference presentations:

[1] Optimization of ridesharing system, The 3rd international research seminar on robomobility, French Ministry of Ecological Transformation, Paris, France, Oral presentation, 2020.09.

[2] Improving ridesplitting services using optimization procedures on a shareability network: A case study of Chengdu, IEEE International Conference on Intelligent Transportation Systems (ITSC), Auckland, New Zealand, Oral presentation, 2019.11.

[3] Demonstrator of automated vehicle prototype, IEEE Intelligent Vehicles Symposium (IV), Paris, France, 2019,07.

[4] The future of robomobility life. The 2nd international research seminar on robomobility, French Ministry of Ecological Transformation, Paris, France, Oral presentation, 2019.06.

ÉCOLE DOCTORALE
Sciences et technologies de l'information et de la communication (STIC)

Titre : Optimisation des services de "ridesourcing" pour le déploiement futur des véhicules autonomes et connectés en milieu urbain

Mots clés : ridesourcing, ridesplitting, véhicules connectés et autonomes, services de mobilité partagée, optimisation, machine learning

Résumé : Les services de transport à la demande sont de plus en plus populaires en raison de leur commodité. Cependant, certaines études font apparaitre que ces services pourraient augmenter les congestions et le niveau de pollution. Le ridesplitting, un nouveau service de mobilité partagée, est un moyen plus durable de se déplacer pour améliorer l'efficacité des transports et réduire les émissions de polluants. Dans ce contexte, ce travail propose un cadre d'optimisation pour un Système de Mobilité Partagée (SMP).

L'originalité et les aspects innovants développés dans cette thèse sont aussi bien théoriques et méthodologiques, qu'appliqués. Du point de vue théorique et méthodologique, le cadre proposé pour le SMP fournit une méthodologie systématique et générique pour la modélisation et la simulation. Les algorithmes d'IA proposés permettent d'analyser et de mieux comprendre les comportements de déplacement des usagers et leur modélisation spatio-temporelle. Pour ce qui est de l'application pratique de ces travaux, le SMP proposé peut améliorer significativement les services de ridesplitting tout en réduisant l'empreinte carbone. De plus, ce SMP est facilement extrapolable aux CAV et aux futurs systèmes de mobilités.

Title : Optimization of ridesourcing services for the future deployment of connected and autonomous vehicles in urban areas

Keywords : ridesourcing, ridesplitting, connected and autonomous vehicles, shared mobility service, optimization, machine learning

Abstract : On-demand ridesourcing services have become increasingly popular due to their convenience. There are some debates claiming that ridesourcing services could increase congestion and pollution. Ridesplitting, a new shared mobility service, is a more sustainable travel mode for improving traffic efficiency and reducing air pollution. Therefore, the motivation of this study is to propose an optimization framework for the shared mobility system (SMS).

The originality and innovative aspects of this dissertation could be summarized according to 2 perspectives. For the value of theory and methodology, the proposed framework for the SMS could provide a systematic methodology for the modelling and simulation. The proposed artificial intelligent algorithms could provide a better understanding for the researches of travel behaviors analysis and spatiotemporal modelling. For the value of practical application, the proposed shared mobility system could help improve ridesplitting service to build a low carbon transport, which could incorporate CAVs for the future mobility.